2

LBL-31631

Lawrence Berkeley Laboratory
UNIVERSITY OF CALIFORNIA

Oligodendroglial Response to Ionizing Radiation: Dose and Dose-Rate Response

R.P. Levy
(Ph.D. Thesis)

December 1991

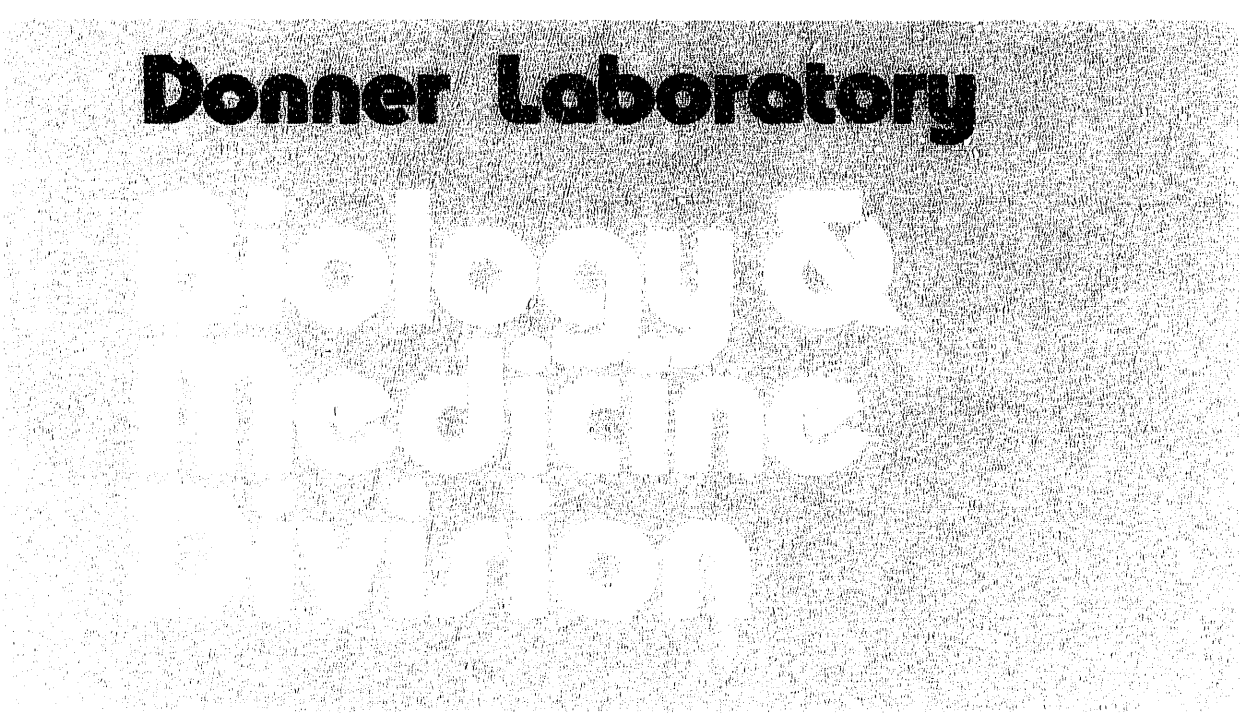

Prepared for the U.S. Department of Energy under Contract Number DE-AC03-76SF00098

LBL--31631

DE92 010307

Oligodendroglial Response to Ionizing Radiation: Dose and Dose-Rate Response

Richard P. Levy

Ph.D. Dissertation

Donner Pavilion and Donner Laboratory
Research Medicine and Radiation Biophysics Division
Lawrence Berkeley Laboratory
University of California at Berkeley
Berkeley, CA 94720

December 1991

This research was supported by the Director, Office of Energy Research, Office of Health and Environmental Research, Medical Applications Division of the U.S. Department of Energy under Contract No. DE-AC03-76SF00098.

Oligodendroglial Response to Ionizing Radiation: Dose and Dose-Rate Response

By

Richard Philip Levy

B.A. (Hofstra University, New York) 1973
M.A. (Hofstra University, New York) 1975
M.D. (Boston University) 1980

DISSERTATION

Submitted in partial satisfaction of the requirements for the degree of

DOCTOR OF PHILOSOPHY

in

BIOPHYSICS

in the

GRADUATE DIVISION

of the

UNIVERSITY OF CALIFORNIA at BERKELEY

* *

Oligodendroglial Response to Ionizing Radiation: Dose and Dose-Rate Response

by

Richard Philip Levy

Oligodendroglial Response to Ionizing Radiation: Dose and Dose-Rate Response

by

Richard Philip Levy

Abstract

An *in vitro* system using neuroglia from neonatal rat brain was developed to examine the morphologic, immunocytochemical and biochemical response of oligodendroglia to ionizing radiation. Following acute γ-irradiation at day-in-culture (DIC) 8, oligodendrocyte counts at DIC 14 were 55% to 65% of control values after 2 Gy, and 29% to 36% after 5 Gy. Counts increased to near-normal levels at DIC 21 in the 2 Gy group and to 75% of normal in the 5 Gy group. Myelin basic protein levels (MBP) at DIC 14 were 60% of control values after 2 Gy, and 40% after 5 Gy. At DIC 21, MBP after 2 Gy was 45% greater than that observed at DIC 14, but MBP, as a fraction of age-matched control values, dropped from 60% to 50%. Following 5 Gy, absolute MBP changed little between DIC 14 and DIC 21, but decreased from 40% to 25% of control cultures. It was concluded that oligodendrocytes in irradiated cultures had significantly lower functional capacity than did unirradiated controls.

The response to *split-dose irradiation* indicated that nearly all sublethal damage in the oligodendrocyte population (and its precursors) was repaired within 3 h to 4 h. At DIC 14, the group irradiated in a single fraction had significantly lower oligodendrocyte counts than any group given split doses; all irradiated cultures had marked depression of MBP synthesis, but no significant differences referable to time interval between doses. At DIC 21, cultures irradiated at intervals of 0 h to 2 h had similar oligodendrocyte counts to one another,

but these counts were significantly lower than in cultures irradiated at intervals of 4 h to 6 h; MBP levels remained depressed at DIC 21 for all irradiated cultures. The oligodendrocyte response to *dose rate* (0.03 to 1.97 Gy/min) was evaluated at DIC 14 and DIC 21. Exposure at 0.03 Gy/min suppressed oligodendrocyte counts at DIC 21 more than did higher dose rates in 5-Gy irradiated cultures.

A new compartmental cell model of radiation response *in vitro* of the oligodendrocyte population is proposed and examined in relation to the potential reaction to radiation injury in the brain. The experimental system developed should prove of value in correlating morphologic observations with tissue responses, investigating cellular repair mechanisms and evaluating radiation sensitizers and protectors.

DEDICATION

To Donna for her love, faith and patience,

and for being my best friend, sweetheart and teddybear

To James, Victoria and Geoffrey

for sharing their Dad with his work

To David and Jean Levy

for a lifetime of parental love and encouragement,

and for instilling in me self-confidence,

perseverance and respect for knowledge

TABLE OF CONTENTS

ACKNOWLEDGMENTS

I wish to express my deepest gratitude to Professor Jacob I. Fabrikant, my colleague, role model, mentor and good friend. His guidance and encouragement have been instrumental in shaping my academic and professional career.

I am very grateful to Professor Edward L. Alpen for his intellectual honesty, kindness and patience, and for sharing with me his extensive knowledge of biophysics and his gift for clear-headed thinking.

I thank Professors Paola S. Timiras and Alexander V. Nichols for their kind encouragement, and for their constructive criticisms during the writing of this dissertation.

I am grateful to Drs. Kenneth A. Frankel and Mark H. Phillips, my trusted confidantes and colleagues at the Donner Pavilion, for their unwavering friendship and their ready willingness to help me with irradiation experiments and computer problems. I have no doubt that we will remain lifelong friends and professional colleagues.

Dr. Adrian Rodriguez has my gratitude for his good humor and friendship, and for his collaboration in fluorescence-activated cell sorting experiments.

Ms. Celina M. Barba, and Messrs. Edward L. McDaniel, David R. Twede and J. Jason Wendel all worked tirelessly with me to develop and carry out the experiments reported in this thesis.

I thank Drs. Eng H. Lo and Neela B. Manley for their friendship, encouragement and advice. The three of us will always share the memories of having completed our doctoral dissertations at the Donner Pavilion.

I am indebted to Drs. Liane Bologa and Araceli Espinosa, and Ms. Ruth Cole from the Brain Research Institute at the UCLA School of Medicine for instructing me in methods of cell culture preparation and immunostaining.

Special thanks are due Mr. Anthony M. Linard for his creative help in obtaining funds for supplies and equipment, and Ms. Kathleen M. Sage and Ms. Dee A. Force for their assistance with countless details in the preparation of this dissertation.

This research was supported by the Director, Office of Energy, Health and Environmental Research of the United States Department of Energy under Contract DE-AC03-76SF00098.

CHAPTER 1
INTRODUCTION AND OUTLINE

1.1 INTRODUCTION

Brain tissue isolated and maintained *in vitro* represents a useful system for evaluation of biochemical and metabolic properties of the various brain cell populations and their interactions under relatively simple and controlled conditions. Some of the important structural and functional attributes of brain cells are well maintained in culture under controlled conditions. Oligodendroglia, for example, differentiate and mature *in vitro*, their morphologic properties correspond well to the *in vivo* situation, and they retain much of their biochemical specificity, including the synthesis of large quantities of myelin membrane. Brain tissue culture is therefore a potentially valuable tool for elucidating fundamental mechanisms of brain injury. The central scientific question addressed in this dissertation is how the oligodendrocyte population and the myelination process in mammalian brain respond to ionizing radiation.

The reaction of mammalian brain tissue to ionizing radiation ranges from minimal physiologic changes to fulminating necrosis, depending on a number of factors, including total dose, dose rate, fractionation, volume of irradiated tissue, and total lifetime dose [36]. Radiation injury of the brain has been classified into acute, early delayed and late delayed categories [35,105,118,119]. After doses in the range used in clinical radiotherapy in patients, acute injury is typically limited to the mitotically active subependymal plate; histologic changes can be detected within 24 h of irradiation [65]. Early delayed response is thought to result primarily from oligodendrocyte injury as manifested by focal demyelination; histopathologic changes can be detected in about 4 mon. Late delayed response

is manifested primarily by vascular degeneration, and may not be apparent for many months or years after irradiation. The observed differences in latency before the onset of manifestations of various categories of injury probably result, to a great extent, from differences in the kinetics of the various cell populations within the brain [35,105,118,119].

Cell culture techniques have been used extensively to study radiation response in rapidly proliferating systems. Quantitative cell-survival curve analysis has been developed toward this end [3]. However, mammalian brain tissue is highly structured with a complex cellular hierarchy, and exhibits only limited proliferative potential. Therefore, a satisfactory *in vitro* model for evaluation of brain irradiation can not rely solely on standard cell culture techniques. A primary objective of this dissertation has been the development of an appropriate experimental tissue-culture-based model for brain irradiation, and particularly for examining the metabolic bases of early delayed radiation injury.

1.2 DISSERTATION OUTLINE

In the first section of Chapter 2, an overview of oligodendrocyte biochemistry, immunocytochemistry, function and pathology is presented as background material. The gross anatomy of the brain and the relationship of the oligodendroglial cells to the other brain cell populations are described briefly. The remaining sections of Chapter 2 are devoted to an introductory survey of brain tissue culture techniques and to a brief description of fundamental principles of cellular neuroradiobiology.

The materials and methods used throughout the dissertation research are described in Chapter 3. In the first section, the preparation of primary mixed glial cell cultures and of oligodendrocyte-enriched secondary cultures is discussed. The preparation of rat glioma cultures is also described briefly, since these cells

were used to evaluate the feasibility of quantifying tritium-labeled thymidine incorporation via fluorescence-activated cell sorting techniques. The second section describes culture evaluation using phase contrast microscopy and indirect immunofluorescent staining methods for both morphologic evaluation and automated cell sorting. The remaining sections detail methods of biochemical analysis and culture irradiation techniques.

In Chapter 4, the morphologic, immunocytochemical and biochemical findings in unirradiated control glial cell cultures are investigated. Primary and secondary cultures are examined qualitatively and quantitatively as a function of culture age and initial plating density. Quantitative endpoints examined include oligodendrocyte counts, incorporation of tritiated galactose and tritiated thymidine, and production of myelin basic protein and total cellular protein. In Chapter 5, these morphologic and biochemical parameters are examined in cultures irradiated with x-rays and ^{60}Co γ-rays. The variables of radiation dose, dose-rate and timing of split-dose irradiation are evaluated as a function of time following irradiation. The morphologic and biochemical parameters examined were generally found to be dependent on dose and culture age, but not to variations in dose-rate in the ranges studied. The response to split-dose irradiation varied as a function of the interval between doses.

The experimental findings of the dissertation research are discussed in Chapter 6. A compartmental *in vitro* model of glial cell proliferation and maturation and stem cell response is proposed to explain the experimental results. This *in vitro* irradiation model is discussed in relation to previously described *in vivo* models. Future research directions are suggested. In Chapter 7, the conclusions of the dissertation are summarized.

CHAPTER 2
BACKGROUND

2.1 INTRODUCTION

The research described in this dissertation draws upon a broad spectrum of topics in neuroscience, including selected areas in neurobiology, neurochemistry and neuroradiobiology. In this chapter, an introductory overview of relevant background material is presented to familiarize the reader with fundamental aspects of these relevant topics. Accordingly, Section 2.2 is devoted to the function of the oligodendrocyte and its relationship to other brain cell populations; the gross anatomy of the brain is described briefly. The biochemistry, immunocytochemistry and pathology of the oligodendrocyte are summarized. In Section 2.3, the techniques of brain tissue culture are discussed. The final section of this chapter discusses fundamental principles of neuroradiobiology and their relationship to radiation injury of the brain.

2.2 OLIGODENDROGLIA

2.2.1 Oligodendrocyte Biology and Function

Gross Anatomy of the Brain

The mammalian brain grossly consists of three basic divisions, the large paired cerebral hemispheres, the brain stem, and the cerebellum (Figure 2.1). The cerebral hemispheres, situated atop the brain stem and cerebellum, are derived embryologically from the telencephalon, the most rostral cerebral vesicle [16]. The hemispheres consist of a highly convoluted gray cortex rich in neurons, an extensive underlying white matter comprised of several types of connecting fibers, and a series of deeply situated neuron collections termed basal nuclei.

The investigations described subsequently in this thesis have been limited to the evaluation of the cerebral cortex component of the brain.

The brain stem consists of the diencephalon, mesencephalon (midbrain), metencephalon (pons) and myelencephalon (medulla) (Figure 2.1) [80]. The diencephalon, the most rostral portion of the brain stem, is almost completely surrounded by hemispheric structures. The myelencephalon, the most caudal portion of the brain stem, tapers gradually into the spinal cord. The cerebellum is an embryologic derivative of the metencephalon [16]. It overlies the the dorsal caudal aspect of the brain stem and extends laterally under the hemispheres to fill most of the posteria fossa of the skull. The ventricular system is a continuum of cavities within the brain, filled with circulating cerebrospinal fluid (CSF). The ependymal-cell lined lateral ventricles are arch-shaped cavities within the cerebral hemispheres (Figure 2.2). The lateral ventricles communicate caudally with the slit-shaped midline "third" ventricle, which in turn communicates with the "fourth" ventricle. From this site, the CSF circulates in the subarachnoid spaces surrounding both the brain and the spinal cord. A detailed discussion of the gross anatomy of the brain is available in reference [80].

Histologic Features of Brain Cells

The brain is a highly complex organ, with a marked hetereogeneity of cell type. Brain tissue of the cerebral cortex is composed primarily of three types of distinct and highly characteristic cells - neurons, astrocytes, and oligodendrocytes - with long elaborate processes which intertwine with one another to form a highly integrated tissue (Figure 2.3). The *neuron* has the primary function of information processing and integration in the brain. The glial cells (astrocytes and oligodendrocytes) help to control the functional environment of the neurons, and they play an essential role in many neuronal functions. Also present in the

Figure 2.1

The major subdivisions of the human brain as viewed in sagittal section. (From Noback CR and Demarest RJ (eds): *The Human Nervous System. Basic Principles of Neurobiology, 3rd ed.* McGraw-Hill, New York, 1981, pg. 2; with permission.)

Figure 2.2

Lateral view of the ventricles of the human brain. (From Noback CR and Demarest RJ (eds): *The Human Nervous System. Basic Principles of Neurobiology, 3rd ed.* McGraw-Hill, New York, 1981, pg. 21; with permission.)

Figure 2.3

Relation of the neuron, astrocyte, oligodendrocyte and nerve terminals in the mammalian nervous system. The axosomatic synapse, axodendritic synapse and axoaxonic synapse in the central nervous system have thickened subsynaptic membranes. Astrocytes are glial cells with thin processes extending either to the walls of the capillaries as perivascular feet or to neurons. The perineuronal oligodendrocytes are glial cells with thick, stubby processes. (From Noback CR and Demarest RJ (eds): *The Human Nervous System. Basic Principles of Neurobiology, 3rd ed.* McGraw-Hill, New York, 1981, pg. 63; with permission.)

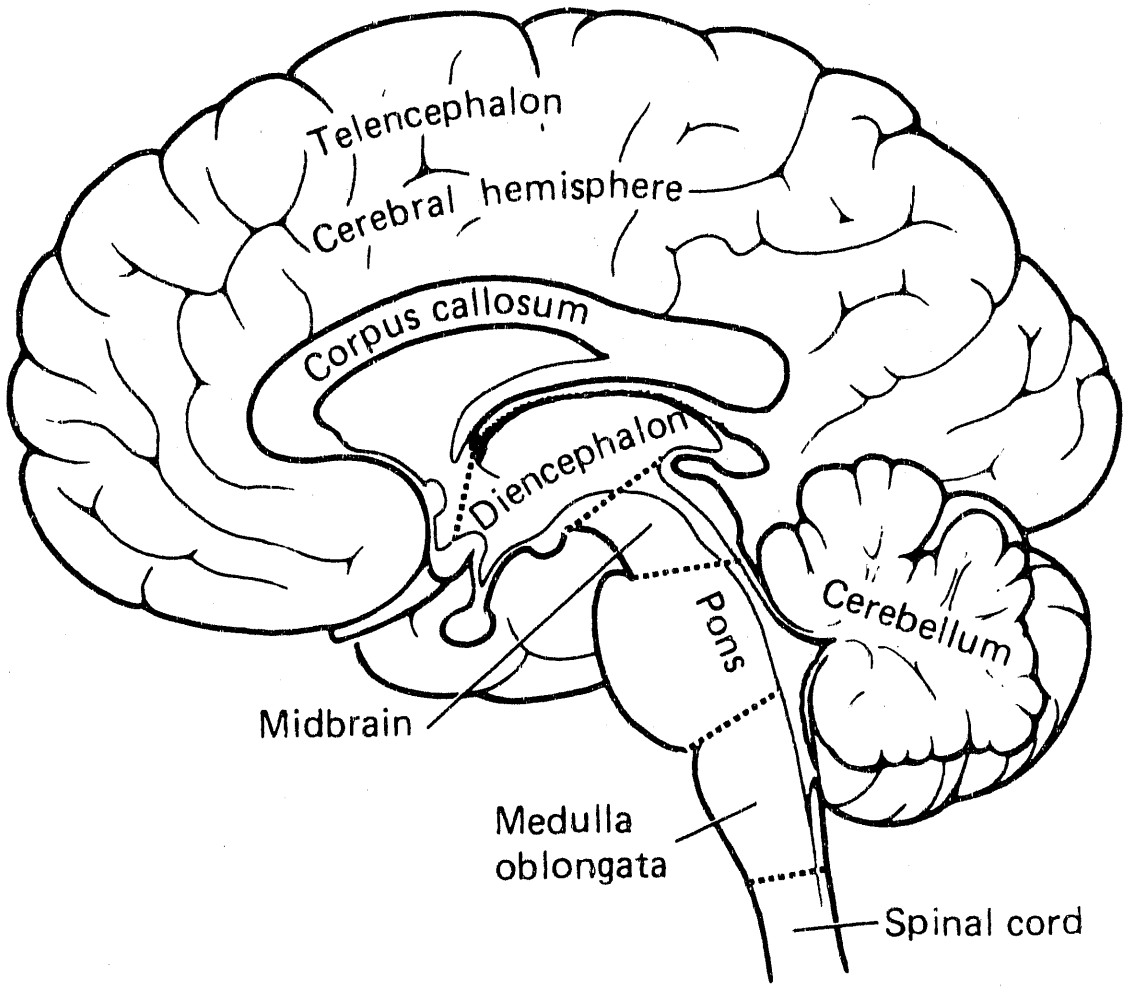
Telencephalon
Cerebral hemisphere
Corpus callosum
Diencephalon
Pons
Cerebellum
Midbrain
Medulla oblongata
Spinal cord
ZBL 910-8007

Figure 2.1

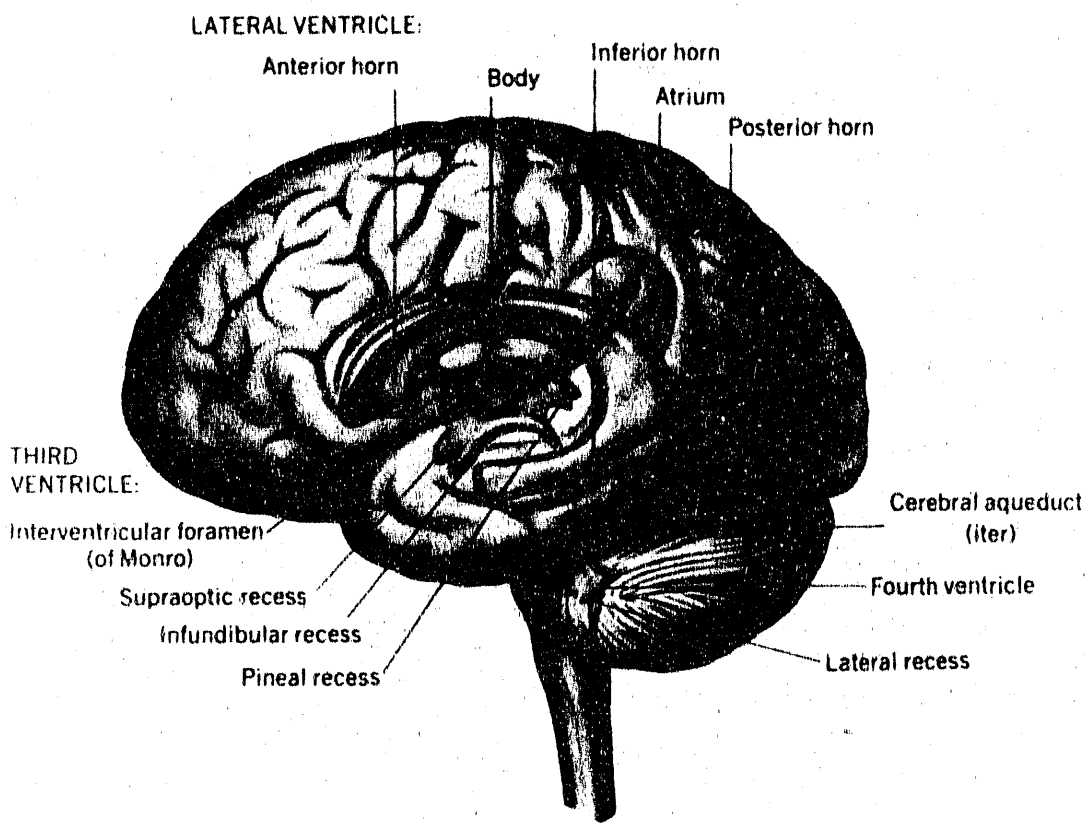
LATERAL VENTRICLE:
Anterior horn
Body
Inferior horn
Atrium
Posterior horn
THIRD VENTRICLE:
Interventricular foramen (of Monro)
Supraoptic recess
Infundibular recess
Pineal recess
Cerebral aqueduct (iter)
Fourth ventricle
Lateral recess
ZBB 910-8009

Figure 2.2

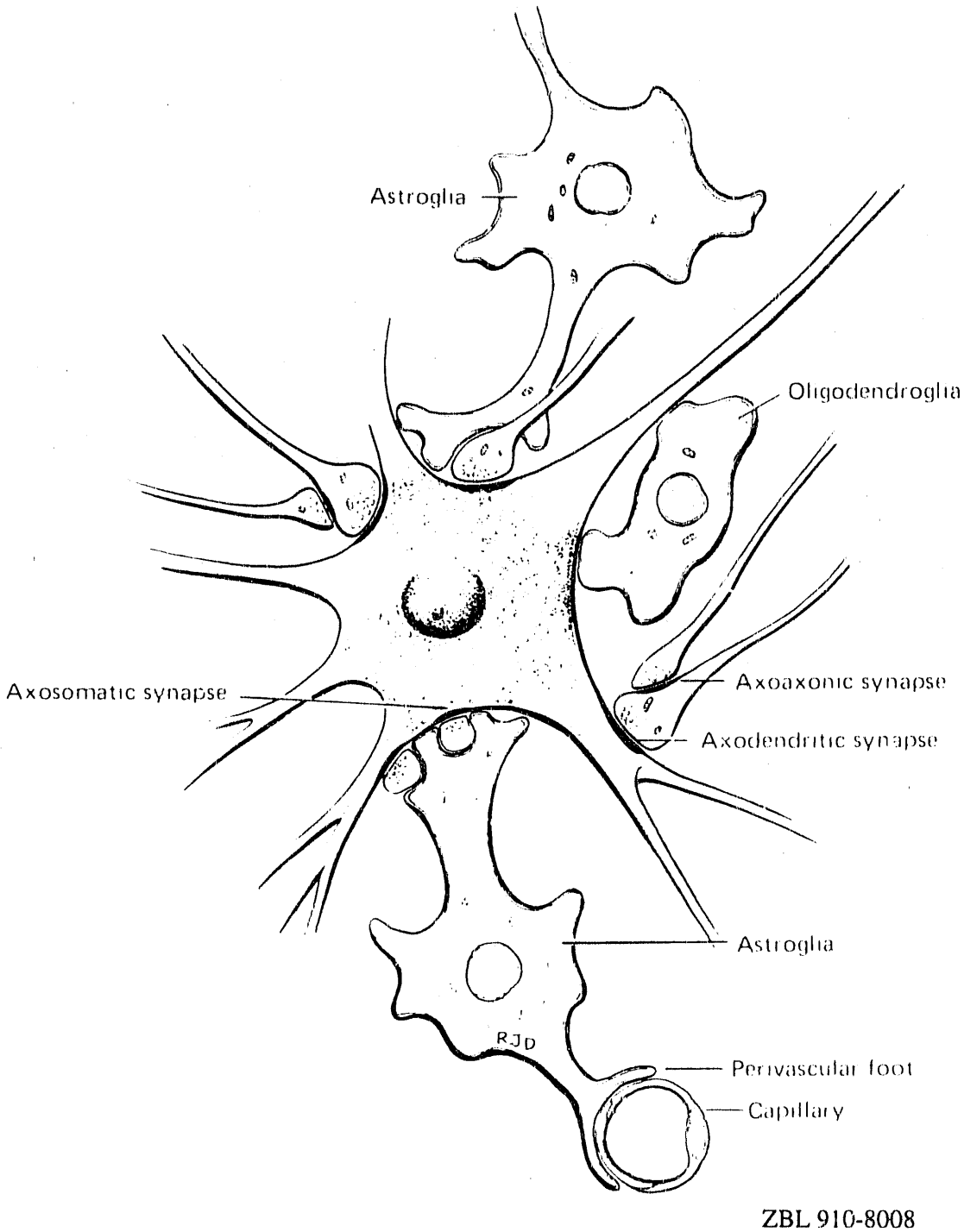
Astroglia
Oligodendroglia
Axosomatic synapse
Axoaxonic synapse
Axodendritic synapse
Astroglia
RJD
Perivascular foot
Capillary
ZBL 910-8008

Figure 2.3

brain are so-called microglia, small cells of mesodermal origin which migrate to sites of injury or degeneration, and transform into large cells that remove and phagocytize cellular debris.

Astrocytes have multiple ramifying processes radiating out in all directions from the cell soma, giving the cell a star-shaped appearance. These cells provide structural support for other parenchymal cells, and they engage in proliferation and repair after brain injury. Astrocytes serve also to isolate and group nerve fibers and terminals, and help to modulate certain metabolic functions in neurons and their synapses [86].

Oligodendrocytes have distinctly fewer and thinner branches than astrocytes; they contain fewer intracellular neurofilaments and glycogen granules than astrocytes, but they have numerous microtubules [86]. The oligodendrocyte's primary function is the production and long-term maintenance of the myelin cell membrane. During development the relatively small cell soma elaborates several times its mass in myelin membrane daily [82]. The oligodendrocyte forms narrow, progressively elongating membrane processes, each of which expands distally into an extensive flattened sheet of myelin membrane (Figure 2.4). This sheet wraps itself around a defined segment of a nearby neuronal axon, forming many layers in a concentrically spiralling fashion. Subsequently, most of the cytoplasm within the flattened sheet is extruded and the adjacent membrane surfaces come into close apposition (or possibly fusion), resulting in compact mature myelin (Figure 2.5). The myelin ensheathment is longitudinally interrupted every 1 to 2 mm by a constriction, i.e., the node of Ranvier. The myelination of each axonal segment appears to be the result of wrapping by a single flattened membrane sheet; this myelinated segment is termed an internode. Each oligodendrocyte is capable of myelinating several internodes on the same or different nearby axons; by contrast, the analogous cell in the peripheral nervous system (the Schwann

Figure 2.4

The oligodendrocyte is shown in relation to the segments of the myelin membrane. **A**, the configuration of the oligodendrocyte soma as reconstructed from serial sections. **B**, the oligodendrocyte in continuity with many segments of the myelin sheath in the usual spiraled and compacted configuration. **C**, the myelin segments in an unrolled configuration. The cytoplasmic extensions of the oligodendrocyte related to myelin have certain similarities to the axonal extensions of neurons. (From Schmitt FO (ed): *The Neurosciences, Second Study Program.* Rockefeller University Press, New York, 1970, pg. 789; with permission.)

Figure 2.5

Relation of oligodendroglia to the axons of the central nervous system, as reconstructed from electron micrographs. The three unmyelinated axons on the left are naked. The two myelinated axons on the right share one oligodendroglial cell. The myelin sheaths of each of the myelinated fibers are continuous through the cytoplasmic *tongue* with the glial cell body. This *tongue* spreads out as a ridge, which extends throughout the entire length of an internode. (From Noback CR and Demarest RJ (eds): *The Human Nervous System. Basic Principles of Neurobiology, 3rd ed.* McGraw-Hill, New York, 1981, pg. 73; with permission.)

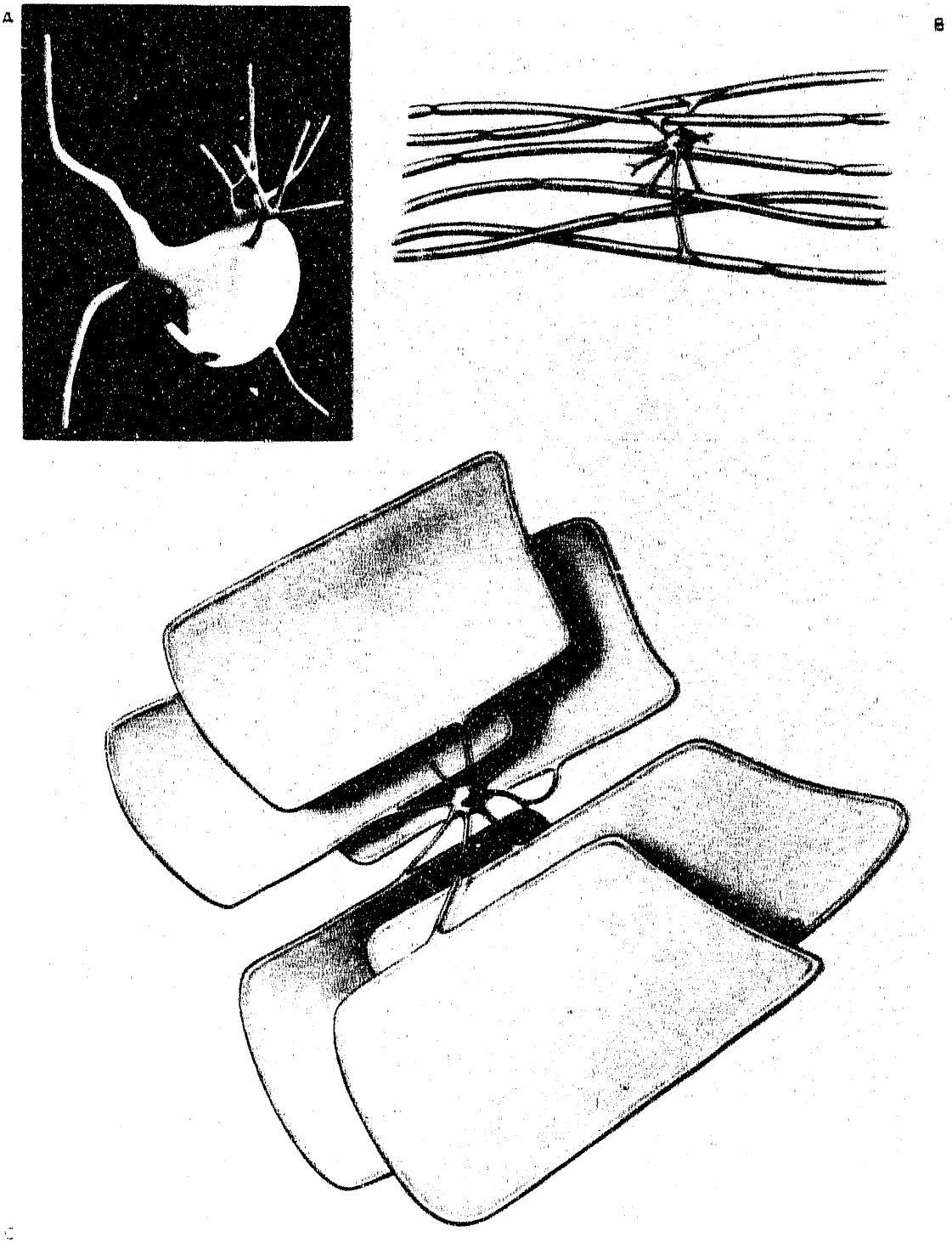

ZBB 910-8006

Figure 2.4

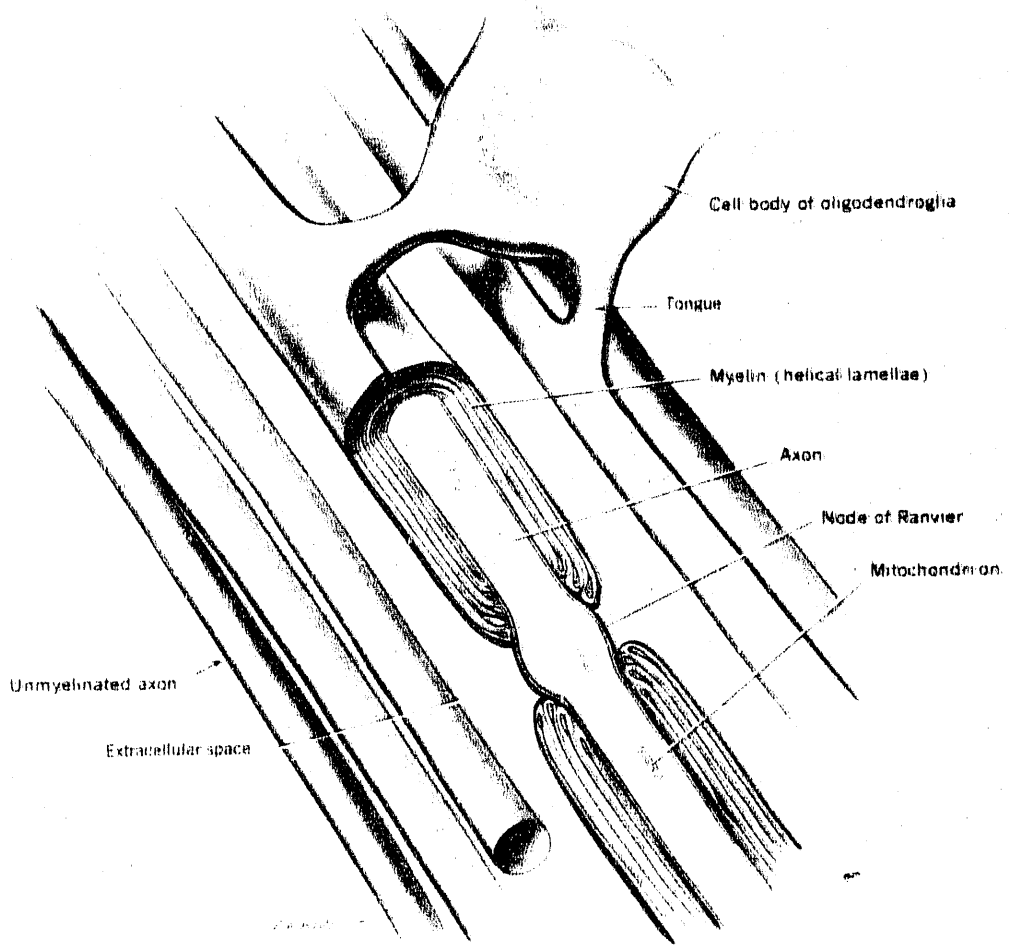

ZBB 910-8010

Figure 2.5

cell) is responsible only for myelination of a single internode [111].

Functional Importance of Oligodendroglia

Myelin ensheathment of axons permits saltatory conduction, a more rapid and energy-efficient means of nerve impulse conduction than would otherwise be possible. Facilitation of impulse conduction is the most crucial role of the oligodendroglia. The mechanism of saltatory conduction is therefore detailed here. Significant injury to the oligodendroglial population, including radiation injury, can compromise impulse conduction and have profoundly deleterious effect on brain function.

According to linear cable theory, passive conduction velocity of an axon can be described by:

$$\theta = \left(\sqrt{\frac{2R_m a}{R_i}}\right)\left(\frac{1}{R_m C_m}\right), \tag{2.1}$$

where θ is the conduction velocity; R_m and C_m are the specific resistance and conductivity of the axon membrane, respectively; R_i is the resistivity of the axon; and a is the radius of the axon [43,109]. When n layers of myelin membrane are wrapped about an unmyelinated axon, R_m increases by a factor roughly equal to n, and C_m decreases by a factor of n, such that the product $R_m C_m$ is constant, assuming myelin has the same electrical properties as the axonal membrane. Since R_i is an intrinsic property of the axoplasm and essentially constant, the net result of myelination of an axon of a given radius is an increase in the passive conduction velocity by a factor of $\sqrt{n}$.

Once an action potential is produced at the proximal end of an axon, the voltage decays exponentially as it propagates distally. The distance within which the voltage decays to $1/e$ of its initial voltage, i.e., the length constant (λ), can be described by:

$$\lambda = \sqrt{\frac{aR_m}{2R_i}}. \tag{2.2}$$

For axons of the size found in the human brain, λ is generally less than 1 mm; thus, signals will travel only very short distances with passive voltage propagation. Active propagation is therefore necessary to maintain sufficient signal strength over greater distances. Propagation of the action potential down the entire length of the axon will maintain satisfactory signal intensity, but it does not increase conduction velocity. Additionally, each action potential increases axoplasmic sodium concentration by about 1.5 μmole, resulting in undesirable ionic equilibrium status after about 500 action potentials. Constant replenishment of the normal ionic potentials would create an excessive metabolic strain. Segmental myelination provides a unique solution to this problem. The insulating effects of the myelinated portions of the axon permit almost no flow of ionic current across the membrane. At the unmyelinated nodes of Ranvier, the presence of a very high local density of sodium channels exposes the central axon to the extracellular ionic milieu. This enables the generation of a new action potential across a very small piece of membrane, resulting in markedly greater energy-efficiency of signal transmission. Thus, segmental myelination permits a succession of action potentials (typically, 2 mm apart), which overcomes the constraint of the length constant in an energy-efficient manner [43,109].

Proliferative Capacity of Oligodendroglia

The proliferative capacity of mature oligodendroglial cells and their ability to mitigate injury are highly important in many brain disorders. For many years it was believed that these cells had no proliferative potential at all. For example, 1-wk-old dissociated brain tissue cultures from neonatal rats were found to have 2 to 5% oligodendrocytes by staining with antibody to galactocerebroside (anti-

GC); the absolute number changed little during 8 wk in culture, suggesting very limited mitotic activity in the oligodendrocyte population in these cultures [75].

The concept that mature oligodendrocytes could proliferate in certain pathologic conditions has only recently gained acceptance [38,60,66,67]. Remyelinating oligodendrocytes take up tritiated thymidine following demyelination by JHM hepatitis virus [38]. In pulse-labeling studies following demyelination mediated by biscyclohexanone oxaldihydrozone (Cuprizone), oligodendrocytes are capable of proliferation and of remyelination of nearby axons. Immature cells seen during the initial glial response to demyelination continue to divide and to mature into myelin-synthesizing forms [61], mimicking the process observed in the developing animal [76]. Oligodendrocyte proliferation appears to slow markedly once synthetic capacity sufficient for remyelination has been achieved [61].

Ludwin [60] demonstrated *in vivo* proliferation of immunohistochemically identified mature oligodendrocytes in adult mice in response to surgical trauma. Oligodendrocyte proliferation, as evidenced by thymidine incorporation, has not been observed in cells engaged in active myelination. However, mature-appearing oligodendrocytes without myelin processes are capable of thymidine incorporation [66]. Therefore, it has been proposed that mature oligodendrocytes must lose their connection to myelin sheaths prior to the acquisition of proliferative potential.

Demyelinating Disease

The oligodendrocyte normally maintains long-term support of its processes; oligodendrocyte death from any cause results in subsequent demyelination, i.e., deterioration of the associated myelin sheaths. This has been observed in a variety of pathologic conditions, experimentally and clinically, in-

cluding progressive multifocal leukoencephalopathy, JHM mouse hepatitis virus encephalomyelitis, and following Cuprizone or ethidium bromide ingestion [59]. In these conditions, progressive myelin breakdown occurs sequentially after morphologically demonstrable oligodendrocyte pathology. Under certain conditions of low-level Cuprizone toxicity the cytoplasm most distal to the perikaryon is the first portion of the oligodendrocyte to degenerate, well before pathologic changes occur in the rest of the cell. Over time the more proximal cytoplasm and perikaryon begin to degenerate. This retrograde deterioration probably results from an inability of the damaged oligodendrocyte to maintain its most distal processes, thereby mimicking conditions where direct damage to the myelin sheath is the mechanism of injury [62]. This suggests that oligodendrocyte injury may be responsible for demyelination in other conditions of uncertain etiology, even when the perikaryon appears to be normal early in the disease process.

Experimental allergic encephalomyelitis, idiopathic polyneuritis (Guillain-Barré syndrome), acute allergic neuritis and canine distemper virus are immune-mediated conditions involving direct injury to the myelin sheath. In other demyelinating diseases, damage to both the oligodendrocyte and myelin sheath is believed to occur in combination, or the precise mechanism is unknown. Multiple sclerosis, the human prototype for demyelinating disease, is of uncertain pathogenesis. A more detailed discussion of the pathology of demyelinating disease is found in reference [59].

2.2.2 Biochemistry of Myelin

Myelin constitutes the bulk of the oligodendrocyte, except during the early stages of the developing nervous system. It is generally assumed that myelin formation directly reflects oligodendrocyte activity. Although the oligodendrocyte perikaryon and the myelin sheath are connected in the developing brain, such

connection has not been demonstrated histologically in mature animals [12,94]. However, myelin maintenance requires extensive biochemical and metabolic support, and persistence of a direct cytoplasmic connection to the oligodendrocyte perikaryon is presumed. A brief overview of the biochemical properties of myelin is required as background for understanding the rationale for selecting some of the analytical methods used in this investigation.

Lipid Biochemistry

Lipid components of myelin are synthesized within the perikaryon and combined there with myelin proteins for transport to the myelin membrane. Compacted mature myelin has a high degree of paracrystalline order, making it one of the few membrane systems amenable to *in situ* polarized light and X-ray diffraction analysis [82]. Oligodendrocytes produce daily more than three times their cell body weight in myelin during the period of peak synthesis. In rats and humans, myelin accounts for 25 and 35% of the dry weight of brain, respectively. The high lipid to protein ratio of myelin is its dominant biochemical feature (Table 2.1). Myelin accounts for 40% of total brain lipids in rats, and over 50% of total brain lipids in humans [82].

TABLE 2.1

Composition of Mature Central Nervous System Myelin[a]

Components	Human	Bovine	Rat
		(% of dry weight)	
Protein	30.0	24.7	29.5
Lipid	70.0	75.3	70.5
		(% of lipid weight)	
Cholesterol	27.7	28.1	27.3
Total galactolipid	27.5	29.3	31.5
cerebroside	22.7	24.0	23.7
sulfatide	3.8	3.6	7.1
Total phospholipid	43.1	43.0	44.0
ethanolamine PG[b]	15.6	17.4	16.7
choline	11.2	10.9	11.3
sphingomyelin	7.9	7.1	3.2
serine PG	4.8	6.5	7.0
inositol PG	0.6	0.8	1.2

[a]Adapted from reference [82]
[b]PG = phosphoglyceride

Human central nervous system (CNS) myelin lipid consists of approximately 28% galactolipid, 28% cholesterol, 43% phospholipid, and small amounts of other lipids; the lipid composition of myelin from other mammalian species is quite similar [81]. Galactocerebroside constitutes about 80% of the galactolipid component; sulfatide (galactocerebroside-3-sulfate) comprises the remainder. Although not exclusively limited to myelin, galactocerebroside is greatly enriched in this membrane, and in fact a highly specific marker for the oligodendrocyte [93]. In addition to the major lipid classes described above, myelin contains small amounts of di- and triphosphoinositide, a series of fatty acid esters of galactocerebroside, several galactosyldiglyceride derivatives, and a series of gangliosides [81].

Protein Biochemistry

The protein composition of CNS myelin is notable for its simplicity; sodium dodecyl sulfate polyacrylamide gel electrophoresis has revealed that the CNS myelin proteins of most species separate into only six prominent bands [82]. Proteolipid protein (PLP) and myelin basic protein (MBP) together comprise 60 to 80% of total myelin protein; the other protein bands include the so-called Wolfgram proteins and myelin-associated glycoproteins. Additionally, numerous enzymatic activities intrinsic to CNS myelin suggest that this membrane is active in metabolism and transport functions [81]. Myelin had previously been assumed to act almost exclusively as a passive insulator to facilitate saltatory axonal conduction, but more recent studies have suggested that myelin may also play some role in cell-to-cell recognition [22] and regulation of the periaxonal ionic milieu [96].

Myelin basic protein comprises about 30% of the myelin proteins of the CNS and is unique to the myelin membrane [112]. During development of rat CNS myelin, radioimmunoassay measurements of initial MBP precede and correlate well with the morphologic detection of compact myelin *in vivo* [23]. Comparison can be made between the synthesis of myelin and the levels of MBP found in rat cerebrum at different developmental stages [8]. At 15 d, postnatally, MBP reaches 30% of adult levels, while myelin is detected at only 10% of adult levels. By 30 d postnatally, the values are in closer agreement, with MBP and myelin at 61% and 53% of adult levels, respectively. Much of the difference at 15 d may be due to the presence of a greater proportion of MBP in the oligodendrocyte soma relative to the myelin sheath at this early stage, as suggested by immunocytochemical studies [112].

Proteolipid protein has a molecular weight of 25,000 and accounts for about 50% of total CNS myelin protein [1]. PLP has unusual physical properties, remaining soluble in chloroform even after nearly all of its bound lipids have been removed. It is very hydrophobic; two-thirds of its amino acids are nonpolar [81]. Total brain PLP levels increase dramatically during the period of myelination, with a six- to ten-fold increase in several brain regions observed to occur in the rat from 10 to 33 d postnatally [14]. Cohen et al [23] have found a two-fold increase in PLP per gram of rat cerebral cortex to occur from 15 to 33 d postnatally, similar to the two-fold increase in MBP observed during this same period. Compared to synthesis of MBP in the rat, PLP synthesis begins somewhat later and does not reach its maximal rate until 22 d postnatally, 4 d later than the peak for MBP [15].

The third major class of myelin proteins is the Wolfgram proteins, including the enzyme 2′,3′-cyclic nucleotide 3′-phosphohydrolase (CNP). Unlike MBP and PLP, CNP can be detected in the rat brain at birth. Total CNP activity increases between 4 and 120 d, with the greatest rate of increase at 2 to 3 wk after birth [107]. A close correlation between CNP and MBP levels was observed between 10 and 60 d. The myelin-associated glycoproteins comprise the last major class of myelin proteins [8]. Like CNP, the most prominent of these glycoproteins (designated MAG) reaches its adult level at an earlier age than MBP.

2.2.3 Immunocytochemistry of Glial Cells

Galactocerebroside, the major myelin glycolipid, was first shown by Raff et al [93] to be a specific immunocytochemical cell-surface marker for oligodendrocytes in culture of the rat optic nerve. More extensive examinations have confirmed the exclusive localization of GC in oligodendroglial soma and processes. The utility of GC as a marker for oligodendrocytes has been demonstrated in

bovine, ovine, feline and rodent species [110].

Antisera to MBP specifically react with myelin and and some oligodendrocytes during the early phase of active myelination. Immunocytochemical studies in dissociated mouse brain cell cultures have demonstrated that GC appears early in the membrane of oligodendrocytes and that cytoplasmic MBP appears later in cells that presumably represent a more differentiated oligodendrocyte population [75].

Glial fibrillary acidic protein (GFAP) is a highly specific immunocytochemical intracellular marker for astrocytes [77]. (GFAP is mentioned here, because of its utility for labeling astrocytes, the primary non-oligodendrocyte population found in the mixed glial cell cultures used extensively in this thesis research.)

A host of other oligodendrocyte-specific antisera have also been studied. Antigens examined include PLP, Wolfgram proteins, CNP, MAG, sulfatide, and a variety of enzymes found exclusively or enriched in oligodendrocytes (e.g., cerebroside sulfotransferase, glycerol-3-phosphate dehydrogenase, and carbonic anhydrase). A more detailed discussion of glial-cell immunocytochemistry is found in reference [110].

2.3 TISSUE CULTURE SYSTEMS

Brain tissue culture investigations have both experimental advantages and disadvantages. In primary brain cell cultures, the normal cellular environment, and topographic and physiologic relationships of the tissue are considerably disrupted. Advantages include control of the physical and chemical environment; isolation from the influences of remote tissues; capability for continuous observation of cells in the living state; and ease of study of biochemical pathways with radiolabeled compounds and other methods. These factors are of special impor-

tance in the study of brain tissue, because of the exceedingly complex structure of the intact brain and its various functionally and morphologically unique cell types.

Any tissue culture method must provide an environment similar to the *in vivo* milieu while permitting suitable experimental simplification and accessibility. Many brain tissue culture strategies have been employed, but several essential criteria are common to all methods:

1. sufficient surface to volume ratio to permit ready diffusion of nutrients and oxygen to all parts of the culture system;
2. suitable substrate for cell attachment;
3. satisfactory nutrient medium, in a balanced salt solution, appropriately buffered, and supplemented by individually determined growth factors and/or animal serum;
4. incubation at 37° C with physiologic pCO_2;
5. lack of toxicity in the culture milieu (e.g., pyrogens, heavy metals); and
6. strict sterile technique at all times.

Over the past 30 years, various methods have been developed to satisfy the above criteria [88]. Three different types of mixed brain cell cultures have been widely used, and are generally referred to as explant, dissociated-reaggregated, and dissociated-attached cultures. In the explant method, a small piece of brain tissue, generally about 0.5 to 1 mm^3, is excised and immobilized on a substrate-coated coverslip, and maintained in nutrient medium with serum and appropriate extracts [64,104]. The fragment size is chosen to be small enough to allow adequate exchanges with the environment, but large enough to maintain organotypic

architecture as much as possible. Within the explant, normal histiocytic relationships are often retained, as are many fiber tracts, and new functional synapses are formed. As many as 75% of neurons are lost soon after explantation, but the surviving cells are fairly stable for some weeks. Peripheral to the primary explant zone, the so-called outgrowth zone initially consists mainly of neurites originating in the explant, and migrating glial cells, connective tissue cells and neurons. After several weeks in culture, the neuritic component of the outgrowth zone degenerates, and glial cell outgrowth expands into a monolayer around the explant. Generally, myelin forms abundantly in the explant and only sparingly in the outgrowth zone.

Dissociation of cells involves a different technical approach. In this technique, a mixed cell population is obtained from dissociation of fetal or neonatal rat brain and placed into culture flasks and dishes with suitable substrate and nutrient medium [69]. Rather than attempting to preserve some histiocytic organization, brain tissue is dissociated by chemical and/or physical means immediately after removal from the intact animal. The cells are then cultured in suspension or plated on plastic or substrate-coated glass surfaces. This type of system is ideal for studying purely cellular aspects and for assessing the importance of tissue-structure integrity in cellular function, morphology, and differentiation.

In dissociated-reaggregated cultures, immature brain tissue (generally, of embryonic origin) is first dissociated to a single-cell suspension by either enzymatic or mechanical means. The cells are then placed in a small flask that is rotated continuously so as to form a gentle vortex, encouraging cellular interactions and aggregation. After a period of reaggregation and recovery, the cells typically sort themselves into complex histiocytic patterns reflective of the stage of brain development at the time of dissociation [88]. Reaggregating fetal and neonatal mouse and rat brain cultures have been demonstrated ultrastructurally

and biochemically to form myelin-like membrane after about 3 wk in culture, associated with a significant degree of neuronal and glial differentiation.

In dissociated-attached cultures, tissue is dissociated into single-cell suspensions and subsequently attaches to a solid substrate (e.g., flask surface or coated glass cover slip) in a quasi-two-dimensional arrangement. The resulting mixed cell culture is readily accessible to immunochemical evaluation. Raff et al [93] found that 5% of cells in dissociated optic nerve cultures from 6 to 8-d-old rats bound anti-GC at day in culture (DIC) 5; these cells had multiple ramifying processes and were morphologically considered to be oligodendrocytes. In the method developed by McCarthy and de Vellis [69], a confluent layer of flat astrocytes, endothelial cells and connective-tissue cells forms over the entire culture dish surface during the first 7 to 10 DIC. On top of this bottom layer, oligodendrocytes form interconnecting networks that adhere loosely to the underlying cells. The oligodendrocytes adhere less firmly than do astrocytes to the plastic culture flask surface. These properties of cellular stratification and differential adhesion in the primary culture can be used to separate oligodendrocytes from the other cells by gentle agitation of the culture dish. The degree of neuronal survival is quite variable, but appears to depend largely on the age and source of the tissue.

The tissue culture systems described above all consist of a mixture of cells, the proportions of which are determined by the experimental conditions. However, substantial effort has been applied to the development of isolated cultures of different cell types, in order to examine specific morphologic and biochemical parameters with greater precision. A variety of methods have been developed for isolation of relatively purified oligodendrocyte cultures. These include bulk isolation techniques involving dissection of white matter [55,83,90], serologically assisted isolation procedures [32,33], and isolation based on differential surface-

adherence in response to mechanical agitation [69]. Highly purified (90 to 95%) oligodendrocyte cultures have been produced with each of these techniques, and these cultures have been determined to satisfy established morphologic, ultrastructural, immunochemical, and biochemical criteria for differentiated oligodendrocyte function [88].

2.4 RADIATION INJURY OF THE BRAIN

Radiation damage of the brain has been categorized into acute, early delayed, and late delayed injury. The temporal patterns of latency prior to onset of each type of injury result to a great extent from differences in the kinetics of the various cell populations and the metabolic reaction to injury of the different cell types within the brain [35,105,118]. In radiation studies with fresh extracts of rodent brain cells that examined selected biochemical endpoints such as unscheduled deoxyribonucleic acid (DNA) synthesis [47,48], and DNA strand unwinding [18,98], populations of neuronal, glial and cerebral endothelial cells demonstrate differing responses to irradiation. In general, oligodendrocytes are the cells most sensitive to radiation injury, followed by the cerebral endothelial cells [98]. The neuronal population is relatively radioresistant, except for the granule cells of the cerebellum, which have proliferative potential even in the adult brain [47,48].

2.4.1 Acute Effects

After doses in the range used in therapeutic radiotherapy (i.e., tens of gray), acute reaction is typically asymptomatic and limited to the subependymal plate just beneath the ventricular ependymal lining. The subependymal plate is the only mitotically active region in the normal adult mammalian brain [118]. Hopewell and Cavanaugh [41] evaluated mitotic activity in rats at intervals after x-irradiation of 2 to 40 Gy. One day following irradiation, the number of

mitoses was markedly reduced for all dose levels, with a rise in mitotic activity noted at 7 d, and another reduction at 14 d. Mitotic counts reached control levels by 3 mon after doses $\leq$ 20 Gy. However, after 40 Gy no mitotic recovery occurred. Six months after irradiation mitotic counts were nearly zero and the subependymal cell population was nearly depleted. Small dark-staining cells, that may represent subependymal plate stem cells, were observed to disappear rapidly after irradiation, while light-staining cells, that may represent slowly proliferating glial precursors, declined more slowly [20,42]. The relationship of these acute effects to delayed permanent radiation damage is incompletely understood. Autoradiographic studies in rodents have demonstrated that the subependymal plate acts as a reservoir for glial cell production for up to 6 mon of age [40]. Korr et al [49] found that subependymal cell replacement proliferation was exponential in character, but that there was extensive cell loss from ineffective proliferation, resulting in cell death, and cell emigration. The cell birth rate and cell loss rate were balanced, thereby maintaining a steady state of cell renewal in the subependymal population. The permanent loss of this population of glial stem cells was thought to be at least partly responsible for the later development of white matter dysfunction [39].

Manley [65] used tritiated thymidine incorporation to evaluate the proliferative activity of the subependymal plate cell in 4-wk-old mouse brain before and 48 h to 1 wk following charged-particle irradiation. The subependymal cell labeling index in the unirradiated animals varied from 10% at the level of the olfactory lobe to 26% at the level of the corpus callosum. The subependymal layer in unirradiated animals was shown to have a growth fraction of about 0.22 and a cell-cycle duration of about 37 h to 39 h. Subependymal cells were considered to be a mixed population, as characterized by cell and tissue kinetics; cells were believed to be at various stages of proliferation, migration and differenti-

ation [49]. Following hemibrain irradiation with helium (10 Gy and 25 Gy) or neon (10 Gy) ions, the subependymal layers in the irradiated and unirradiated cortices of the same mouse showed comparable perturbations in cell and tissue kinetics within 48 h to 1 wk, although histologic changes were limited only to the irradiated cortex. A decrease in labeling index was observed in both cortices of the irradiated animals and was demonstarted to be dose- and ion-dependent. A marked decrease in the growth fraction of both the irradiated (to 0.08) and unirradiated (to 0.09) subependymal layers was observed in irradiated animals 48 h following exposure to 45 Gy helium ions.

2.4.2 Delayed Effects

The complex pathology of delayed radiation injury in the mammalian brain has been described in detail [13,29,119,120]. However, the underlying cellular mechanisms of delayed injury are still poorly understood. The oligodendrocytes and the cerebral endothelial cells appear to be the most likely target cells involved in the development of injury [29,39,78,105,118,119,120]. Early delayed radiation injury is thought to be mediated primarily by damage to the oligodendrocyte population; late delayed injury is believed to result primarily from damage to the endothelial cell population.

Early delayed radiation injury may be detected histologically from 4 mon to a few years after brain irradiation, after a latent period inversely related to dose [39,119]. The lesions consist primarily of foci of demyelination in the white matter, and these foci may progress to necrosis. It is believed that white matter necrosis results primarily from loss of oligodendrocytes, and that the slow turnover rate of these cells accounts for the delayed onset of these effects. Those glial cells in the white matter of the hippocampus and corpus callosum have the highest thymidine labeling index [49]; radiation necrosis following irradiation

with doses of 20 to 40 Gy occurs most readily in these same regions [39]. In contrast, the cerebral cortex shows the lowest turnover of glial cells, and necrosis there is induced only by significantly higher doses (above 50 Gy).

Late delayed radiation injury may not be apparent for many months or years after irradiation. This category of brain injury appears to be mediated primarily by the cerebrovascular system [13,39,95,119]. Focal irradiation of the rat brain produced transient or permanent disruptions in local blood-brain-barrier permeability [44,63,97,124]. Severe vascular lesions were seen in the basilar artery of cats sacrificed 7 d to 220 d after focal ^{60}Co γ-irradiation with doses of 100 to 300 Gy [79]; pathologic findings increased with dose and time after irradiation. Vascular effects have been found invariably to precede the appearance of parenchymal necrosis in rats examined as long as 5 mon following focal proton-beam irradiation with doses of 100 to 200 Gy [50]. Decreased regional cerebral blood flow occurred 4 to 5 mon following 35 Gy focal x-irradiation of the occipital lobe in monkeys, prior to the onset of severe edema and increased intracranial pressure [114].

Early radiation-induced changes in small vessels include varying degrees of swelling, degeneration and necrosis of endothelial cells, and degeneration of the elastic and muscular layers. These changes were observed in goats 1 to 4 mon following brain irradiation with narrow beams of protons at doses of 200 to 400 Gy [53], and in cats following 100 to 200 Gy ^{60}Co γ-irradiation [79]. Early post-irradiation changes may be subtle and scattered. With progressive vascular damage, increasing areas of the small vessel bed undergo degenerative and fibrotic change. Medium and large arteries also show degenerative intimal, medial and adventitial changes, although these arteries are not as severely damaged as are arterioles and capillaries. In the late period following irradiation, excessive proliferation of the endothelial cells and subendothelial connective tissue may

occur with narrowing or total occlusion of small-vessel lumina, while larger vessels have a greater margin for change before patency is compromised [53,79]. In larger vessels, medial degeneration may also occur, and there is evidence of progressive sclerosis with subsequent occlusion of the vasa vasorum leading to segmental vessel obliteration.

In rats and dogs, single doses below 25 to 30 Gy x-rays have been found to induce primarily endothelial cell injury with accompanying perturbations in cerebrovascular function, whereas at higher doses ($\geq$30Gy), damage to glial elements and direct injury to neuronal function may predominate [13,89,95,116,119]. However, a study in rabbits has shown that single focal doses of 60 Gy x-irradiation induced subtle perturbations in blood-brain barrier and regional cerebral blood flow without extensive parenchymal injury [58]. Various studies at the cellular level have also indicated that cerebral endothelial and glial cells possess different dose-response characteristics [98].

Generally, the induction of focal white-matter necrosis (presumed to represent oligodendroglial injury) appears to occur at somewhat higher doses (e.g., 30 to 50 Gy) and occurs with a shorter latency, whereas vascular injury without concomitant necrosis appears to be favored by somewhat lower doses (e.g., 15 to 25 Gy) and occurs with a longer latency [39,116,119]. However, the distinction between these two mechanisms of delayed injury is arbitrary and the transition between them most likely represents an overlapping and interdependent relationship [13].

2.4.3 Repair of Sublethal Radiation Damage

The concept of sublethal radiation injury and repair in mammalian cells was first developed by Elkind and Sutton [27]. For some cell types, a single intracellular radiation "hit" is considered sufficient to effect cell death. For other

cell types, however, it appears that cell death requires that a critical threshold number of sublethal radiation events be accumulated over time (at least for a portion of the cell population). In the latter case, intracellular processes capable of repairing sublethal damage can prevent cellular death if the damage is repaired quickly enough (i.e., before the critical number of unrepaired sublethal events has been accrued). This phenomenon can be demonstrated under a variety of experimental conditions wherein cells are subjected to irradiation delivered in small enough increments to permit timely repair of sublethal damage. These conditions include: (1) split-dose irradiation (dividing the total dose typically into two equal halves, separated in time by minutes to hours); (2) fractionation (dividing the total dose into multiple fractions over a period of days or weeks); and (3) continuous irradiation delivered at sufficiently low dose rates to permit repair of damage between successive sublethal intracellular events in a given cell.

Split-Dose Irradiation and Fractionation

Experimentally determined fractional cell survival (S/S_0) for mammalian cells after irradiation can be described by the relationship,

$$S/S_0 = e^{-(\alpha d + \beta d^2)}, \tag{2.3}$$

where cell death is considered to be the product of two mechanisms, "single-hit" injury described by an exponential curve ($e^{-\alpha d}$), and "multihit," or accumulative, injury described by a continuously downward-bending curve ($e^{-\beta d^2}$), where the two mechanisms of injury for any dose (d) are related by the coefficients α and β [127]. Late effects appear to be mediated by accumulative-injury mechanisms to a greater extent than are early effects; this phenomenon is expressed in radiobiologic terms as a smaller α/β ratio ($\sim$ 2 Gy) for late-responding tissues, such as the brain, and a larger ratio ($\sim$ 10 Gy) for early-responding tissues, such as

the skin [126].

When mammalian cell cultures are subjected to split-dose irradiation, the width of the survival-curve shoulder is positively correlated with cellular capacity for repair of sublethal radiation damage [27,28]. The shoulder of the curve can be restored fully (i.e., sublethal damage repaired fully) by sufficiently lengthening the interval between an initial conditioning dose and a second exposure. According to this formulation, late-responding brain and spinal cord tissues consisting of oligodendrocytes and cerebral endothelial cells would be expected to demonstrate greater capacity for repair of sublethal injury than would early-responding tissues [52,120,126,128].

When the total dose of irradiation is fractionated into a series of small daily doses (e.g., 2 Gy) spread over a number of weeks, four primary phenomena have been found to influence the biologic response in clinical cancer patients. These are the repair of sublethal damage, repopulation by surviving cells in the irradiated tissues, redistribution of cells throughout the cell-division cycle, and reoxygenation of hypoxic cells [28,37,45]. The first two phenomena result primarily in sparing of normal tissues; dividing a high dose into multiple fractions permits normal cells to repair sublethal damage between dose fractions and, if the overall course of irradiation is sufficiently long, allows repopulation of normal cells in the radiation field. The latter two phenomena result in increased radiation damage to malignant tumor tissue; dividing a dose into multiple smaller fractions increases the overall response to radiation of the tumor, by allowing for reoxygenation of relatively radioresistant hypoxic tumor tissue and by permitting the redistribution of tumor cells into more radiosensitive phases of the cell cycle.

Dose-Rate Effects

Dose rate is one of the more important factors that determine the biologic

effects of a given dose of radiation [31]. In general, the effects of radiation decrease as dose rate decreases. The dose-rate effect is most pronounced in the range 0.01 to 0.05 Gy/min, the phenomenon being a manifestation of repair of sublethal damage [108]. As the dose rate falls below some threshold level, the rate of accumulation of sublethal intracellular events no longer overwhelms the repair capabilities of the average cell in the population at risk. Some cell death will still occur, since sublethal events occur in a random Poisson distribution rather than uniformly throughout the population; however, the incidence of cell death can be expected to decrease progressively as dose rate decreases.

The radiation tolerance of the central nervous system shows a dose-rate dependency analogous to that seen in many other tissues (e.g., skin, gastrointestinal tract, lung, kidney); bone marrow stem cells are a notable exception, showing little or no dose-rate dependency [31]. With ^{60}Co irradiation of rats *in utero* at dose rates of 0.01, 0.03, 0.1 and 0.47 Gy/min, a dose-rate effect (decrease in brain weight and cellular content at birth and up to 160 d) was observed at doses of 0.8 to 2.4 Gy [68]. At lower doses (0.42 Gy), changes in postnatal growth were independent of dose rate. When 9-d-old rat embryos were x-irradiated with 1.44 Gy, a dose rate of 0.96 Gy/min was found to be ten times more effective for inducing anencephaly than 0.0115 Gy/min [11].

A canine model was used to examine dose-rate effects from interstitially implanted single sources of ^{125}I, ^{192}Ir or ^{198}Au [84]. For a total accumulated dose of 260 Gy at 5 mm from the source, the necrotic lesion was smaller in size and slower to develop with mean dose rates of 4.3×10^{-4} to 6.3×10^{-4} Gy/min than with mean dose rates of 3.6×10^{-3} to 4.4×10^{-3} Gy/min.

Radiation tolerance of the spinal cord was also found to be strongly dose-rate dependent [100,121]. Within 6 to 8 mon and up to 15 mon after irradiation of the cervical spinal cord, rats developed foreleg paralysis caused by white mat-

ter necrosis and intramedullary vascular damage. For a 50% incidence of foreleg paralysis at 9 mon, the dose-rate factor (i.e., the ratio of the isoeffect dose for a given dose rate to the isoeffect dose for the reference dose rate) relative to a reference dose rate of 1.79 Gy/min was found to increase from 1.28 at 0.245 Gy/min to 1.71 at 0.065 Gy/min to $>$ 2.1 at 0.033 Gy/min, although latency for the development of paralysis was independent of dose rate [100]. Following lumbosacral irradiation, rats developed radiation radiculopathy with muscular atrophy and impaired motor function [121]. The ED_{50}[1] for radiculopathy increased from 19.5 to 25.5 Gy with decrease in dose rate from 3.0 to 0.065 Gy/min.

[1] ED_{50} = dose required to produce a given effect in 50% of animals irradiated

CHAPTER 3
MATERIALS AND METHODS

3.1 INTRODUCTION

In this chapter, the materials and experimental techniques used in the dissertation research are described and organized for subsequent reference. In the first section, the preparation of primary and secondary neonatal rat glial cell cultures is detailed, and the culturing of rat glioma cells is introduced. In the second section, culture evaluation by phase contrast microscopy, immunocytochemical methods and automated cell sorting is described. The final sections consider techniques of biochemical and metabolic analysis, and culture irradiation methods. All chemicals were obtained from Sigma Chemical Co. (St. Louis, MO), unless otherwise stated.

3.2 TISSUE CULTURE PREPARATION

3.2.1 Preparation of Primary Mixed Glial Cell Cultures

The method of preparation of primary mixed brain cell cultures was developed in our laboratory as a modification of the method of McCarthy and de Vellis [69]. A mixed glial cell primary culture, rich in oligodendrocytes and astrocytes, was obtained from disaggregated neonatal rat cerebral cortex. Viable neurons do not survive this method of preparation.

One-day-old Sprague Dawley rats were sacrificed by scissors decapitation. The protocol and euthanasia technique were approved by the Animal Welfare and Research Committee at Lawrence Berkeley Laboratory (AWRC No. 1902). Using sterile technique, the brains were removed and placed in a plastic culture dish containing nutrient medium (1:1 Hams F-12 (Gibco, Grand Island, NY):

Dulbecco's Modified Eagle's Medium (Gibco), with 10% fetal calf serum, 15 mM Hepes buffer, and 1.2 g/l sodium bicarbonate). The excised brains were washed immediately with additional nutrient medium to rinse off extraneous cellular debris and surface blood. The cortices were teased away from the more caudal portion of the brain, and the meninges were gently removed from the cortices. The cortices in the medium were then poured into a 210 μm pore nylon monofilament bag, and dissociated into fresh medium by gentle stroking with a glass rod. The cellular filtrate was then filtered sequentially through 230 μm and 140 μm mesh stainless steel screens. Fetal calf serum was added to the final cellular filtrate prior to centrifugation at 800 rpm for 5 min. The pellet was then resuspended in fresh medium and the cells were plated in 25 cm^2 (3.5 ml cell suspension) or 75 cm^2 (10.0 ml cell suspension) plastic culture flasks (Falcon, Becton-Dickinson Labware, Lincoln Park, NJ) at a concentration of about 1.5×10^6 cells per 1.0 ml medium, or in 24-well plates (Corning Glass Inc., Corning, NY) at 0.5×10^6 cells per 1.0 ml medium. The primary culture flasks were maintained at 37° C in a water-jacketed incubator at 5% CO_2 in humidified air. The first media change was on day-in-culture (DIC) 5; subsequent media changes took place on DIC 7, 9, 12, 14, 16, 19, etc. (i.e., three times weekly).

3.2.2 Preparation of Oligodendrocyte-Enriched Secondary Cell Cultures

On DIC 7 to 9, the primary culture 75 cm^2 plastic flasks were examined daily to determine when astrocyte proliferation had resulted in the formation of a confluent bed layer of cells on the surface of the flask. The flasks were then tightly sealed and placed on a rotary shaker at 200 rpm for 6 h at 37° C; this agitation separated out loosely adherent macrophages and cellular debris, which were then discarded. Fresh media was added and the flasks were returned to the shaker

for an additional period of 18 h at 200 rpm; this procedure loosened oligodendrocytes preferentially from the more tightly-adherent astrocyte bed layer. The oligodendrocyte-rich cell suspensions of the shaken flasks were poured aseptically into new flasks (4 shaken flasks per 1 new flask) and incubated at 37° C at 5% CO_2 in humidified air; after 24 h the media was replaced with 10 ml fresh media per flask and the flasks were placed on the rotary shaker at 200 rpm for another 24 h in order to produce a more enriched oligodendrocyte suspension which could then be used for further study.

When the oligodendrocyte-enriched cell suspensions were first decanted from the original primary culture flasks after the initial 24 h agitation period, large numbers of oligodendrocytes still remained adherent to the astrocyte bed layer. In order to harvest these cells, fresh media was added to these original flasks and shaking at 200 rpm was continued for an additional 24 h. Thus, two batches of oligodendrocyte-enriched cell suspensions were produced, separated by 24 h. In each case, these cell suspensions were decanted through a 25 μm stainless steel sieve immediately following the last shaking step. These mechanical agitation procedures separated out oligodendrocytes with about 95% purity [69].

3.2.3 Preparation of Rat Glioma Tumor Cell Cultures

A rat-glioma-cell clone (marked "9-L" and provided by Dr. A. Rodriguez) was used to evaluate the feasibility of quantifying tritiated thymidine incorporation in a discrete cell population meeting designated immunofluorescent criteria. A frozen tumor-cell aliquot was thawed and cultured in nutrient medium (see Section 3.2.1), and incubated at 37° C in a 75 cm^2 plastic flask in a water-jacketed incubator at 5% CO_2 in humidified air. The culture was examined daily to determine when cellular proliferation had resulted in the formation of a confluent layer

of cells on the surface of the flask. The primary culture was then dissociated by successive incubation with trypsin and trypsin inhibitor (see Section 3.3.4) and subcultured into multiple flasks for subsequent manipulation and assay.

3.3 CULTURE EXAMINATION

3.3.1 Phase Contrast Microscopy

Phase contrast microscopy was used to assess the condition of living brain cell preparations in plastic culture flasks or on coated glass cover slips. Cultures were examined at each media change (and as required) for cellular viability, cell density, and fungal and bacterial contamination. A bed layer of phase-light astrocytes proliferates to confluence over a period of days, and is readily distinguished from more superficial phase-dark process-bearing oligodendrocytes. Scanning at $\times 100$ magnification is suitable to assess whether the astrocyte carpet is complete, and to determine the extent of cellular stratification. Screening for fungal contamination is done at the same time. Observation at $\times 400$ magnification is preferable to establish the morphologic maturity and integrity of the oligodendrocytes, check for cellular fragmentation, and to screen for early bacterial contamination.

Oligodendrocyte Counting

The oligodendrocyte population in the mixed glial culture was quantified using phase contrast microscopy at $\times 400$ magnification. Characteristic phase-dark cells were counted in a 1 mm $\times$ 1 mm square grid in ten randomly positioned flask regions (the perimeter of the flask was not sampled in order to avoid regions that might be unrepresentative due to pooling effects). The extreme high and low oligodendrocyte counts were ignored, and the mean value of the remaining eight regions was calculated.

3.3.2 Preparation of Antisera

Polyclonal anti-galactocerebroside (anti-GC) was prepared[1] by immunizing rabbits with bovine galactocerebroside sonicated with fatty-acid-free bovine serum albumin and Freund's complete adjuvant. Sera was then affinity-adsorbed against bovine serum albumin to improve specificity. The anti-GC sera was used at 1:10 dilution for cover slip culture immunofluorescent staining and for automated-fluorescence activated cell sorting (FACS). Commercially available anti-GC (Advanced Immunochemical Services, Inc., Long Beach, CA) was also used in selected procedures at 1:50 to 1:200 dilution.

Antibody to myelin basic protein (anti-MBP) (Diagnostics Systems Laboratory, Webster, TX) was used at 1:25 to 1:100 dilution for cover slip culture immunofluorescent staining and FACS procedures. Mouse monoclonal or rabbit polyclonal anti-glial fibrillary acidic protein (anti-GFAP) was used at 1:8 to 1:100 dilution for these immunofluorescence procedures.

Goat anti-rabbit IgG-fluorescein isothiocyanate conjugate (FITC) was used at 1:100 to 1:300 dilution for cover slip culture immunofluorescent staining and FACS procedures. Goat anti-mouse IgG-FITC and goat anti-mouse IgG-tetramethylrhodamine isothiocyanate conjugate (TRITC) were used at 1:100 to 1:300 dilution for cover slip culture immunofluorescent staining and FACS procedures.

3.3.3 Indirect Immunofluorescent Staining for Cover Slip Cultures

For immunofluorescent staining procedures, primary or secondary cultures were plated onto glass cover slips previously incubated in 10 μg/ml poly-D-lysine (50-70K Dalton). Cultures were washed several times in cold (4° C) phosphate

[1] In collaboration with Berkeley Antibody Company, Berkeley, CA

buffered saline (PBS), and then fixed in 3.7% formaldehyde in PBS for 30 min or 70% ethanol at -20° C for 30 min. After thorough washing in cold PBS, the cell preparations were incubated with primary antibody for 30 to 60 min at room temperature or overnight at 4° C. Primary antibodies (rabbit polyclonal or mouse monoclonal) were prepared at appropriate titer in PBS supplemented with 10% pre-immune goat serum as a blocking agent; cell permeabilization with 0.01% Triton X-100 was used to access internal antigens after formaldehyde fixation procedures, but was later found to be unnecessary following ethanol fixation. Pre-immune rabbit and mouse serum were used as controls for the primary antibodies. After thorough washing in cold PBS, the cultures were then incubated for 30 min at room temperature with secondary fluorescein-conjugated goat anti-rabbit and/or rhodamine-conjugated goat anti-mouse antibodies at appropriate titer in PBS supplemented with 10% pre-immune goat serum. The washed cover slips were then mounted in 90% glycerol (PBS-buffered), sealed with clear nail polish, viewed for immunofluorescence and photographed.

3.3.4 Automated Cell Sorting by Optical Scatter Properties

Automated cell sorting procedures can be used to analyze and separate mixed glial cell populations based on either differential optical or fluorescent-antiserum-binding parameters. The principal is that a stream of single cells intersects a laser beam (typically, a 488-nm argon laser), which is focused on the stream. Light scattering or emitted fluorescence are monitored by detectors. When a cell generates a specific signal of designated value, a charging voltage pulse is applied to the stream which has been broken into droplets by low-power ultrasonic vibration. Those droplets containing the cells which have exhibited the specific designated signal remain charged after separation from the stream and are then deflected by an electric field into a collection vial.

Cells in plastic culture flasks were washed twice in cold PBS (Ca-, Mg-free) with 0.02% EDTA, then suspended in trypsin (3 ml per 10-ml flask) at 37° C for 5 min or until the cellular mass floated loose from the flask surface. This suspension was then pipetted up and down repeatedly to break up any residual cellular clumps. Each flask was then incubated with 3 ml media supplemented by 2 mg/ml soybean trypsin inhibitor and 80 μg/ml DNase I for an additional 15 min at 37° C. A plastic cell scraper was used to dislodge any remaining cells from the flask surface into suspension. After the cellular suspension was centrifuged at 1500 rpm for 5 min, the pellet was resuspended and washed twice in PBS, fixed in 3.7% formaldehyde in PBS for at least 30 min and then filtered through a 40 μm Millipore filter to remove cellular clumps. (The fixed-cell suspension can be stored at 4° C for several weeks at this stage before further processing.)

An aliquot of the fixed-cell suspension was injected into a FACS IV[2] fluorescence-activated cell sorter where frequency histograms of cell distributions were generated for forward and side optical scatter channels. These parameters were bracketed as desired for automated cell sorting, so that those cells matching the designated criteria could be counted and/or separated for further analysis.

3.3.5 Indirect Immunofluorescent Staining for Cell Sorting

For sorting glial cells by fluorescent antibody labeling, cells fixed with formaldehyde or 70% ethanol (as prepared in Section 3.3.4) were pelleted by centrifugation at 1500 rpm for 5 min. After washing twice in PBS, the cells were resuspended and incubated for 30 min at room temperature with primary antibody appropriately diluted in PBS with 10% goat serum. (For formaldehyde-fixed cells, the diluent was supplemented with 0.01% Triton X-100 if internal antigens were to be labeled.) The cells were pelleted and washed three times,

[2] Becton-Dickinson, Mountain View, CA

and then incubated for 30 min at room temperature with secondary antibody at appropriate titer in PBS with 10% goat serum, washed 3 times in PBS, and resuspended in 1 ml aliquots in PBS.

3.3.6 Automated Fluorescence-Activated Cell Sorting

Each 1-ml aliquot of the cell suspensions prepared as above (Section 3.3.5) was gently suspended in 2 ml propidium iodide solution (50 mg/l) and permitted to incubate for 10 min at room temperature. Propidium iodide is a selective fluorescent stain for DNA. The final cell suspension was then injected into the FACS, and frequency histograms for fluorescence intensity were generated. Those cells satisfying the designated fluorescence-intensity criteria for both intact nucleus (i.e., positive propidium iodide label) and oligodendrocyte identification (i.e., positive anti-GC label) or astrocyte identification (i.e., positive anti-GFAP label) were counted and sorted into collection vials for subsequent assay. Propidium-iodide-labeled cells not satisfying the cell-type-specific criteria of a given experiment were also counted and sorted into collection vials for subsequent assay.

Fluorescent excitation of FITC, TRITC and propidium iodide molecules in the FACS cellular stream was provided by a 488-nm argon laser. A 600-nm long pass filter (designed to transmit wavelengths $\geq$ 600 nm) was used to detect emitted red fluorescence from propidium iodide or TRITC. A 530-nm band pass filter (designed to transmit wavelengths of 530 $\pm$ 15 nm) was used to detect emitted green fluorescence from FITC (Figure 3.1).

The FACS can be programmed to trigger when a red-fluorescence-emission event (denoting propidium iodide label) of sufficient intensity (i.e., higher than background noise) is detected; this event represents a nonspecific cell with an intact nucleus. All such cells are in turn assessed for the presence of cell-specific

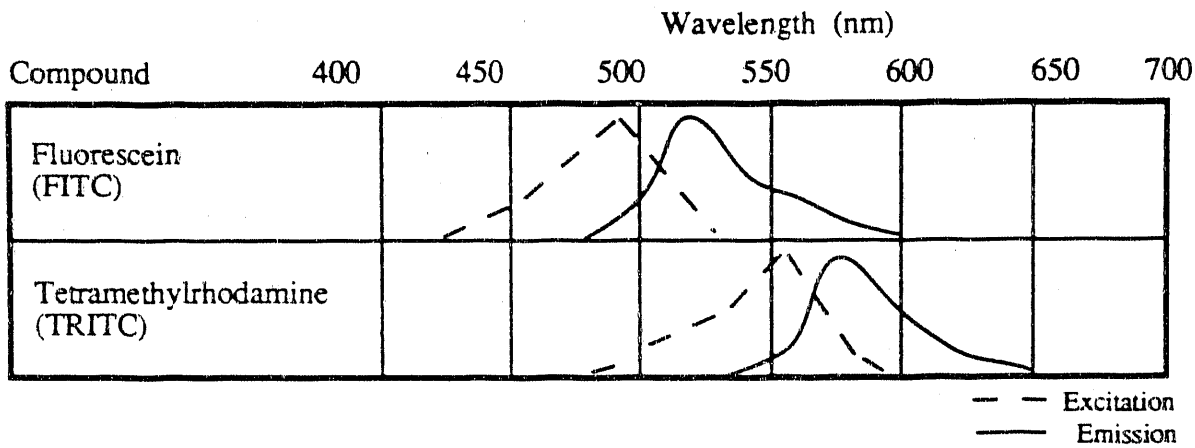

Figure 3.1. The excitation (dashed line) and emission (solid line) spectra are shown for fluorescein isothiocyanate (FITC) and tetramethylrhodamine isothiocyanate (TRITC). See Section 3.3.6.

indirect immunofluorescent labeling (i.e., green-fluorescence emission of sufficient intensity). The appropriate green-fluorescence-sorting parameters are determined by visual inspection of the initial fluorescence-log-intensity histograms. Alternately, the propidium-iodide-labeling step can be skipped, and cells sorted simultaneously according to the presence of either of two discrete and noncross-reacting cell-specific indirect-immunofluorescent labels (e.g., oligodendrocytes labeled with FITC-anti-GC and astrocytes labeled with TRITC-anti-GFAP).

The FACS can also be programmed to analyze relatively homogeneous cell populations without cell-specific-immunofluorescent labeling, e.g., formaldehyde-fixed 9-L tumor cells. In this case, a 1-ml aliquot of tumor-cell suspension was gently suspended in 2 ml propidium iodide solution (as above) and the final cell suspension was injected into the FACS. Each appropriate red-fluorescence-emission event was taken to designate a discrete tumor cell, which was then counted and sorted into a collection vial for subsequent assay.

3.3.7 Photomicrography Technique

All phase-contrast and fluorescent micrographs in this dissertation were photographed with a Nikon FM2 camera and Diaphot-TMD[3] inverted microscope with epi-fluorescence capability. Tri-X pan[4] 400 ASA black-and-white negative 35-mm film was exposed at the 800 ASA setting. Magnification factors were reported as present at the film plane (i.e., $\times 25$ for *low power* or $\times 100$ for *high power*). These images were further enlarged four times for final formatting, but without any improvement in resolution.

[3]Nikon Corp., Tokyo, Japan
[4]Eastman Kodak Co., Rochester, NY

3.4 METABOLIC ANALYSIS

3.4.1 Tritiated Precursor Incorporation

Primary mixed glial cell cultures (or 9-L glioma cultures) were incubated for periods ranging from 6 to 48 h at 37° C in a humidified 5% CO_2 atmosphere with various concentrations (up to 40 μCi/7.5 ml medium) of tritiated thymidine (6.7 Ci/mmol) or tritiated galactose (60.0 Ci/mmol) (NEN Research Products, Boston, MA) in prewarmed nutrient medium. For selected experiments, the tritiated medium was replaced with standard nutrient medium for 24 h prior to sacrificing the cultures, in order to "chase" any tritiated precusors that had not been structurally incorporated into the glial cells. After washing twice with PBS, the cells were trypsinized and fixed (see Section 3.3.4). Glial cells were stained for galactocerebroside with fluorescein-conjugated indirect immunofluorescence technique (see Section 3.3.5), and sorted and counted by an automated fluorescent antibody cell sorter (see Section 3.3.6). Glioma cells were stained only with propidium iodide before sorting (see Section 3.3.6). The sorted cell aliquots were then mixed with liquid scintillation fluid and analyzed for tritium content in a Tri-Carb Model 2000 CA liquid scintillation analyzer [5].

3.4.2 Myelin Basic Protein Radioimmunoassay

The cell cultures were gently washed 4 times with PBS at 4° C, and then bathed in 0.02 M Tris-acetate buffer (4° C) at pH 7.2 containing 0.02 M NaCl, 0.1% Triton X-100 and 0.1% aprotinin. A plastic cell scraper was used to dislodge the cells from the flask surface and into suspension in the Tris buffer; the suspension was then sonicated, incubated overnight at 4° C, and then centrifuged at 1,500 g for 20 to 30 min at 4° C. Aliquots of the supernatant were then analyzed

[5] Packard Instrument Co., Inc., Downers Grove, IL

for MBP by radioimmunoassay (or collected for other biochemical assays) or stored at -15° C for later assay.

Radioimmunoassay procedures were performed with a modification of a commercially available kit (Diagnostics Systems Laboratory, Webster, TX). Briefly, ^{125}I-labeled MBP competes with appropriately diluted (1:1 to 1:20) unlabeled MBP from standards or unknowns for binding sites on anti-MBP molecules. The MBP-antibody complexes were precipitated and assayed in a Packard 5000 Gamma Counter[6] after centrifugation and decanting of any unbound radiolabel. A curve-fitting logistic program was developed to calculate MBP concentrations.

3.4.3 Total Cellular Protein Spectrophotometric Assay

Aliquots (600 μl) of the supernatant prepared as described in Section 3.4.2 were assayed for total protein content, using an ASTRA spectrophotometric (545 nm) analyzer[7] calibrated for cerebrospinal fluid. In this analytical method, the peptide bonds of the protein are rapidly chelated by an alkaline copper sulfate reagent to form a dark blue copper tripeptide chelate. This method has a correlation coefficient of 0.971 versus known standards, and a precision of 5% at one standard deviation.

3.5 CULTURE IRRADIATION

3.5.1 Preparation for Irradiation

Culture flasks were prepared for irradiation in a laminar flow hood[8]. Lucite filters for "build-up" of electronic equilibrium were taped in place (for ^{60}Co irradiation). Flasks were placed and sealed into zip-locked plastic bags prior to

[6]Packard Instrument Co., Inc., Downers Grove, IL
[7]Beckman Instruments, Fullerton, CA
[8]SterilGARD Hood, Baker Co., Inc., Sanford, ME

transportation to the irradiation site; the zip-locked bags remained sealed until the cultures were returned to the hood. Cultures were irradiated in the upright position, and were maintained at 37° C during and following irradiation. For experiments requiring irradiations in excess of 40 min, irradiated culture flasks (and control flasks) were filled completely with nutrient media to prevent drying of the cell surface. For lesser exposure times, no additional media was used.

3.5.2 Irradiation Parameters

For irradiation with 225 kVp X-rays, a Philips RT 250 Irradiator[9] was used with a 0.35 mm Cu filter; a dose rate of 0.70 Gy/min was present at the culture surface. For irradiation with ^{60}Co γ-rays, a Gammabeam 150 C Unit[10] was used with a 5-mm thick Lucite filter taped to the surface of the flask. Dose rates of γ-irradiation employed varied from about 0.03 Gy/min to 2.0 Gy/min, with a rate of about 0.5 Gy/min present at 1.0 m from the point source. In all experiments, randomly selected control cultures were handled identically to the irradiated cultures, except for the actual irradiation. For example, controls were transported to the irradiation site along with the cultures to be irradiated. The control flasks were assigned randomly to be positioned upright for the same length of time as required for either the shortest or longest irradiation exposure; these "short-exposure" and "long-exposure" controls were compared with each other following each experiment to verify that the physical handling of the specimens did not contribute to any differences observed following irradiation.

3.6 STATISTICAL EVALUATION

Multiple groups within an experiment were compared statistically with

[9]Philips Medical Systems, Eindhoven, Netherlands
[10]Atomic Energy of Canada Limited, Ottawa, Canada

each other for all permutations, using analysis of variance (Fisher's protected least significant difference (PLSD) test) [125]; significance was evaluated at the 95% level. The Kruskal-Wallis mean rank test was used for non-parametric analysis of groups consisting of ratios of two random variables [125]; here, the standard deviation was taken as the square root of the variance of ratios [5].

CHAPTER 4
RESULTS: UNIRRADIATED GLIAL CELL CULTURES

4.1 INTRODUCTION

A systematic characterization of the metabolic properties of brain cells under optimal culture conditions was considered essential prior to initiating studies of glial cell reaction to radiation injury. A variety of morphologic, immunocytochemical and biochemical assays was developed toward this end. The qualitative and quantitative experimental findings in unirradiated glial cultures are described in this chapter.

4.2 MORPHOLOGIC EVALUATION

4.2.1 Primary Mixed Glial Cell Cultures

At day-in-culture (DIC) 5, the oligodendrocyte and astrocyte populations were beginning to demonstrate the morphologic characteristics on phase contrast microscopy typical of more mature glial cells. Many glial cells still had a relatively undifferentiated rounded-up appearance. Large bare areas on the plastic flask surface (or culture-well bottom) were common. Heavily vacuolated cells were plentiful and were seen to be loosely adherent to the developing cell monolayer or floating freely in the medium. Clumped cellular debris was also found to be floating or loosely attached to the monolayer. The majority of the cellular debris and vacuolated cells were removed during the first media change, and the residual unwanted cellular elements were discarded progessively during successive media changes.

At DIC 7, an increasingly confluent monolayer of flat phase-light astrocytes took on a cobblestone carpet appearance (Figure 4.1). At this stage, mor-

phologically distinct phase-dark, process-bearing cells were present overlaying and adherent to the astrocyte layer. These phase-dark cells were demonstrated by immunocytochemical means to be oligodendrocytes (see Section 4.3). Oligodendrocytes adhered directly to the flask surface in areas where the astrocyte carpet was interrupted. In these astrocyte-free regions, the oligodendrocytes elaborated complex processes (often in apparent interaction with processes from adjacent oligodendrocytes) with increasing maturational age (Figure 4.2). In astrocyte-populated regions, the oligodendrocyte processes became successively intertwined with and anchored to the astrocyte monolayer. With increasing culture age, astrocyte proliferation continued until the surface of the flask was fully covered with a confluent layer of astrocytes. The astrocytes adhered very tightly to the surface and they appeared to crowd out the oligodendrocytes, progressively forcing the soma of the oligodendrocytes to assume their final position atop the astrocyte monolayer (Figures 4.3 and 4.4).

The appearance of mixed primary glial cell cultures under the phase microscope depended on a number of factors, including the time required for culture preparation and the initial cellular plating density. The viability and/or reproductive integrity of the glial cells was compromised by prolonged *ex situ* preparation time of the primary culture. Culture quality and quantity of surviving cells improved as the dissection and culture-preparation procedures became more efficient. A substantial degree of culture inhomogeneity, however, was apparent even under optimal conditions of culture preparation. Thorough mixing of the primary cell suspension prior to plating was not sufficient to assure a uniform distribution of oligodendrocytes in the final culture. Careful evaluation demonstrated oligodendocyte enriched and depleted regions to be present in nearly all primary cultures. Similarly, the astrocyte monolayer typically (at least in younger cultures) exhibited acellular holes scattered among regions of cellular

Figure 4.1

Phase contrast photomicrograph of a primary mixed glial cell culture at day-in-culture (DIC) 7. An oligodendrocyte-free region is selected to illustrate the nearly confluent layer of relatively amorphous astrocytes and to demonstrate the characteristic "cobblestone carpet" appearance of the astrocyte monolayer. ×100.

Figure 4.2

Phase contrast photomicrograph of a primary mixed glial cell culture at DIC 13. An oligodendrocyte-enriched region is selected to demonstrate the characteristic phase-dark oligodendrocytes in their customary position on top of the astrocyte monolayer. The branching oligodendrocyte processes are best seen where they adhere directly to the flask surface in regions where the astrocyte carpet is interrupted (at left). ×100.

Figure 4.3

Phase contrast photomicrograph of a primary mixed glial cell culture at DIC 19. Oligodendrocytes appear as phase-dark cells with elongated processes overlying an amorphous astrocyte monolayer (cf Figure 4.4). ×25.

Figure 4.4

Phase contrast photomicrograph of the primary mixed glial cell culture at DIC 19 (cf Figure 4.3) shown at higher power. ×100.

Figure 4.1

XBB 904-3376A

Figure 4.2

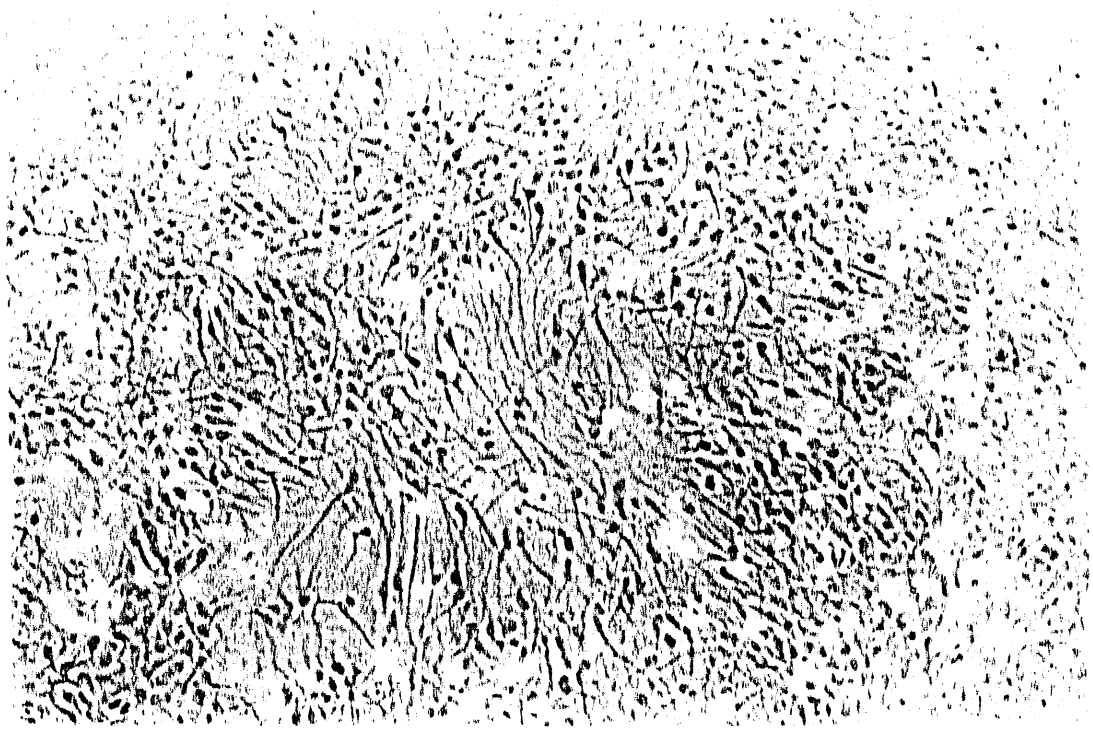

Figure 4.3

XBB 910-8168A

Figure 4.4

confluence.

Decreased initial plating density tended to favor the development of astrocyte-enriched cultures, because the astrocyte population continued to proliferate until a confluent monolayer was ultimately formed. On the other hand, oligodendrocytes appeared to exhibit very limited proliferative capabilities in culture (see Section 4.3.2), and their final population therefore reflected more directly the concentration of viable oligodendrocytes in the initial culture.

4.2.2. Oligodendrocyte-Enriched Secondary Cell Cultures

Considerable effort was applied to obtain secondary cultures highly enriched in oligodendrocytes in an effort to isolate this population for cell-specific evaluation. It was possible to obtain purified oligodendrocytes in limited quantities sufficient for immunocytochemical staining and selected fluorescence-activated cell sorting (FACS) procedures (see Sections 4.3 and 4.4). Additionally, clusters of oligodendrocytes were obtained for observation in an astrocyte-free environment, where the morphologic qualities of the individual oligodendrocytes and their network of processes could be demonstrated more clearly (Figure 4.5). Very few oligodendrocytes appeared to survive the secondary culture preparation procedure with their elaborate processes intact. Within 24 h of replating, however, the formation of new processes was noted. Extensive branching processes began to form within 48 to 72 h after replating, often demonstrating complex multicell networks corresponding to that seen in primary mixed glial cultures.

The oligodendrocyte yield in the secondary cultures was generally too low to permit reliable quantitative biochemical and/or morphologic evaluation. Certain observations were possible which may contribute ultimately to solving the problem of poor oligodendrocyte yield.

The quality and quantity of the secondary culture was noted to be highly

dependent on the initial conditions of the primary culture. Stratification of the oligodendrocytes and astrocytes typically required 7 to 9 days in culture. If the mechanical sorting technique described in Section 3.2.2 were attempted prior to the time the astrocyte bed layer attained confluence, rounded-up proliferating astrocytes would shake off into suspension, thereby contaminating the oligodendrocyte preparation. If mechanical separation were delayed more than 1 or 2 d after astrocyte confluence was attained, some astrocytes would begin to cluster above the bed layer and break up into suspension during the sorting procedures. Moreover, with increasing cell age the oligodendrocyte processes became firmly intertwined with and adhered more strongly to the astrocyte layer; the mechanical shaking process thereby became less efficient and the oligodendrocytes became susceptible to injury and death from mechanical shearing. Thus, it was imperative that the primary cultures were plated with the appropriate cell density to assure that complete astrocyte confluence was achieved prior to extensive differentiation and anchoring of the oligodendrocytes. Daily evaluation with phase contrast microscopy was required to determine the optimal time for commencing the cell separation procedures.

Modifications of the duration and speed of the shaking procedures had predictable effects on the nature of the resulting secondary cultures. Shortening the initial shaking period (following which the media is discarded) increased the oligodendrocyte yield, but resulted in greater contamination of the secondary cultures with vacuolated cells, loose astrocytes, and cellular debris. Lowering the shaking speed from 200 rpm to 100 rpm resulted in oligodendrocytes which were less likely to have process-shearing injury, but at the expense of a lower cell yield. Generally, the oligodendrocyte output of the second day's shaking gave a lower yield, but of higher purity, than the first day's output. The optimal cell-separation parameters have yet to be firmly established.

4.2.3. Astrocyte-Enriched Secondary Cell Cultures

While specific evaluation of the astrocyte population was not a primary goal of this investigation, the procedures for obtaining oligodendrocyte-enriched secondary cultures left astrocyte-enriched cultures behind in the original culture flasks. Extending the period of mechanical agitation for a period of several additional days reliably resulted in astrocyte cultures of extremely high purity (Figure 4.6). These cultures served as the material for selected immunocytochemical staining and FACS procedures (see Sections 4.3 and 4.4). The yield and quality of the astrocyte-enriched cultures was generally excellent and, although not pursued further in the research described in this thesis, these secondary cultures shall serve readily as the starting point for quantitative *in vitro* evaluation of the astrocyte population in planned future investigations.

4.2.4 Oligodendrocyte Quantitation in Mixed Glial Cell Cultures

Quantitation of the oligodendrocyte population in mixed primary glial cell cultures was carried out by grid counting of morphologically characteristic phase-dark oligodendrocytes (see Section 3.3.1). A group of primary culture flasks was dedicated exclusively to serial quantitation of the oligodendrocyte population. These cultures were counted every few days from DIC 7 until DIC 33 or until contamination intervened. The oligodendrocyte population, as quantified by morphologic criteria, could be seen to increase sharply between DIC 7 and DIC 14 and to reach a plateau at about DIC 14 or shortly thereafter (Figure 4.7). The mild fluctuations in oligodendrocyte counts seen in the plateau region of the curve illustrate the uncertainty inherent in random sampling of an intrinsically heterogeneous plated cell population.

Figure 4.5

Phase contrast photomicrograph of an oligodendrocyte-enriched secondary cell culture at DIC 18 demonstrates an extensive network of ramifying cytoplasmic processes. ×100.

Figure 4.6

Phase contrast photomicrograph of an astrocyte-enriched secondary cell culture at DIC 27. Phase-light astrocytes elaborate a network of long processes which typically have relatively fewer branches than do oligodendrocyte processes (cf Figure 4.5). ×100.

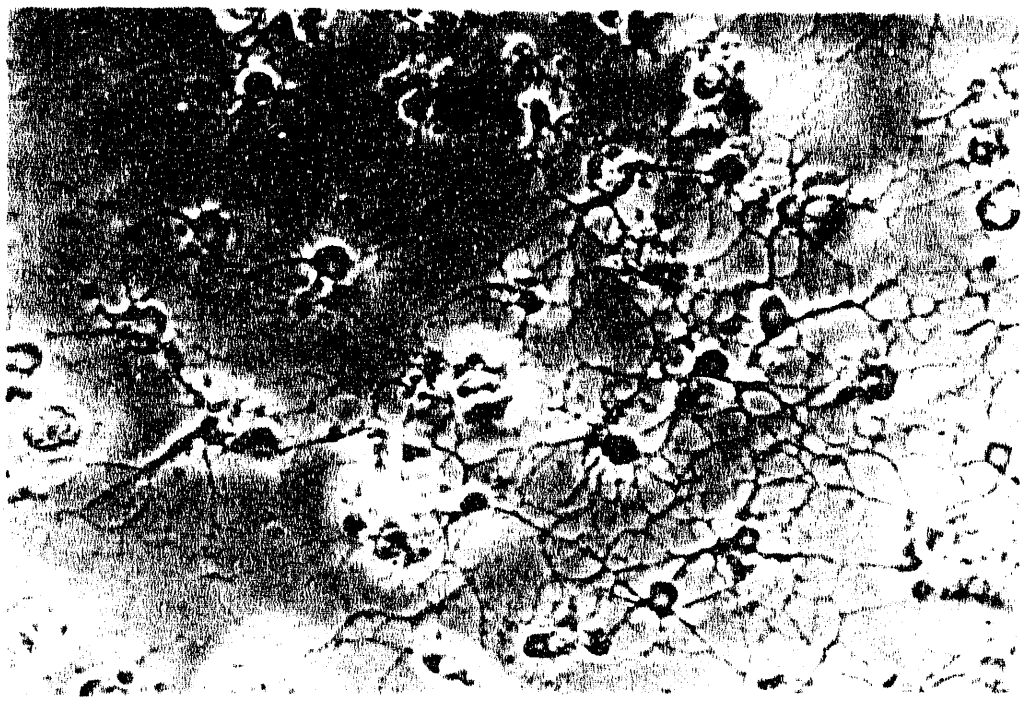

Figure 4.5

XBB 910-8902A

Figure 4.6

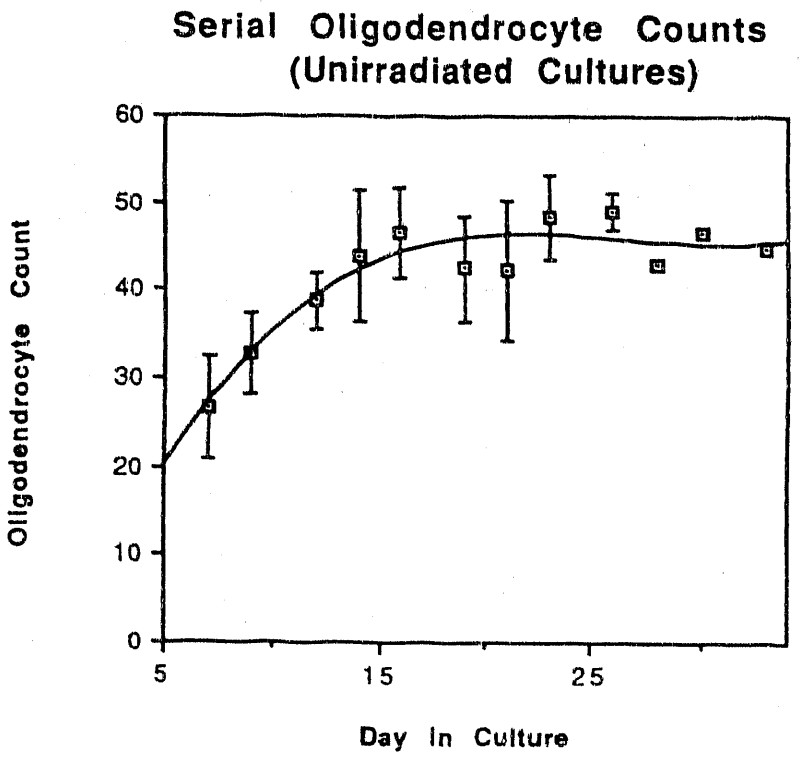

Figure 4.7. Serial oligodendrocyte counts (mean ± S.D.) in unirradiated primary mixed glial cultures are shown as a function of DIC. Morphologically characteristic phase-dark oligodendrocytes were grid-counted at ×400 magnification (see Section 3.3.1). Cultures were counted every few days from DIC 7 to DIC 33 or until contamination intervened. Cell counts increased sharply between DIC 7 and DIC 14 and reached a plateau shortly thereafter.

4.3 INDIRECT IMMUNOFLUORESCENT STAINING

4.3.1 Mixed Glial Cell Cultures

Indirect immunofluorescent staining in cover-slip cultures was an effective means of labeling specific cell subpopulations within a heterogeneous mixed glial cell culture. Those phase-dark cells morphologically identified as oligodendrocytes (see Section 4.2) were labeled by anti-galactocerebroside (GC) with nearly one-to-one correspondence as early as DIC 7 (Figures 4.8 - 4.13). Antisera to myelin basic protein (MBP) was also highly specific for oligodendrocytes, but was not as sensitive as anti-GC, especially in cultures younger than 10 DIC (Figures 4.14 and 4.15).

Indirect immunofluorescent staining with anti-glial fibrillary acidic protein (GFAP) selectively labeled phase-light glial cells morphologically identified as astrocytes (see Section 4.2). Evaluation of paired fluorescent and phase-contrast micrographs demonstrated very high correspondence of GFAP staining with astrocyte-dominated regions of the culture (Figures 4.16 - 4.19). It was difficult to determine the precise degree of astrocytic labeling with GFAP in primary mixed glial cultures, since the astrocytes were so densely clustered as to preclude accurate quantitation. When higher concentrations of anti-GFAP were used, the fine reticular pattern of the filamentous intracellular proteins was evident (Figure 4.20).

4.3.2 Secondary Glial Cell Cultures

The immunofluorescent staining properties demonstrated in mixed glial cell cultures (see Section 4.3.1) were well maintained in secondary cultures of either oligodendrocytes or astrocytes. In mature secondary oligodendrocyte cultures, extensive flattened processes adherent to the polylysine-coated cover slips

Figure 4.8

Indirect immunofluorescent photomicrograph of a primary mixed glial cell culture at DIC 9. Staining was performed with rabbit anti-galactocerebroside (anti-GC) primary antibody at 1:100 dilution and FITC-conjugated goat anti-rabbit secondary antibody at 1:100 (cf Figure 4.9). ×25.

Figure 4.9

Phase contrast photomicrograph corresponding to the indirect immunofluorescent field shown in Figure 4.8. ×25.

Figure 4.10

Indirect immunofluorescent photomicrograph of a primary mixed glial cell culture at DIC 8. Staining was performed with rabbit anti-GC primary antibody at 1:100 dilution and FITC-conjugated goat anti-rabbit secondary antibody at 1:100 (cf Figure 4.11). ×100.

Figure 4.11

Phase contrast photomicrograph corresponding to the indirect immunofluorescent field shown in Figure 4.10. The characteristic phase-dark cells identified morphologically as oligodendrocytes were labeled with anti-GC with approximately one-to-one correspondence. ×100.

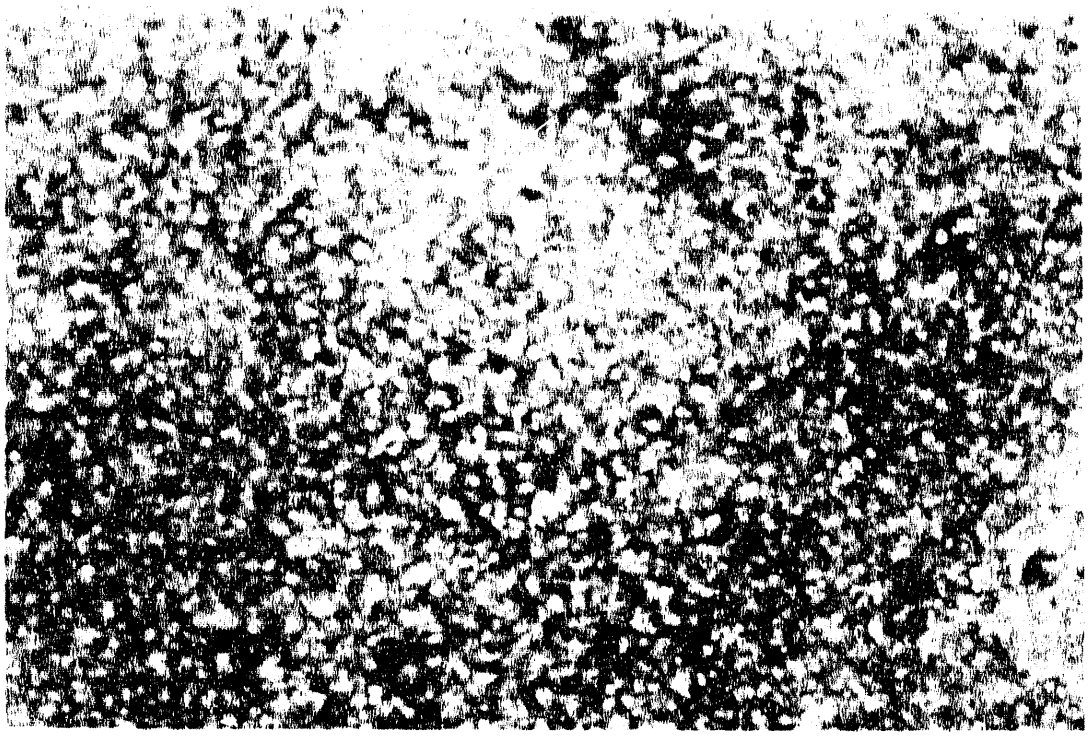

Figure 4.8

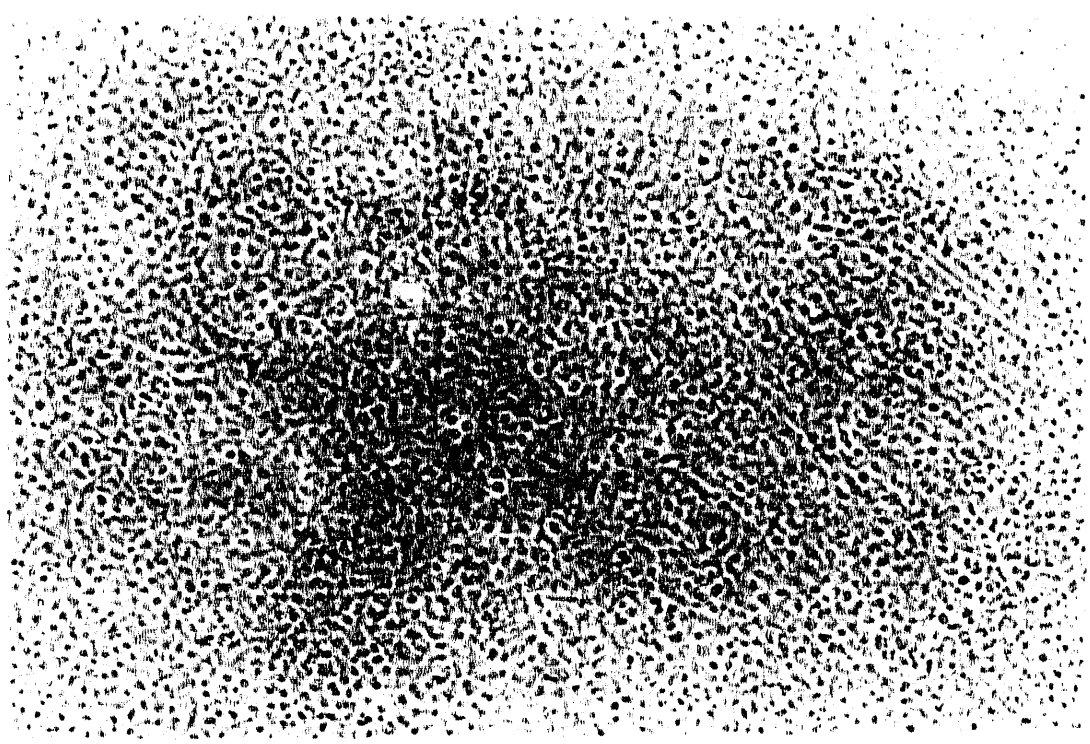

XBB 910-8663A

Figure 4.9

Figure 4.10

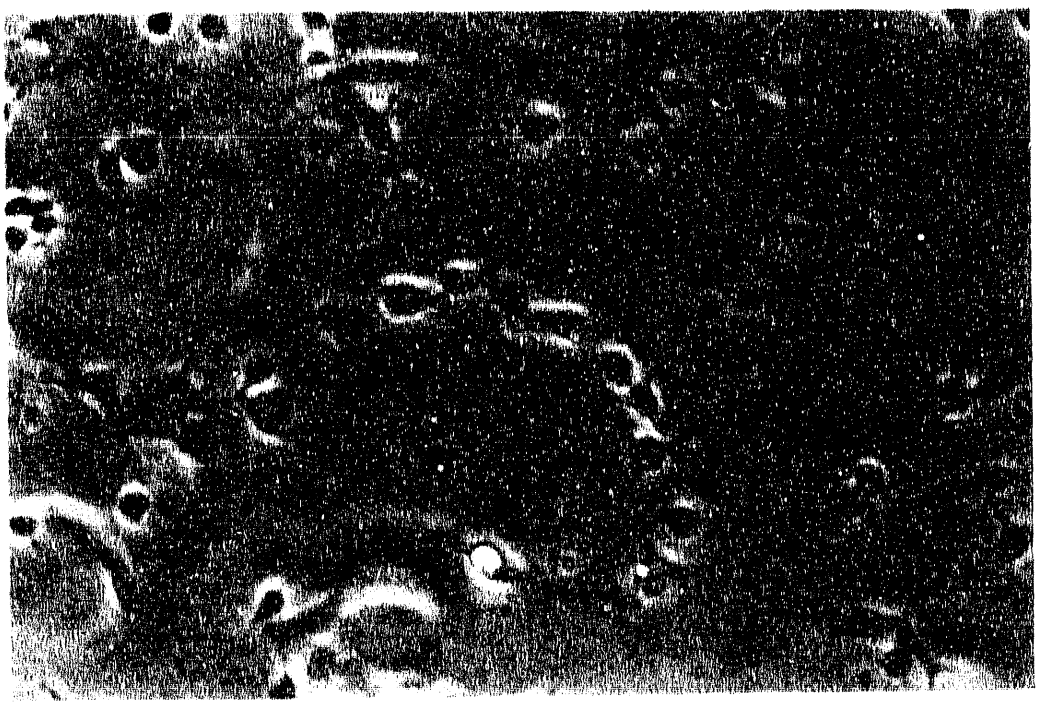

CBB 910-8011A

Figure 4.11

Figure 4.12

Indirect immunofluorescent photomicrograph of a primary mixed glial cell culture at DIC 9. Anti-GC labeling is apparent in the fine processes extending from the cell soma (analogous to the cytoplasmic tongues illustrated in Figure 2.5), and fainter labeling can be detected in the flattened adjacent structures (possibly analogous to the flattened myelin segments illustrated in Figure 2.4). Staining was performed with rabbit anti-GC primary antibody at 1:100 dilution and FITC-conjugated goat anti-rabbit secondary antibody at 1:100 (cf Figure 4.13). $\times 100$.

Figure 4.13

Phase contrast photomicrograph corresponding to the indirect immunofluorescent field shown in Figure 4.12. There is correspondence of morphologic and immunologic criteria for identification of oligodendrocytes. $\times 100$.

Figure 4.14

Indirect immunofluorescent photomicrograph of a primary mixed glial cell culture at DIC 8. Staining was performed with rabbit anti-myelin basic protein primary antibody at 1:25 dilution and FITC-conjugated goat anti-rabbit secondary antibody at 1:100 (cf Figure 4.15). $\times 100$.

Figure 4.15

Phase contrast photomicrograph corresponding to the indirect immunofluorescent field shown in Figure 4.14. The characteristic phase-dark cells identified morphologically as oligodendrocytes were labeled with anti-myelin basic protein (anti-MBP) with approximately one-to-one correspondence. $\times 100$.

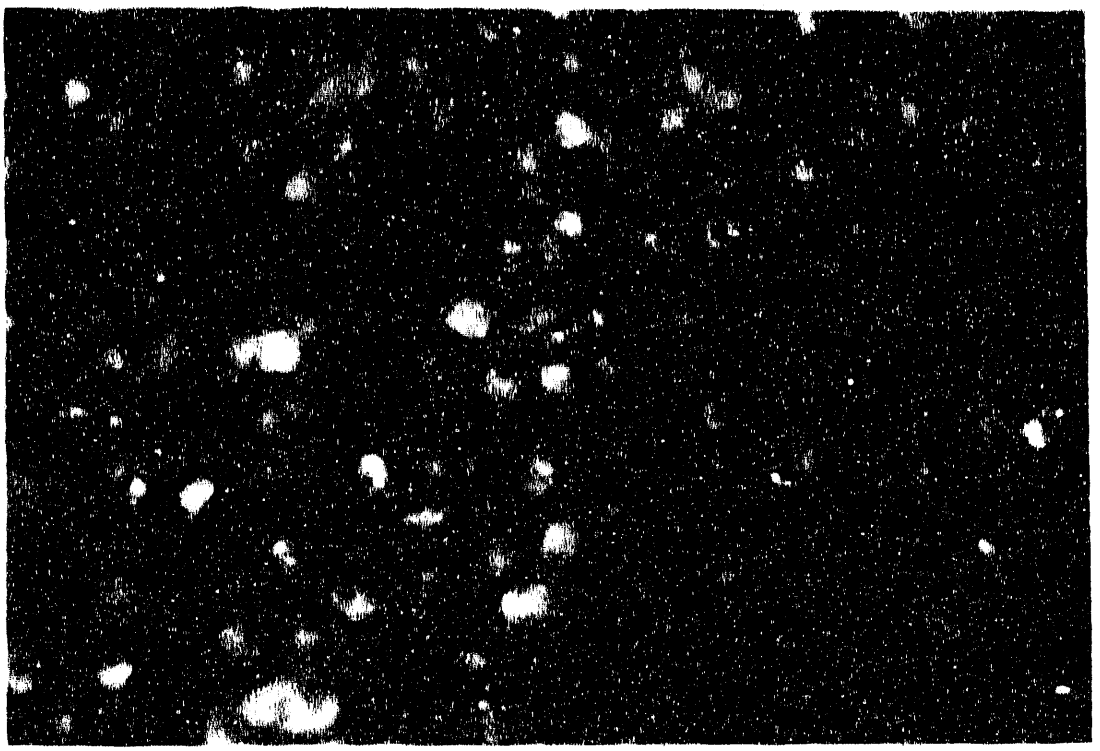

Figure 4.12

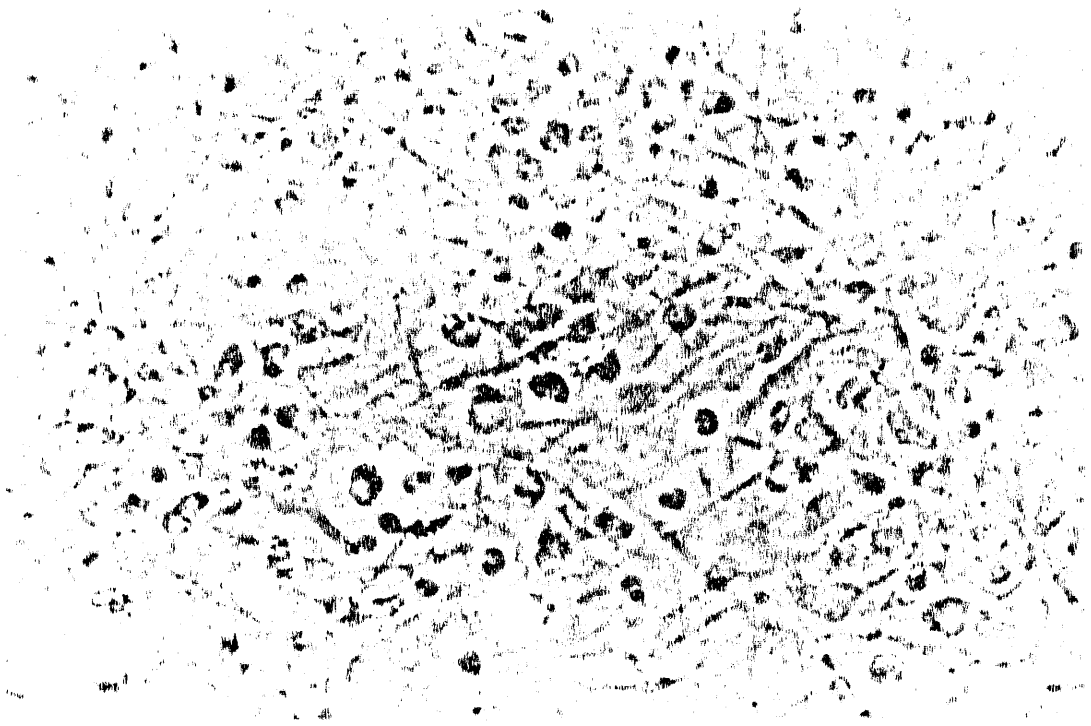

Figure 4.13

XBB 910-8661A

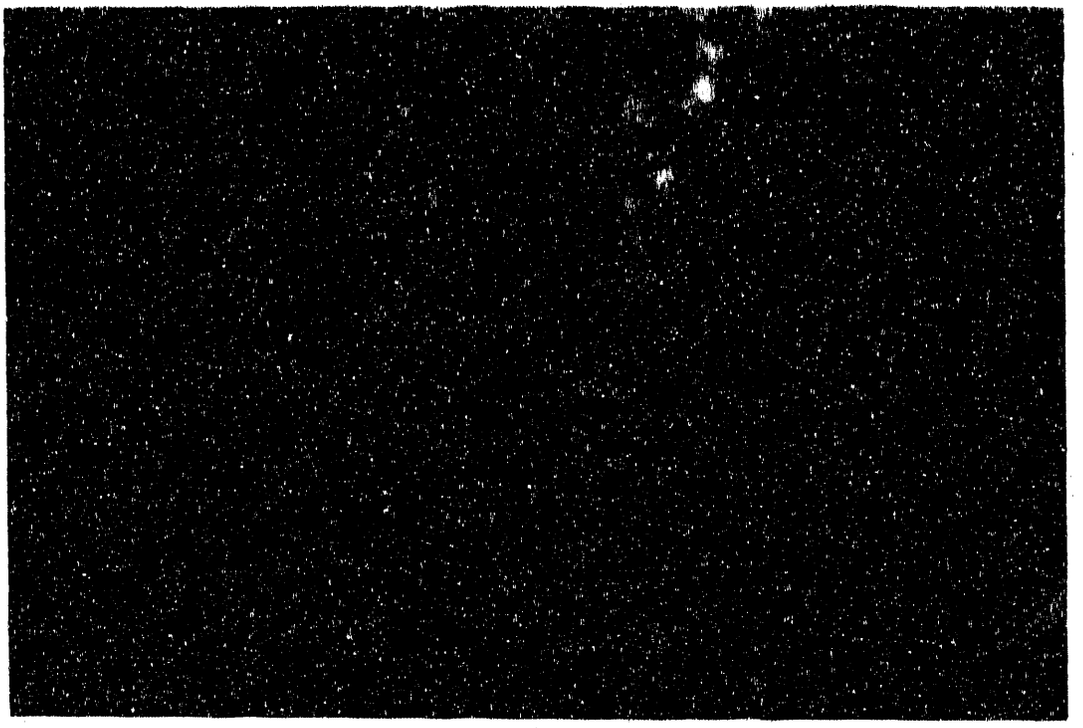

Figure 4.14

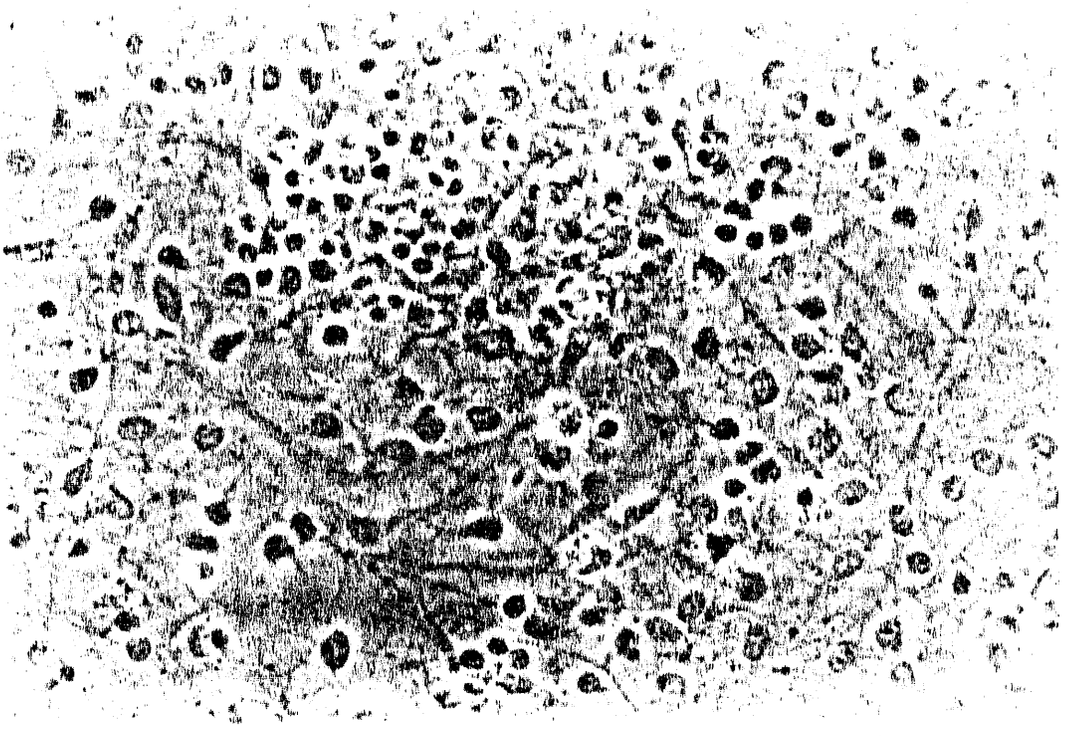

XBB 910-8669A

Figure 4.15

Figure 4.16

Indirect immunofluorescent photomicrograph of a primary mixed glial cell culture at DIC 7. Glial fibrillary acidic protein (GFAP) is an intermediate filament located in the cytoplasm of astrocytes which manifests an immunostaining pattern quite different from that seen with membrane antigens, such as GC and MBP (cf Figures 4.12 and 4.14). Staining was performed with rabbit anti-GFAP primary antibody at 1:50 dilution and FITC-conjugated goat anti-rabbit secondary antibody at 1:100 (cf Figure 4.17). $\times 25$.

Figure 4.17

Phase contrast photomicrograph corresponding to the indirect immunofluorescent field shown in Figure 4.16. $\times 25$.

Figure 4.18

Indirect immunofluorescent photomicrograph of a primary mixed glial cell culture at DIC 7. The linear immunofluorescent staining pattern is consistent with the filamentous nature of GFAP. Staining was performed with rabbit anti-GFAP primary antibody at 1:50 dilution and FITC-conjugated goat anti-rabbit secondary antibody at 1:100 (cf Figure 4.19). $\times 100$.

Figure 4.19

Phase contrast photomicrograph corresponding to the indirect immunofluorescent field shown in Figure 4.18. The astrocytes are densely clustered and have indistinct margins, precluding reliable cell matching with the paired immunofluorescent photomicrograph. $\times 100$.

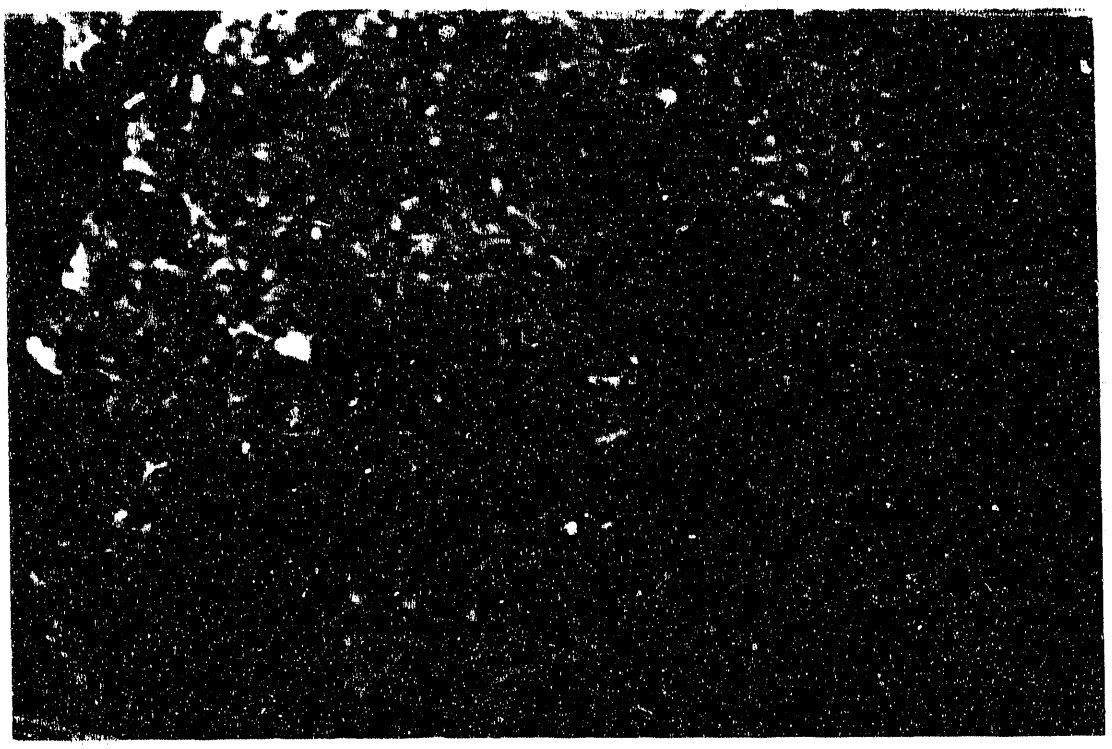

Figure 4.16

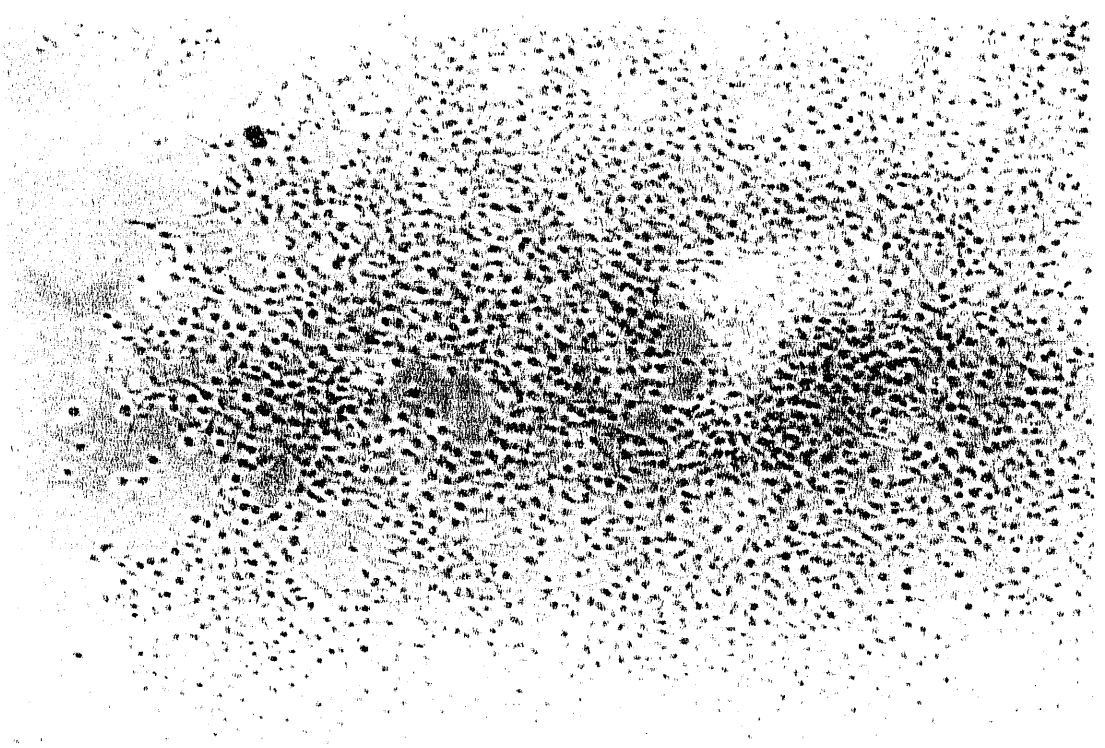

XBB 910-8169A

Figure 4.17

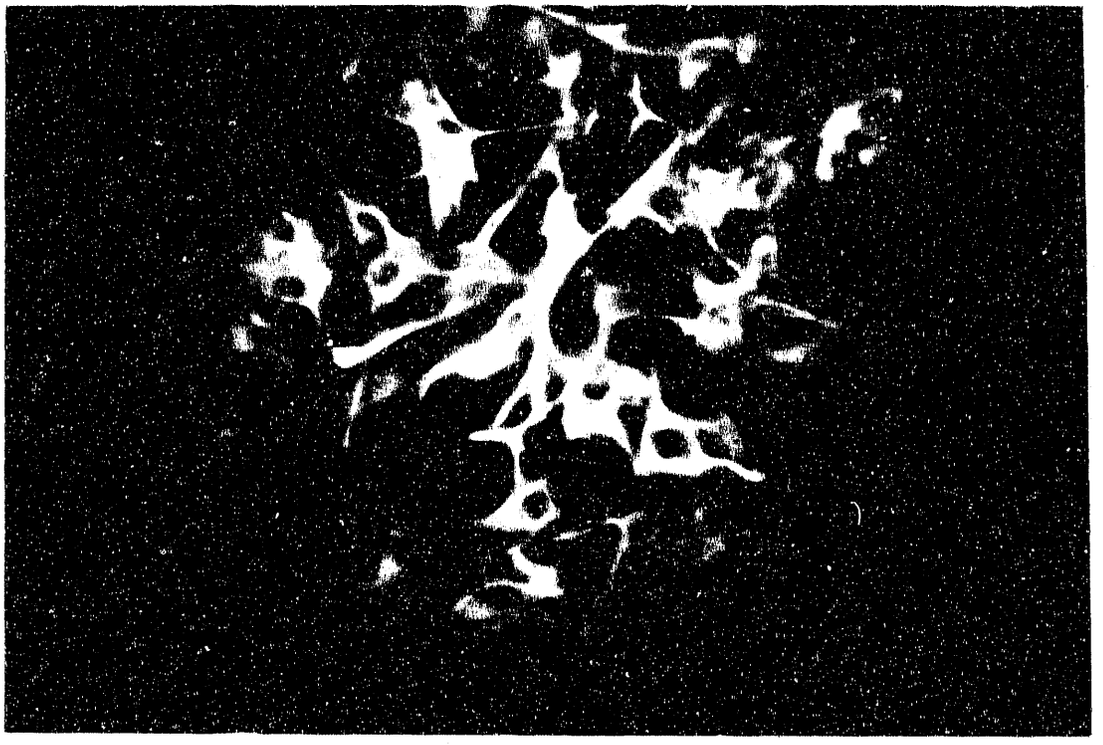

Figure 4.18

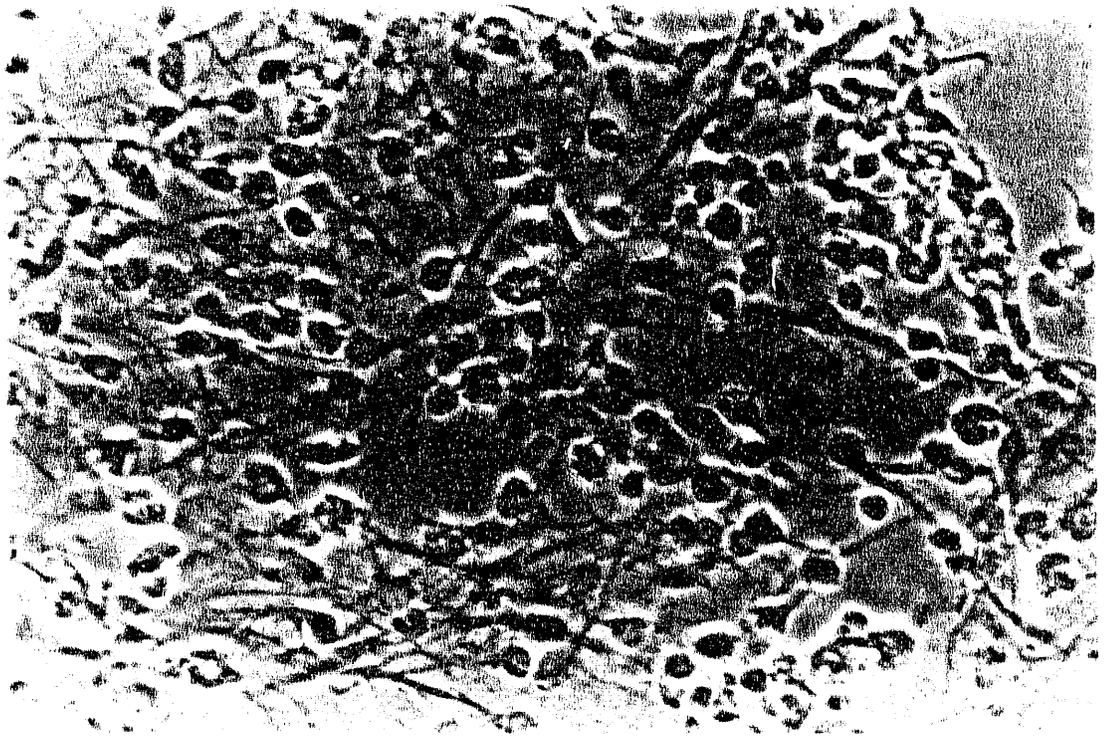

XBB 910-8172A

Figure 4.19

stained with anti-GC (Figures 4.21 and 4.22). In mixed glial cultures, the oligodendocyte processes did not appear nearly as extensive as those seen in the secondary cultures, much of the processes having apparently been intertwined with and obscured by the astrocytes. Secondary oligodendrocyte cultures also stained well with MBP (Figures 4.23 and 4.24). Secondary astrocyte cultures exhibited GFAP staining with very high specificity and sensitivity (Figures 4.25 – 4.30.)

4.4 FLUORESCENCE-ACTIVATED CELL SORTING

Fluorescence-activated cell sorting (FACS) techniques were applied to the evaluation of primary and secondary glial cultures to assess selected biochemical and histochemical properties of glial cell populations.

4.4.1 Tritiated Precursor Studies

Rat Glioma Tumor Cell Cultures

A rat glioma cell clone (9-L [73]) was prepared for FACS evaluation (as described in Sections 3.2.3, 3.3.4 and 3.3.6) to evaluate the feasibility of using FACS techniques to quantify the cellular incorporation of tritiated precursors. The 9-L glioma culture consisted of actively dividing tumor cells that were expected to incorporate tritiated thymidine reliably, and therefore this clone represented a model system for comparison with other cell populations. After incubation with tritiated thymidine for 6 h, approximately 2.0×10^5 tumor cells were sorted by FACS for each of a series of cultures. The tumor cell nuclei were stained with propidium iodide, and characteristic propidium-iodide fluorescence signals were used to trigger counting and sorting of tumor cells. The net tritium incorporation (after correcting for background radioactivity) and net tritium incorporation per tumor cell are shown in Table 4.1 as a function of tritiated thymidine concentra-

Figure 4.20

Indirect immunofluorescent photomicrograph of a primary mixed glial cell culture at DIC 7. When concentrated anti-GFAP was used as a primary antibody, a fine reticular pattern was demonstrated in the cytoplasm. Staining was performed with rabbit anti-GFAP primary antibody at 1:8 dilution and FITC-conjugated goat anti-rabbit secondary antibody at 1:100. $\times 100$.

Figure 4.21

Indirect immunofluorescent photomicrograph of a secondary oligodendrocyte-enriched culture at DIC 11. Anti-GC labeling is apparent in the fine processes extending from the cell soma, and fainter labeling is seen in adjacent structures. Staining was performed with rabbit anti-GC primary antibody at 1:100 dilution and FITC-conjugated goat anti-rabbit secondary antibody at 1:100 (cf Figure 4.22). $\times 100$.

Figure 4.22

Phase contrast photomicrograph corresponding to the indirect immunofluorescent field shown in Figure 4.21. $\times 100$.

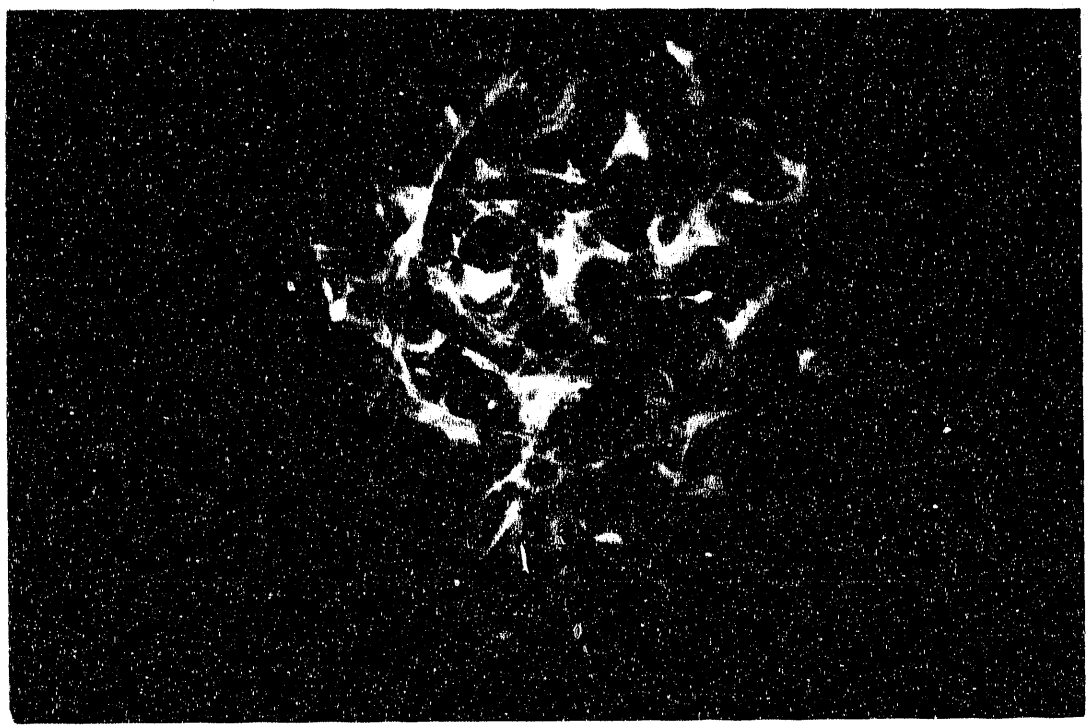

XBB 910-8166

Figure 4.20

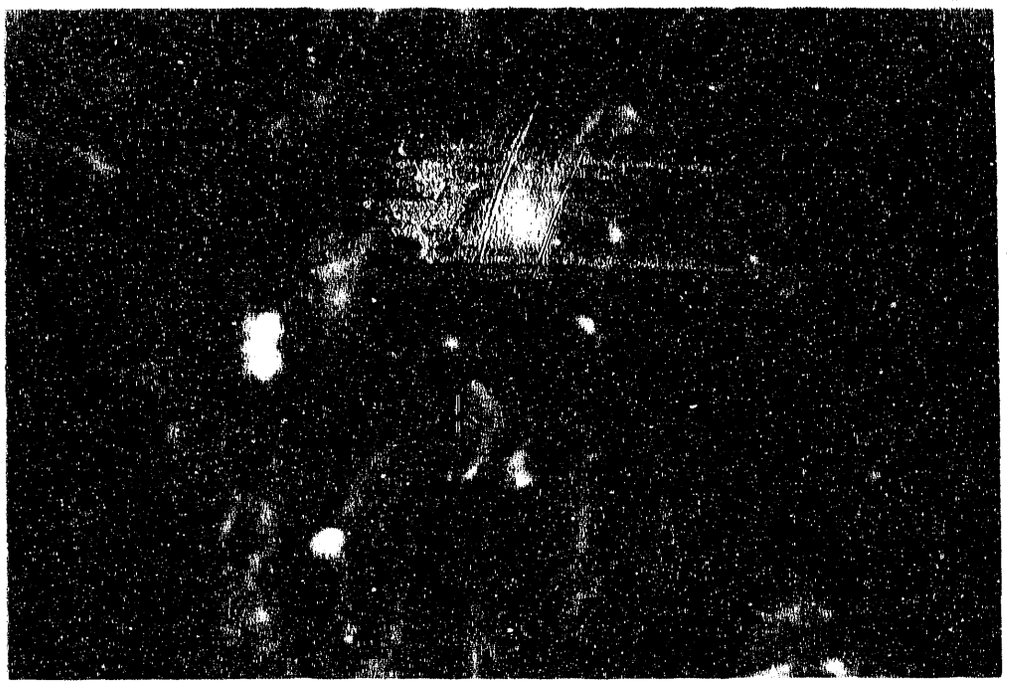

Figure 4.21

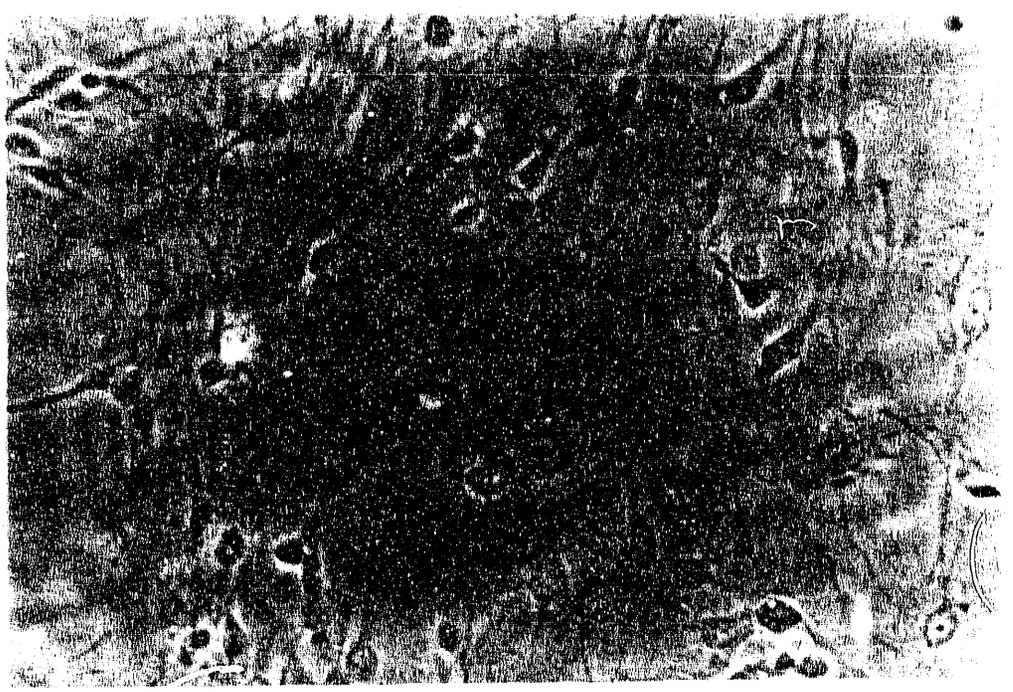

XBB 910-8677B

Figure 4.22

Figure 4.23

Indirect immunofluorescent photomicrograph of a secondary oligodendrocyte-enriched culture at DIC 10. Staining was performed with rabbit anti-MBP primary antibody at 1:50 dilution and FITC-conjugated goat anti-rabbit secondary antibody at 1:100 (cf Figure 4.24). ×100.

Figure 4.24

Phase contrast photomicrograph corresponding to the indirect immunofluorescent field shown in Figure 4.23. The characteristic phase-dark cells identified morphologically as oligodendrocytes were labeled with anti-MBP with approximately one-to-one correspondence. ×100.

Figure 4.25

Indirect immunofluorescent photomicrograph of a secondary astrocyte-enriched culture at DIC 29. Staining was performed with rabbit anti-GFAP primary antibody at 1:100 dilution and FITC-conjugated goat anti-rabbit secondary antibody at 1:100 (cf Figure 4.26). ×25.

Figure 4.26

Phase contrast photomicrograph corresponding to the indirect immunofluorescent field shown in Figure 4.25. ×25.

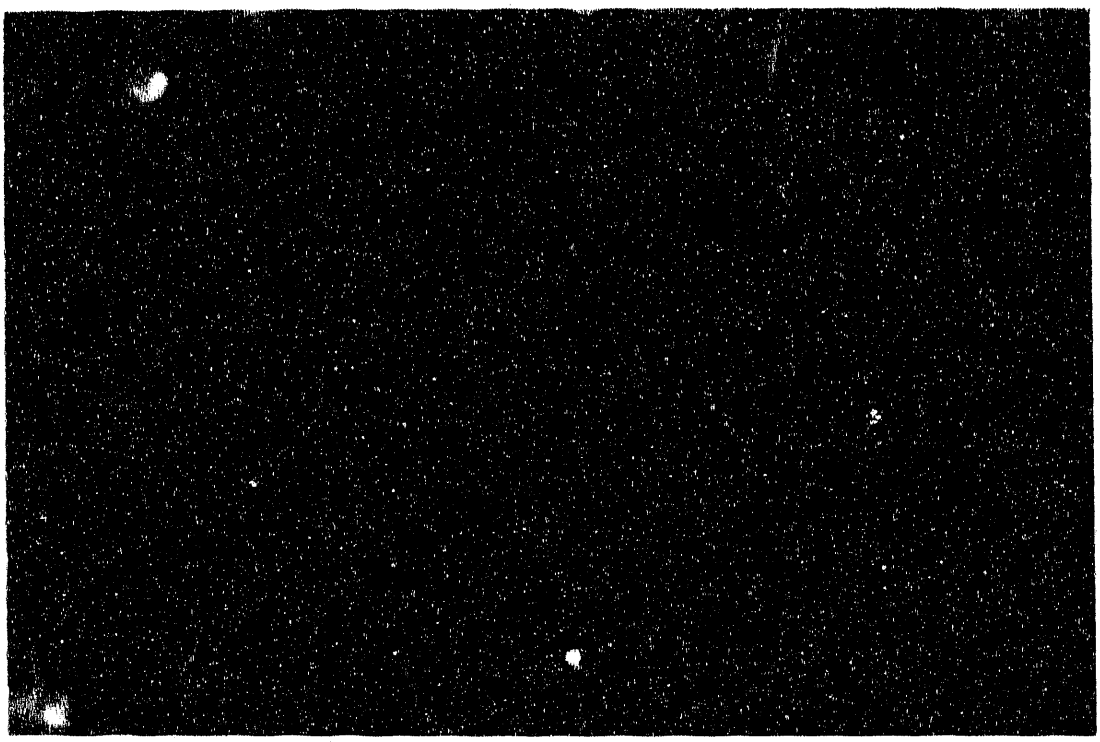

Figure 4.23

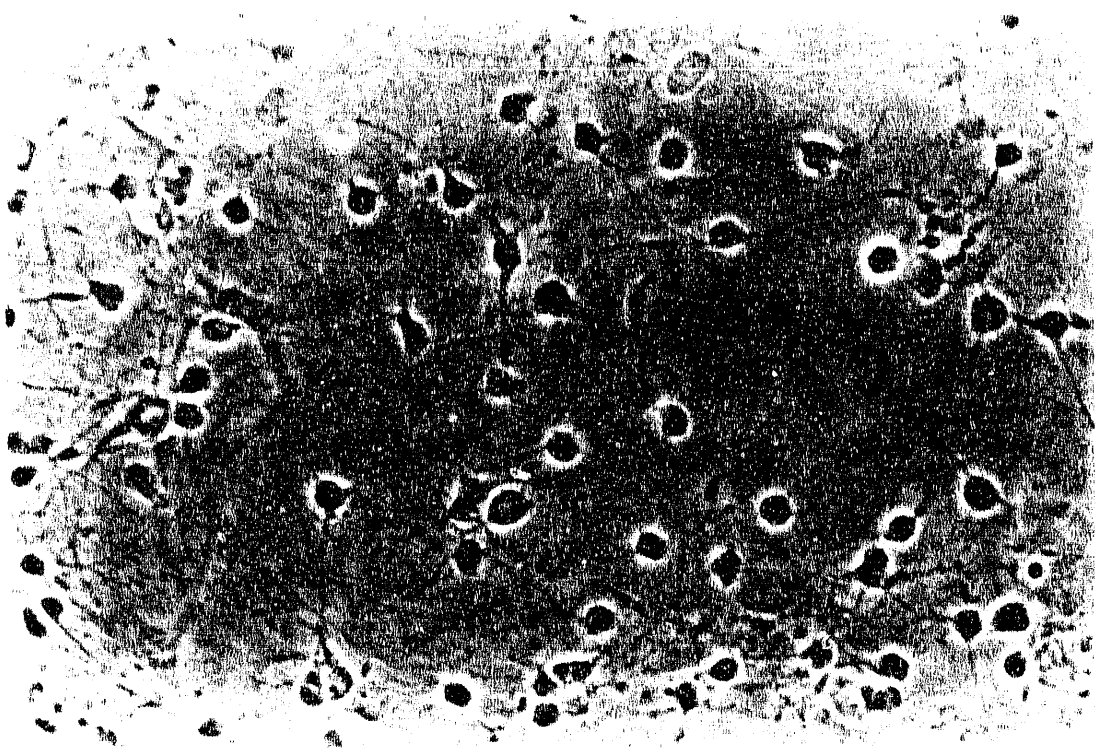

XBB 910-8665A

Figure 4.24

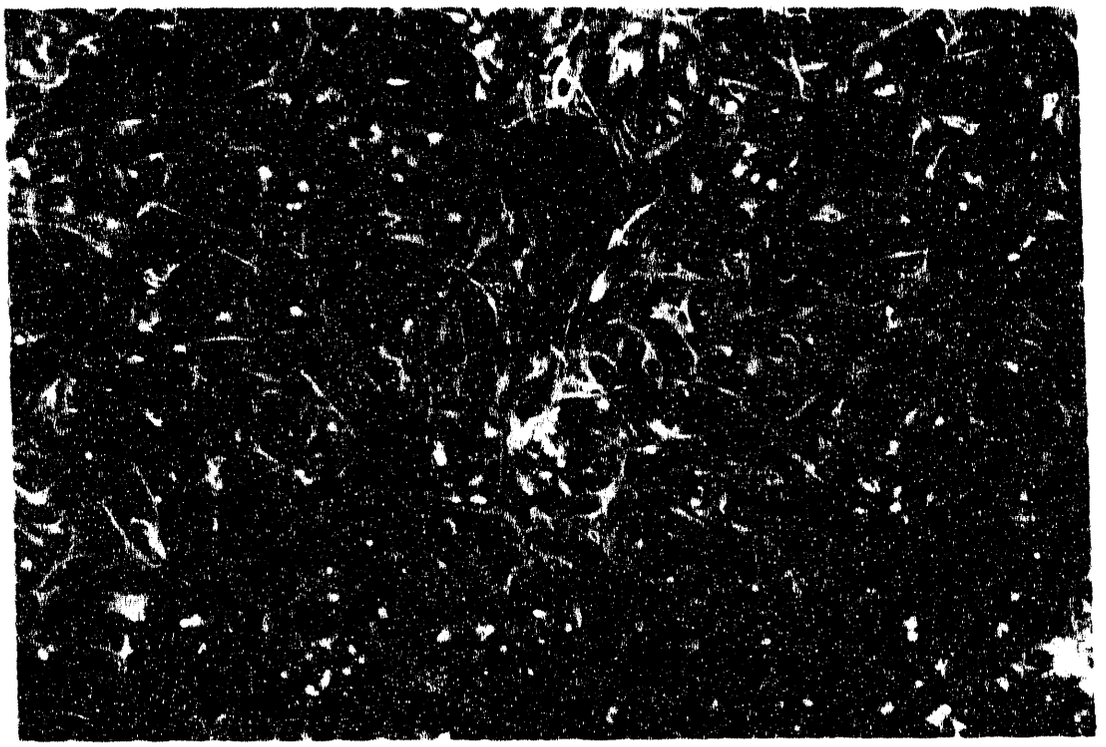

Figure 4.25

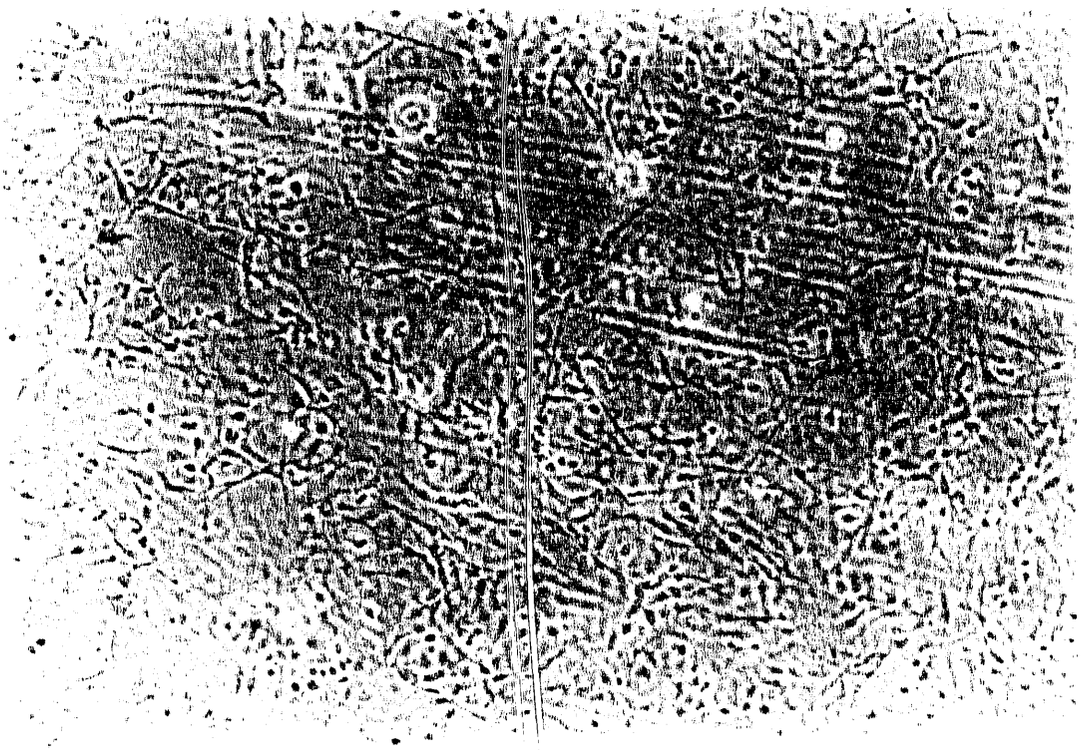

Figure 4.26

XBB 910-8671A

Figure 4.27

Indirect immunofluorescent photomicrograph of a secondary astrocyte-enriched culture at DIC 29. The elongated processes of the astrocytes show strong labeling with anti-GFAP. Staining was performed with rabbit anti-GFAP primary antibody at 1:100 dilution and FITC-conjugated goat anti-rabbit secondary antibody at 1:100 (cf Figure 4.28). $\times$100.

Figure 4.28

Phase contrast photomicrograph corresponding to the indirect immunofluorescent field shown in Figure 4.27. $\times$100.

Figure 4.29

Indirect immunofluorescent photomicrograph of a secondary astrocyte-enriched culture at DIC 29. The cytoplasmic intermediate filaments label strongly with anti-GFAP. Staining was performed with rabbit anti-GFAP primary antibody at 1:100 dilution and FITC-conjugated goat anti-rabbit secondary antibody at 1:100 (cf Figure 4.30). $\times$100.

Figure 4.30

Phase contrast photomicrograph corresponding to the indirect immunofluorescent field shown in Figure 4.29. $\times$100.

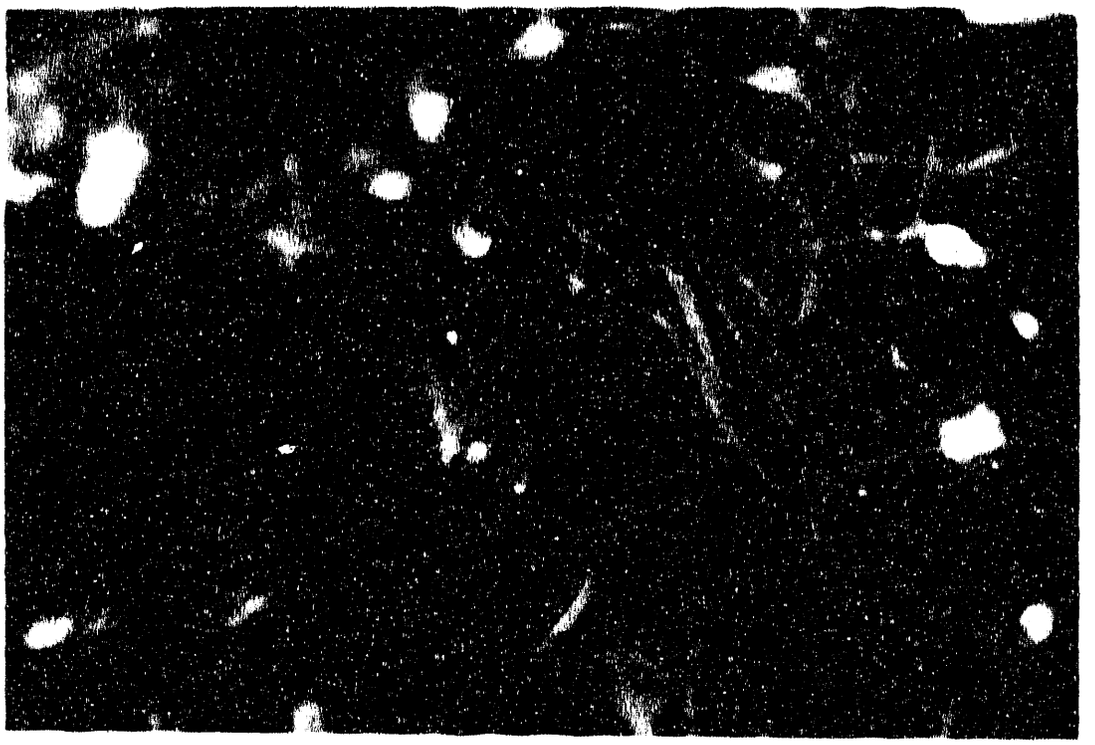

Figure 4.27

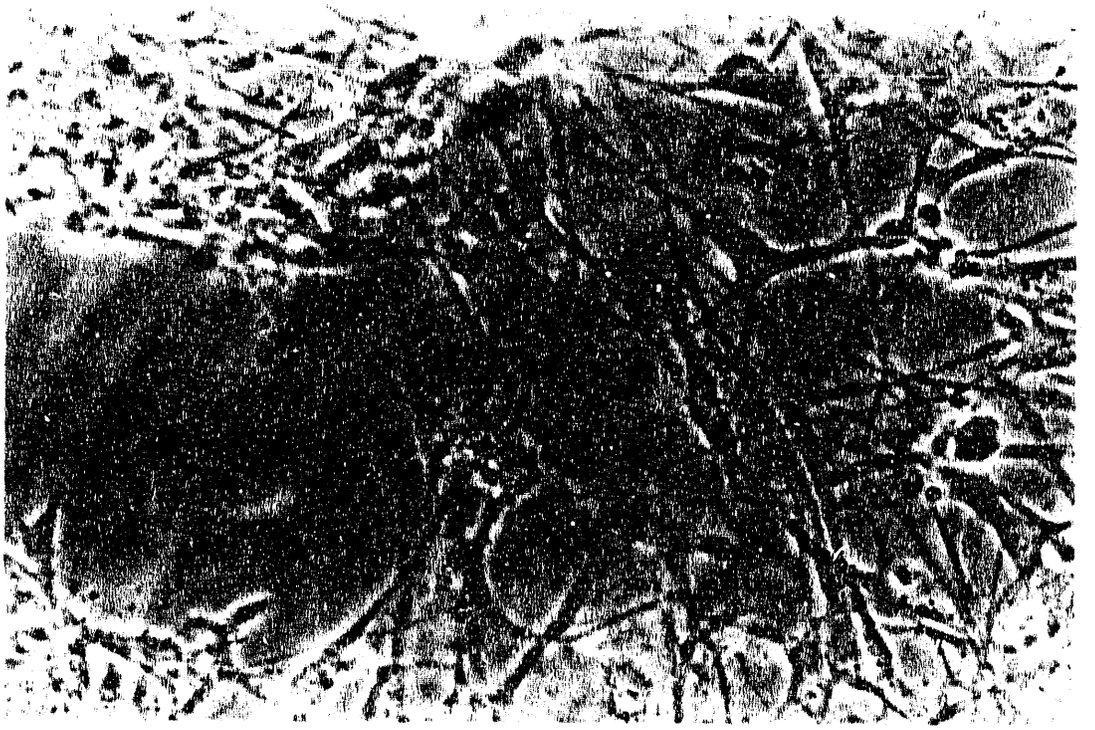

XBB 910-8677A

Figure 4.28

Figure 4.29

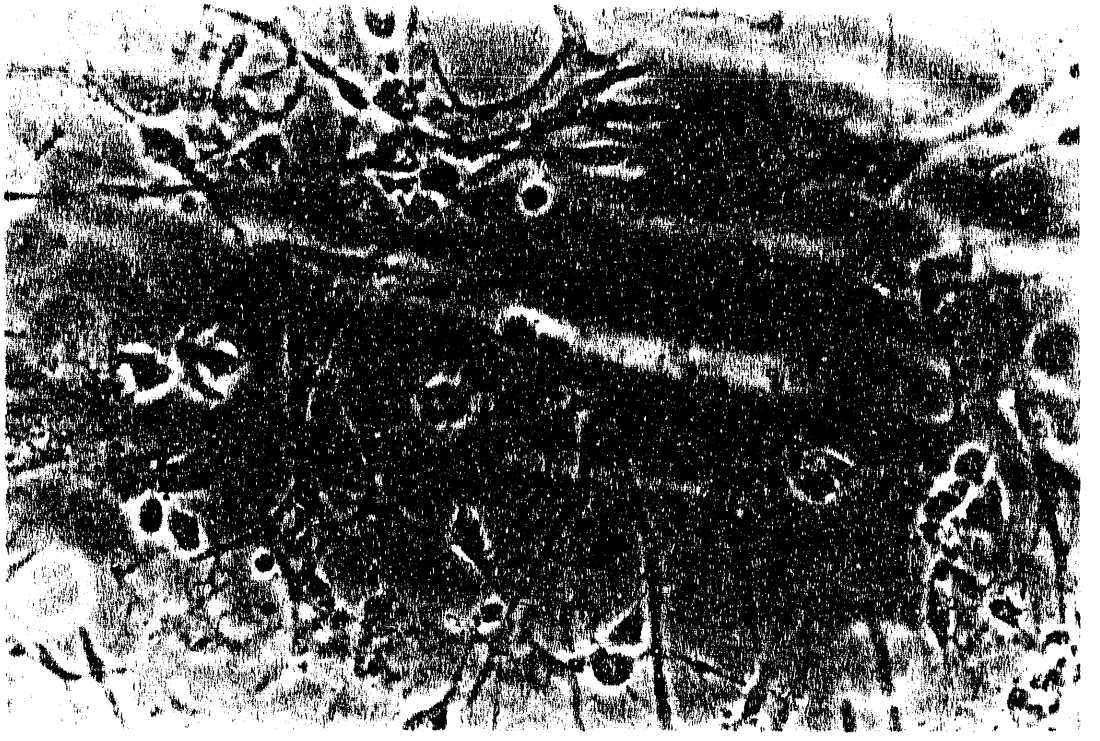

Figure 4.30

XBB 910-8673A

tion in the media. Labeled precursor incorporation was found to be detectable at all thymidine concentrations tested and was seen to increase with thymidine concentration. These findings were taken to confirm the feasibility of using FACS techniques to analyze tritiated precursor incorporation in glial cell populations.

TABLE 4.1

Tritiated Thymidine Incorporation in 9L-Glioma Cells (Propidium-Iodide Sorted)

Specimen No.	[^{3}H][b]	FACS[a] Events ($\times 10^5$)	Net DPM[c]	Net DPM/FACS Event ($\times 10^{-4}$)
1	0 μCi	2.01	0	–
2	0 μCi	2.01	0	–
3	1 μCi	2.02	56.1	2.78
4	1 μCi	2.02	29.0	1.43
5	2 μCi	2.01	41.6	2.07
6	2 μCi	2.01	39.4	1.96
7	4 μCi	2.01	165	8.21
8	4 μCi	2.00	119	5.97
9	8 μCi	2.03	520	25.6
10	8 μCi	2.01	719	35.7

[a]FACS = fluorescence-activated cell sorting
[b]μCi ^{3}H-thymidine per 3.5 ml flask
[c]Net DPM = (total disintegrations/min [DPM]) - (background DPM [here, 51.87])

Mixed Glial Cultures

Initial FACS experiments with glial cell cultures were performed to evaluate oligodendrocyte incorporation of specific tritiated precursors. Preliminary studies were performed to determine optimal settings for the FACS fluorescence

channels; a linear fluorescence scale was used initially. Mixed glial cultures were prepared for FACS in three different manners: (1) unstained; (2) nonspecific staining (fluorescent secondary antibody only); and (3) specific staining (indirect immunofluorescent staining against GC). The distribution of FACS events according to fluorescence channels is shown in Table 4.2. Since high-fluorescence intensity was presumed to represent specific staining for oligodendrocytes ("GC-positive" cells), it was tentatively concluded that fluorescence-channel settings of 103–255 would falsely identify 4.4% of GC-negative cells as being GC-positive, and that channel settings of 121–255 would falsely identify 1.2% of GC-negative cells as being GC-positive. Given these assumptions, a series of experiments was conducted to assess galactose incorporation in oligodendroglial cells.

TABLE 4.2

Linear Fluorescence-Channel Characterization (Mixed Glial Cell Cultures)

Fluorescence Channels	FACS Events[a] No Staining	Nonspecific Staining[b]	Specific Staining[c]
121–255	0 (0%)	154 (1.2%)	3,268 (12%)
103–255	0 (0%)	547 (4.4%)	3,879 (14%)
22–255	28,653	12,334	27,275

[a]FACS = fluorescence-activated cell sorting. For each category of cell staining, FACS events bracketed by fluorescence channels shown are also given as percent of total FACS events (i.e., channels 22–255).
[b]Fluorescent secondary antibody only
[c]Primary antibody to galactocerebroside and fluorescent secondary antibody

Tritiated galactose incorporation was determined in mixed glial cell cultures at DIC 7. After 70 h incubation with tritiated galactose concentrations

of 20 to 40 μCi per 7.5 ml flask, cell suspensions stained for GC were evaluated by FACS (Table 4.3). Using the fluorescence channel settings determined as described above, "GC-positive" oligodendrocytes (i.e., channels 103–255) were found to incorporate tritiated galactose similarly or somewhat less well than "GC-negative" astrocytes (i.e., channels 001-102). When more stringent criteria were used to identify GC-positive cells (i.e., channels 121–255), tritium incorporation per GC-positive cell (i.e., DPM/FACS event) was not enhanced. These findings appeared to suggest that the majority of tritiated galactose incorporation found in this experiment was utilized for purposes other than structural incorporation into the myelin membrane (likely, as a cellular energy source).

TABLE 4.3

Tritiated Galactose Incorporation in Mixed Glial Cells

Specimen No.	[^{3}H][c]	Fluorescence Channels	FACS[a] Events ($\times 10^3$)	Net DPM[b] ($\times 10^3$)	Net DPM/ FACS Event
1	20 μCi	103–255	69.3	9.60	0.14
		001–102	269	37.6	0.14
2	20 μCi	103–255	78.5	7.19	0.09
		001–102	535	81.4	0.15
3	40 μCi	103–255	94.7	21.5	0.23
		001–102	343	116	0.34
4	40 μCi	121–255	59.7	10.5	0.18
		001–120	441	107	0.24

[a]FACS = fluorescence-activated cell sorting
[b]Net DPM = (total disintegrations/min [DPM]) - (background DPM [here, 54.35])
[c]μCi ^{3}H-galactose per 7.5 ml flask

In order to evaluate the structural incorporation of tritiated galactose into the myelin membrane, a precursor "chase" experiment was conducted. Glial cells

at DIC 7 were incubated in tritiated medium for 24 h, and then incubated in normal medium for another 24 h to permit any galactose not structurally incorporated to be dissipated. The cell suspensions were stained for GC and evaluated by FACS (Table 4.4). Using the fluorescence channel settings previously described, however, no significant tritium incorporation could be ascertained in either oligodendrocyte or astrocyte populations.

TABLE 4.4

Tritiated Galactose Incorporation in Mixed Glial Cells (Following 24-hour "Wash-Out")

Specimen No.	$[^3H]^b$	Fluorescence Channels	FACS[a] Events ($\times 10^3$)	Net DPM[c]
1	10 μCi	103–255	10.1	16.0
		001–102	12.8	14.1
2	10 μCi	103–255	62.6	24.4
		001–102	83.8	118
3	10 μCi	103–255	3.90	2.58
		001–102	23.6	27.7
4	10 μCi	103–255	7.80	-4.33
		001–102	53.2	47.7

[a]FACS = fluorescence-activated cell sorting
[b]μCi ^{3}H-galactose per 7.5 ml flask
[c]Net DPM = (total disintegrations/min [DPM]) - (background DPM [here, 62.10])

When logarithmic fluorescence scales were used in FACS procedures, discrete glial cell populations were sorted with much improved accuracy (see Section 4.4.2). This technique was used to evaluate thymidine incorporation in mixed glial cultures. After incubation with tritiated thymidine for 24 h, GC-

stained cultures at various DIC were sorted and tritium incorporation measured for GC-positive oligodendrocytes and GC-negative astrocytes (Table 4.5). Net tritium uptake per FACS event was used as an index of thymidine incorporation. Oligodendrocytes did not incorporate measureable quantities of thymidine at any DIC or thymidine concentration tested, suggesting that proliferative activity in this population was minimal. The astrocyte population, however, incorporated thymidine readily at all DIC examined. Thymidine uptake in astrocytes at DIC 7 increased with increasing thymidine concentration in the medium. Low thymidine incorporation in one astrocyte sample (specimen 7 in Table 4.5) may have been due to the astrocytes in that culture having attained confluence prior to the beginning of the experiment and no longer being in a proliferating state; this conclusion was supported by the very high astrocyte numbers found in that specimen. Based on these findings, no further investigation of thymidine uptake in oligodendrocytes was carried out. However, this approach appeared promising for future investigation of the astrocyte population.

TABLE 4.5

Tritiated Thymidine Incorporation in Mixed Glial Cells

Spec. No.	DIC[c]	[^{3}H][d]	Fluorescence Channels	FACS[a] Events ($\times 10^3$)	Net DPM[b] ($\times 10^2$)	Net DPM/FACS Event ($\times 10^{-2}$)
1	7	0 μCi	135–250	2.85	0.00	–
			001-134	85.2	0.06	–
2	7	20 μCi	135–250	2.74	0.04	–
			001-134	15.7	2.70	1.73
3	7	20 μCi	135–250	2.92	-0.01	–
			001-134	17.5	3.30	1.88
4	7	40 μCi	135–250	3.13	0.03	–
			001-134	40.5	9.83	2.43
5	7	40 μCi	135–250	4.01	0.04	–
			001-134	85.0	20.7	2.44
6	12	40 μCi	135–250	3.87	0.01	–
			001-134	119	12.3	12.3
7	12	40 μCi	135–250	4.24	0.07	–
			001-134	383	7.69	0.20
8	12	40 μCi	135–250	2.70	0.16	–
			001-134	33.7	8.97	2.66
9	15	0 μCi	135–250	3.12	0.02	–
			001-134	117	0.08	–
10	15	40 μCi	135–250	2.40	0.09	–
			001-134	122	28.7	2.35
11	15	40 μCi	135–250	3.80	0.12	–
			001-134	197	61.3	3.11

[a]FACS = fluorescence-activated cell sorting
[b]Net DPM = (total disintegrations/min [DPM]) - (background DPM [here, 51.45])
[c]DIC = day-in-culture at beginning of ^{3}H-thymidine exposure
[d]μCi ^{3}H-thymidine per 7.5 ml flask

4.4.2 Cell Population Studies

For the initial FACS experiments described in this dissertation cells were sorted according to fluorescence intensity displayed on a linear scale (see Section 4.4.1). When the FACS procedure was amended to use a logarithmic fluorescence scale, it was possible to define GC-positive and GC-negative populations of glial cells much more precisely. The preliminary findings with the amended technique are described briefly in this section.

Mixed Glial Cultures

Mixed glial cell cultures labeled with indirect immunofluorescent (FITC) staining against GC were represented by FACS by two distinct fluorescence peaks (Figure 4.31). The smaller high-fluorescence peak and the larger low-fluorescence peaks were considered to correspond to the oligodendrocyte and astrocyte populations, respectively. These populations were quantified readily by calculating the areas under the respective curves. GFAP-stained mixed cultures exhibited biphasic FACS patterns, comparable to GC-stained cultures; however, GFAP cultures generally had a larger high-fluorescence peak consistent with the larger astrocyte population.

Oligodendrocyte-Enriched Cultures

Oligodendrocyte-enriched secondary cultures and mixed glial primary cultures were labeled with indirect immunofluorescent staining against GC. The FACS pattern of the oligodendrocyte culture was a single peak in the high-fluorescence region, which was seen to match precisely with the high-fluorescence FACS peak of the mixed culture (Figure 4.32). This correspondence of FACS patterns confirmed the interpretation of high-fluorescence FACS events made during earlier FACS experiments.

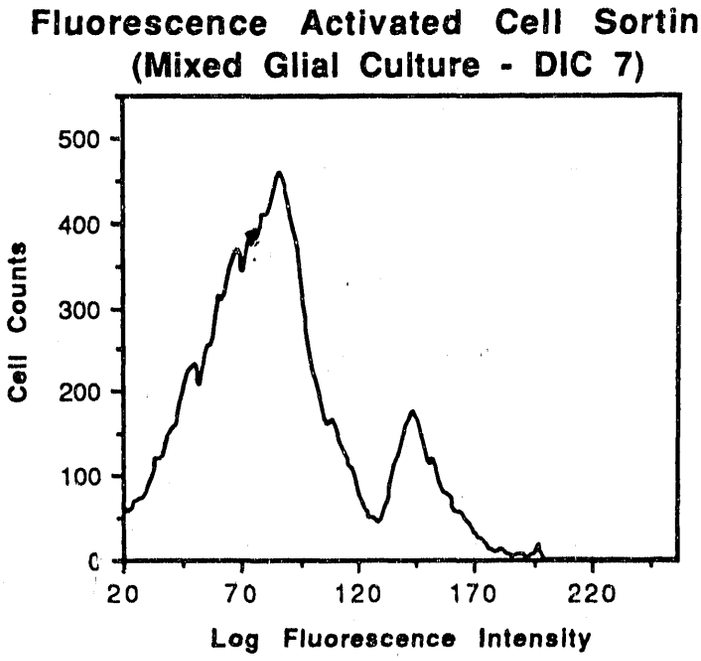

Figure 4.31. Fluorescence-activated cell sorting analysis for an unirradiated primary mixed glial cell culture at DIC 7, stained with anti-GC. The frequency histogram is plotted as a function of the logarithm of fluorescence intensity. Two distinct fluorescence peaks are seen. The smaller high-fluorescence peak reflects cells labeling specifically with anti-GC (i.e., oligodendrocytes); the larger low-fluorescence peak reflects cells with nonspecific staining and/or autofluorescent properties (e.g., cytochromes) and is considered to correspond to the astrocyte population (cf Figures 4.32 and 4.33).

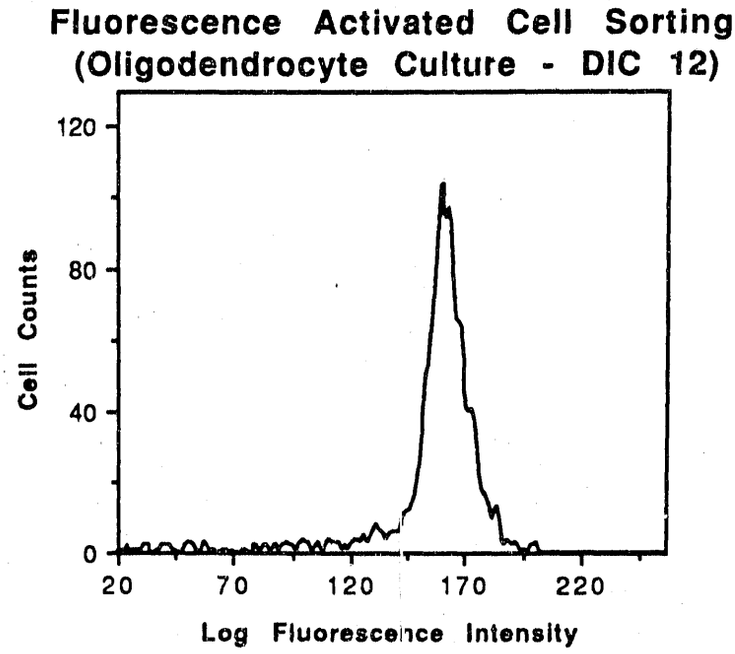

Figure 4.32. Fluorescence-activated cell sorting analysis for an unirradiated secondary oligodendrocyte-enriched cell culture at DIC 12, stained with anti-GC. The frequency histogram is plotted as a function of the logarithm of fluorescence intensity. A single high-fluorescence peak corresponds closely to the oligodendrocyte peak seen in mixed glial cultures (cf Figure 4.31).

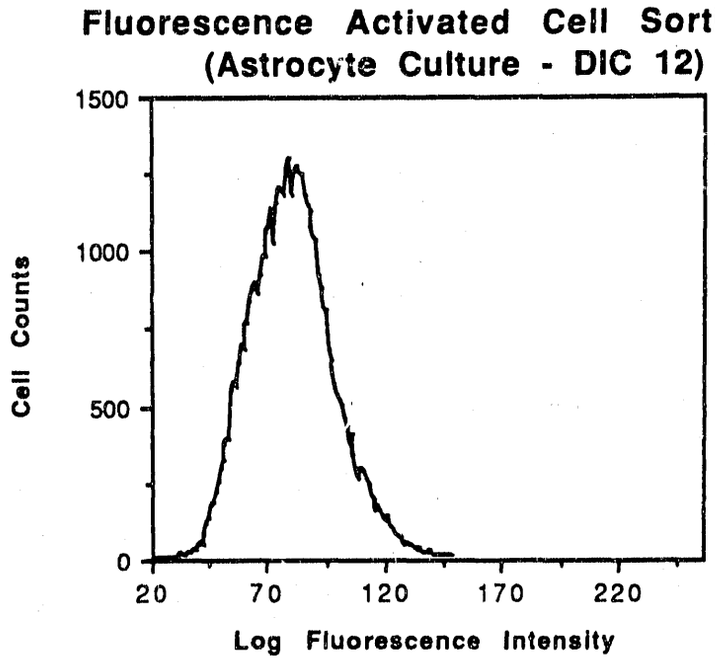

Figure 4.33. Fluorescence-activated cell sorting analysis for an unirradiated secondary astrocyte-enriched cell culture at DIC 12, stained with anti-GC. The frequency histogram is plotted as a function of the logarithm of fluorescence intensity. A single large low-fluorescence peak reflects cells with nonspecific staining and/or autofluorescent properties (e.g., cytochromes); this peak corresponds closely to the astrocyte peak seen in mixed glial cultures (cf Figure 4.31).

Astrocyte-Enriched Cultures

Secondary astrocyte cultures prepared concurrently with secondary oligodendrocyte and mixed glial cultures (as above) demonstrated complementary FACS patterns. GC-stained astrocyte cultures exhibited a single low-fluorescence peak, corresponding to the astrocyte peak described in the mixed glial cultures (Figure 4.33). This low-fluorescence peak was considered to represent nonspecific staining. When secondary astrocyte cultures were stained against GFAP, a single high-fluorescence peak was seen; this corresponded to the high-fluorescence peak in GFAP-stained mixed cultures.

4.5 BIOCHEMICAL EVALUATION

The biochemical endpoints selected as representative of the general metabolic condition of the glial cultures were MBP and total cellular protein. MBP is highly-specific to the oligodendrocyte membrane and immunochemical measurement of MBP correlates very well with synthesis of mature myelin *in vivo* [23]. Measurement of total cellular protein, though not specific for a given cell type, can be used reliably as an index of cell density in general and of the astrocyte population in particular. Astrocytes constitute the great majority of glial cells in primary mixed cultures at DIC 7, and preferential astrocyte proliferation results in progressively more heavily astrocyte-weighted cultures thereafter. Total protein measurements therefore strongly reflect the contribution of the astrocyte population.

Since quantitative biochemical analysis of MBP and total cellular protein required sacrificing the cultures at the DIC of interest, it was not possible to obtain serial data on individual cultures. These data were therefore accumulated by random sampling of groups of primary culture flasks at periodic intervals following the initial plating.

4.5.1 Myelin Basic Protein Synthesis

The results of six separate experiments with comparable initial plating conditions were pooled to determine the general pattern of MBP accumulation as a function of DIC (Figure 4.34). It was found that the concentration of MBP in culture increased very rapidly with DIC. Mean MBP values increased from 8 ng/ml at DIC 7 to 63 ng/ml at DIC 14 to 133 ng/ml at DIC 21 to 281 ng/ml at DIC 28.

4.5.2 Total Cellular Protein Synthesis

As was the case with analysis of MBP production (see Section 4.5.1), the pattern of total cellular protein synthesis was determined by random sampling of groups of primary culture flasks at weekly intervals. The results of six separate experiments with comparable initial plating conditions were pooled (Figure 4.35). It was found that the concentration of total protein in culture increased steadily with DIC. Mean total protein values increased from 148 μg/ml at DIC 7 to 237 μg/ml at DIC 14 to 378 μg/ml at DIC 21 to 612 μg/ml at DIC 28.

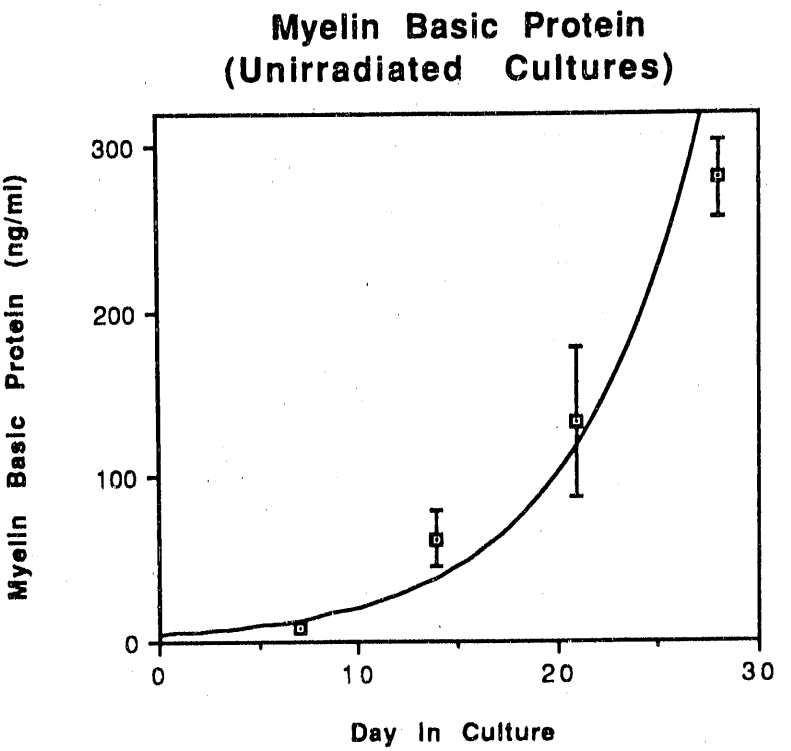

Figure 4.34. MBP levels (mean ± S.D.) in unirradiated primary mixed glial cultures are shown as a function of DIC. The results of six separate experiments with comparable initial plating conditions are pooled. MBP levels increase at a nearly exponential rate (solid line) from DIC 7 to DIC 28.

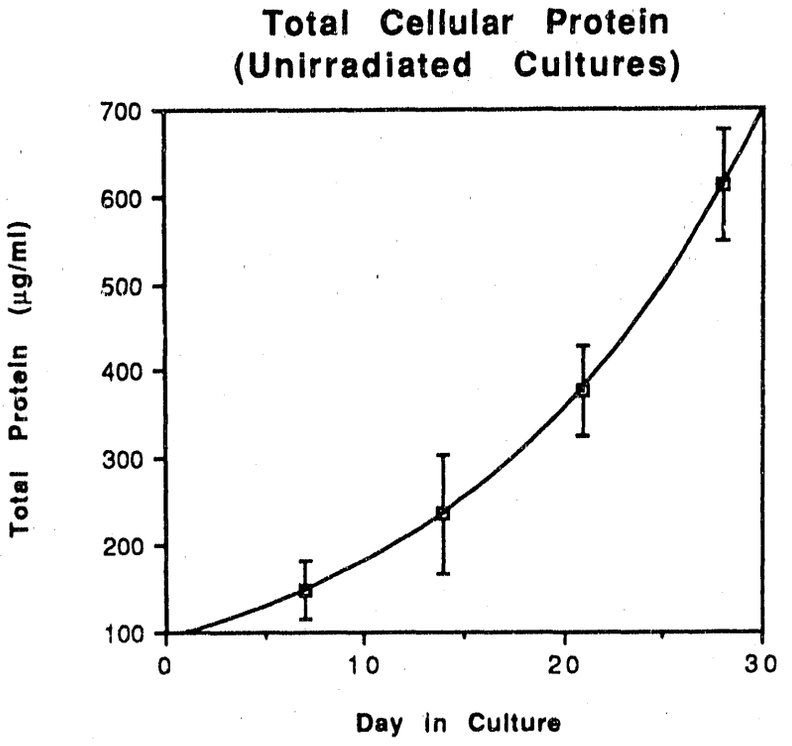

Figure 4.35. Total cellular protein levels (mean ± S.D.) in unirradiated primary mixed glial cultures are shown as a function of DIC. The results of six separate experiments with comparable initial plating conditions are pooled. Total protein levels increase at an exponential rate (solid line) from DIC 7 to DIC 28.

CHAPTER 5

RESULTS: IRRADIATED GLIAL CELL CULTURES

5.1 INTRODUCTION

In this chapter, the responses to ionizing radiation of the oligodendrocyte population *in vitro* and the myelination process are examined. Morphologic and biochemical findings in glial cell cultures are described qualitatively and quantitatively as a function of radiation dose and culture age. The oligodendrocyte response to total dose, dose rate and split-dose irradiation is characterized.

5.2 GLIAL CELL RESPONSE TO 225 kVp X-RAYS

Initial irradiation experiments were conducted with 225 kVp x-rays to determine the general response to irradiation of glial cell populations growing in culture, and of the oligodendrocyte population in particular. Preliminary studies were designed to establish the appropriate experimental range for radiation dose and optimal days-in-culture (DIC) for data collection. Phase contrast microscopy was used to evaluate the morphologic response of mixed glial cultures following irradiation at DIC 6. Cultures were randomly selected for irradiation with doses of 1, 2, 5, 10 and 30 Gy. Irradiated and unirradiated cultures were compared at DIC 7, 9, 12, 14, 19 and 21.

Definite morphologic changes were consistently demonstrated within 24 h following irradiation with single doses as low as 2 Gy, and marked changes were seen after 5 Gy (Figures 5.1–5.18). The population of phase-dark oligodendrocytes was markedly reduced in response to irradiation, and this response was maintained at least to DIC 19. These observations are illustrated most clearly by representative high-power phase contrast micrographs. However, the

Figure 5.1

Representative high-power (×100) phase contrast photomicrograph of an unirradiated primary mixed glial cell culture at DIC 7. Phase-dark oligodendrocytes overlie an astrocyte monolayer that has not yet reached confluence. (Cf Figure 5.2.)

Figure 5.2

A representative low-power (×25) phase contrast photomicrograph from the unirradiated primary mixed glial cell culture shown in Figure 5.1. Phase-dark astrocytes are plentiful and scattered heterogeneously throughout the field.

Figure 5.3

Representative high-power (×100) phase contrast photomicrograph of a primary mixed glial cell culture at DIC 7, 24 h following 2 Gy 225 kVp x-irradiation. Compared with unirradiated controls (cf Figure 5.1), fewer phase-dark oligodendrocytes are seen, and there are more interruptions in the astrocyte monolayer. (Cf Figure 5.4.)

Figure 5.4

A representative low-power (×25) phase contrast photomicrograph from the 2-Gy irradiated primary mixed glial cell culture shown in Figure 5.3.

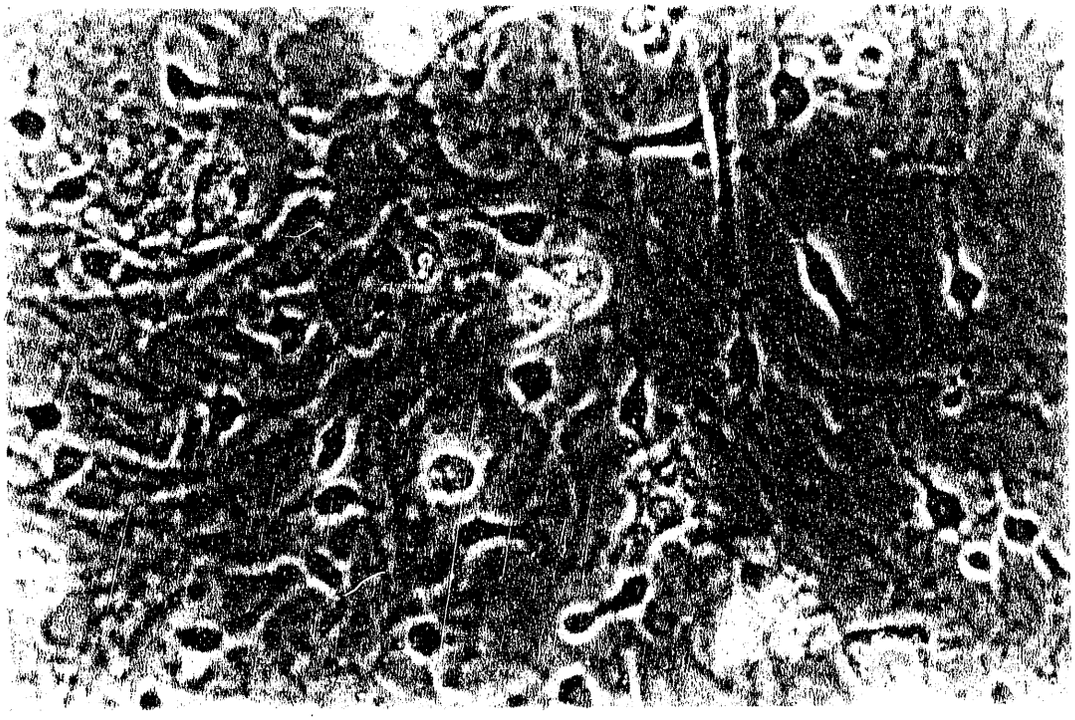

Figure 5.1

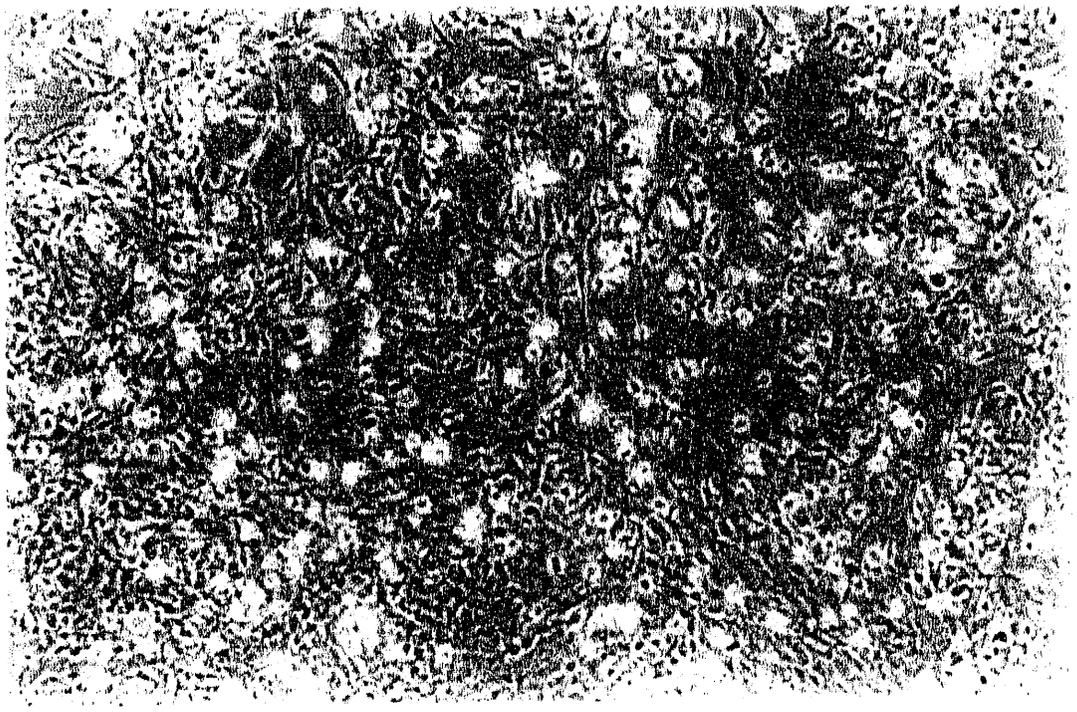

XBB 908-6575A

Figure 5.2

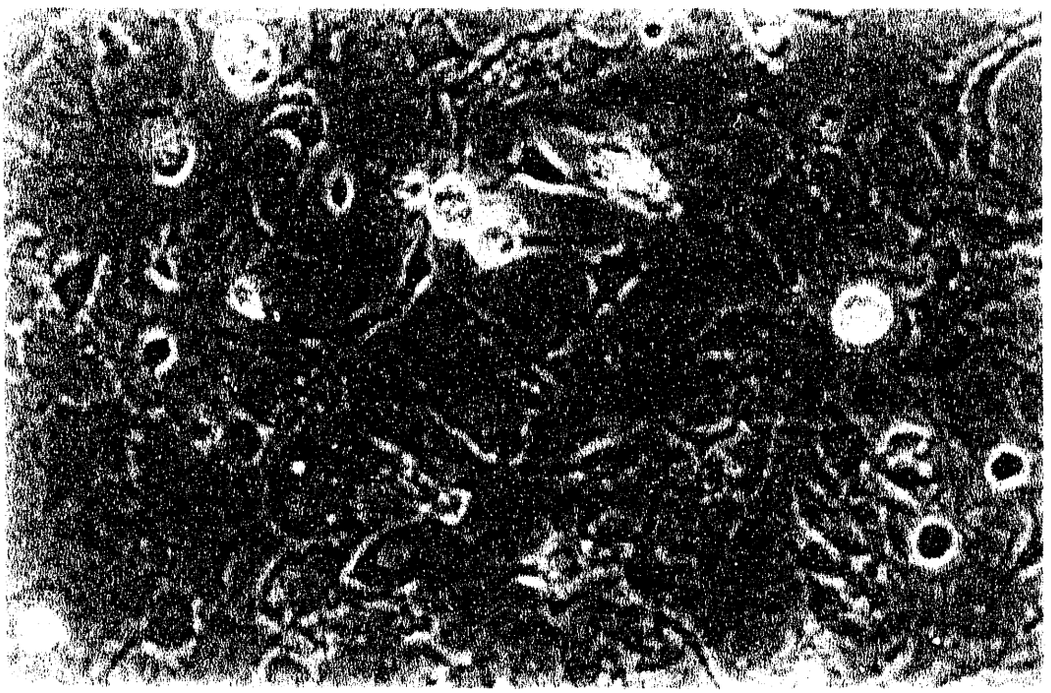

Figure 5.3

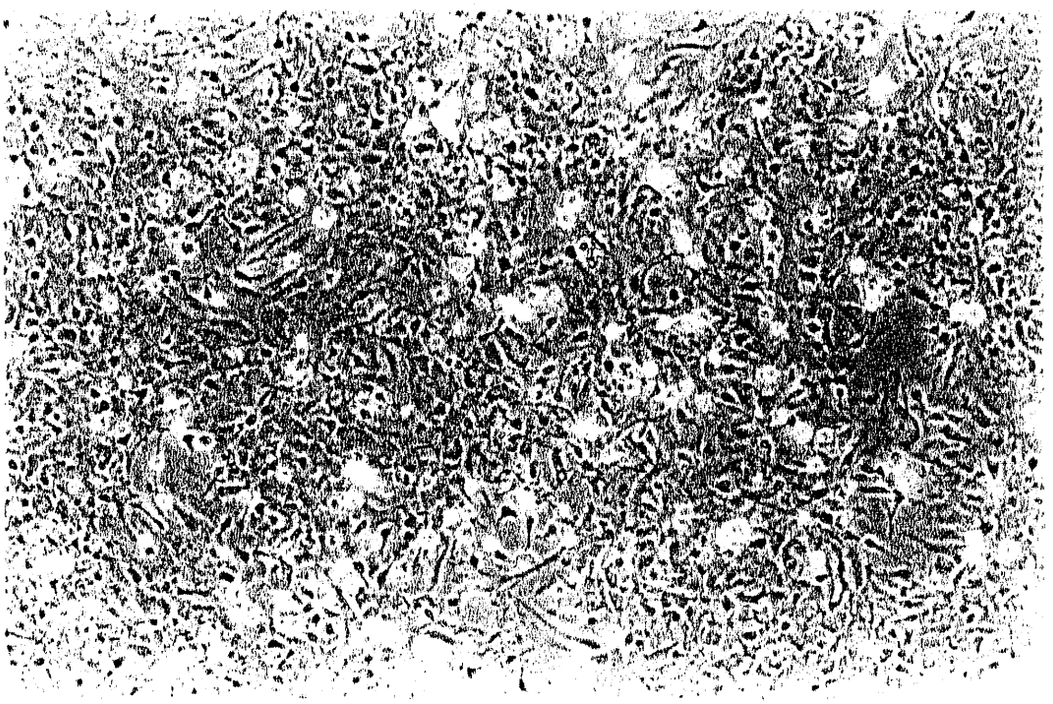

Figure 5.4

XBB 908-6579A

Figure 5.5

Representative high-power (×100) phase contrast photomicrograph of a primary mixed glial cell culture at DIC 7, 24 h following 5 Gy 225 kVp x-irradiation. Compared with unirradiated controls (cf Figure 5.1) and 2-Gy irradiated cultures (cf Figure 5.3), oligodendrocytes are scarce and the astrocyte monolayer is markedly damaged. (Cf Figure 5.6.)

Figure 5.6

A representative low-power (×25) phase contrast photomicrograph from the 5-Gy irradiated primary mixed glial cell culture shown in Figure 5.5. The degree of oligodendrocyte loss can be appreciated by comparison with unirradiated and 2-Gy irradiated cultures (Figures 5.2 and 5.4).

Figure 5.7

Representative high-power (×100) phase contrast photomicrograph of an unirradiated primary mixed glial cell culture at DIC 9. Phase-dark oligodendrocytes are more plentiful than at DIC 7 and they exhibit increased formation of cytoplasmic processes (cf Figure 5.1). The astrocyte monolayer is now fully confluent. (Cf Figure 5.8.)

Figure 5.8

A representative low-power (×25) phase contrast photomicrograph from the unirradiated primary mixed glial cell culture shown in Figure 5.7. Phase-dark oligodendrocytes are plentiful and distributed throughout the field.

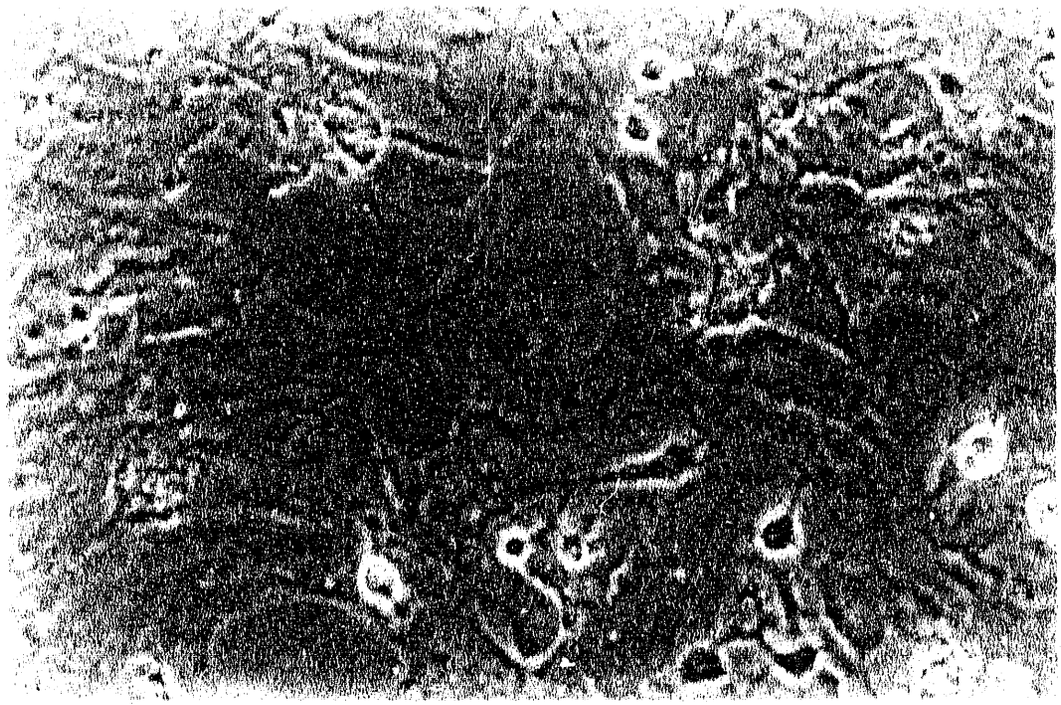

Figure 5.5

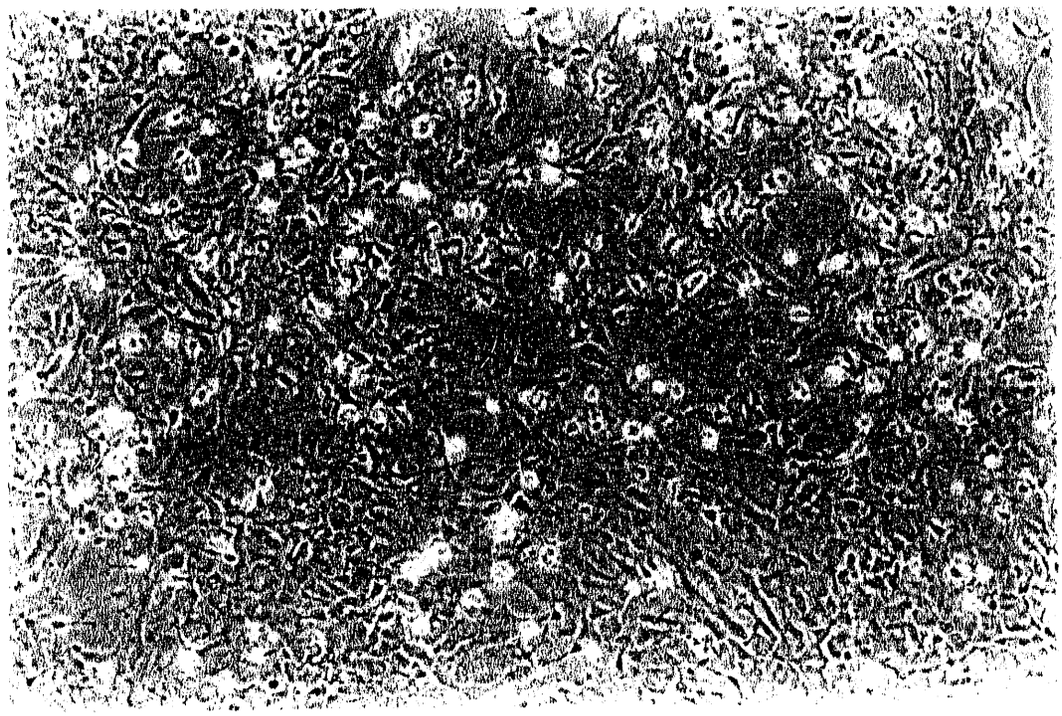

XBB 908-6581A

Figure 5.6

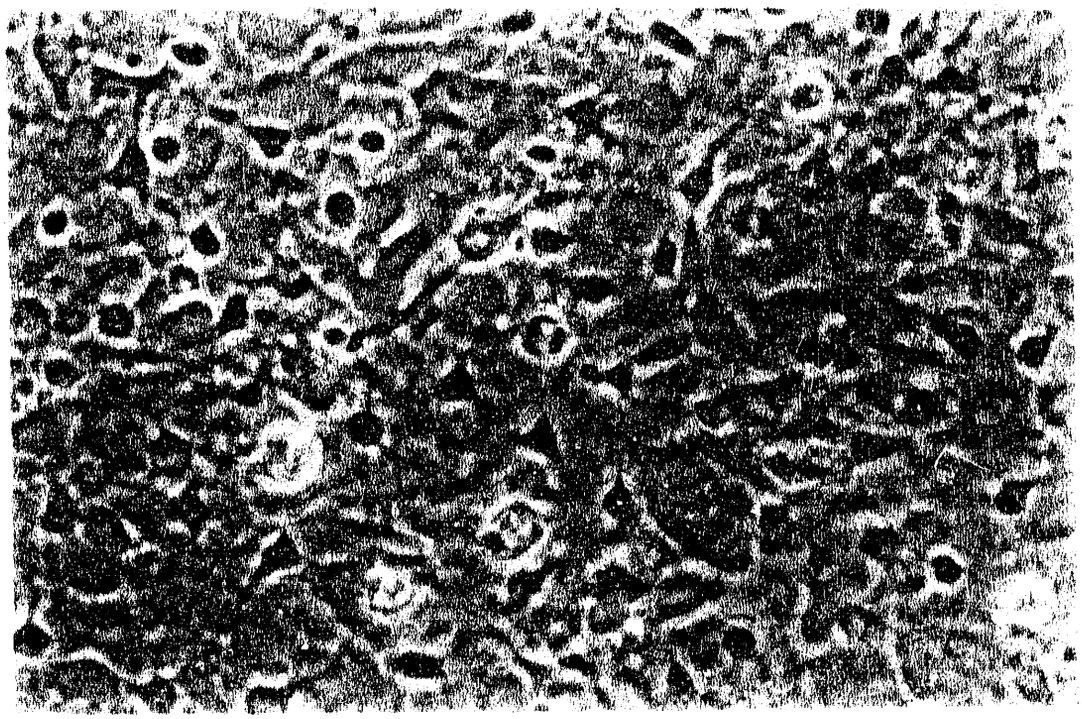

Figure 5.7

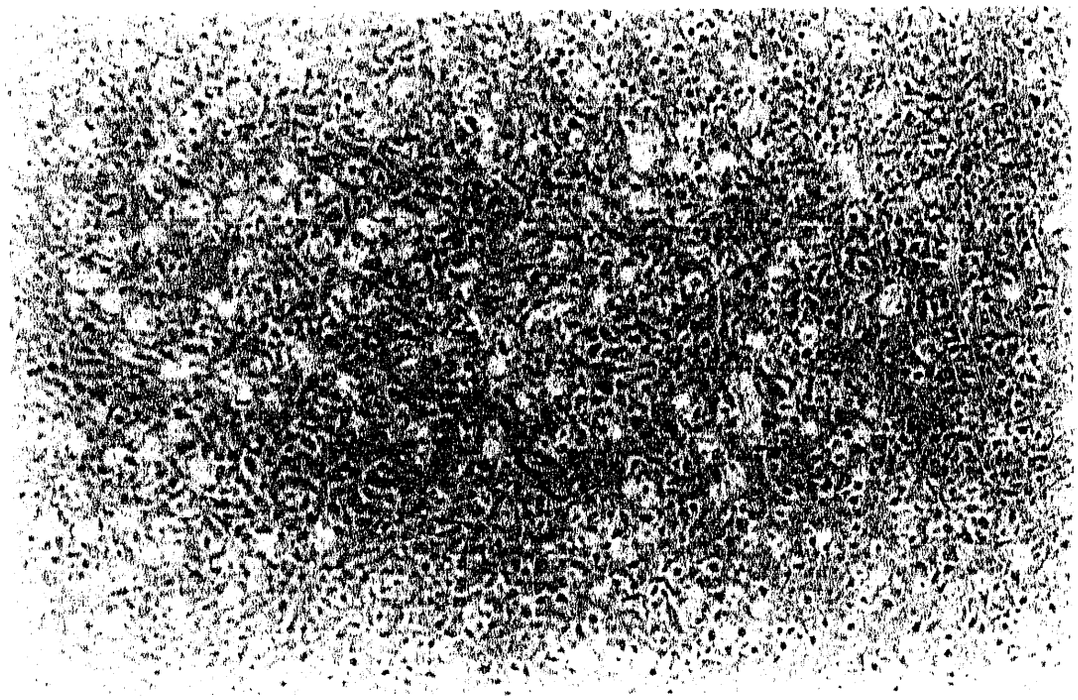

XBB 908-6564A

Figure 5.8

Figure 5.9

Representative high-power (×100) phase contrast photomicrograph of a primary mixed glial cell culture at DIC 9, 3 d following 2 Gy 225 kVp x-irradiation. Compared with unirradiated controls (cf Figure 5.7), fewer phase-dark oligodendrocytes are seen. (Cf Figure 5.10.)

Figure 5.10

A representative low-power (×25) phase contrast photomicrograph from the 2-Gy irradiated primary mixed glial cell culture shown in Figure 5.9. The astrocyte monolayer is nearly confluent.

Figure 5.11

Representative high-power (×100) phase contrast photomicrograph of a primary mixed glial cell culture at DIC 9, 3 d following 5 Gy 225 kVp x-irradiation. Compared with unirradiated controls (cf Figure 5.7) and 2-Gy irradiated cultures (cf Figure 5.9), oligodendrocytes are sparse. (Cf Figure 5.12.)

Figure 5.12

A representative low-power (×25) phase contrast photomicrograph from the 5-Gy irradiated primary mixed glial cell culture shown in Figure 5.11. The extent of oligodendrocyte loss is illustrated by comparison with Figures 5.8 and 5.10. The astrocyte monolayer is nearly confluent.

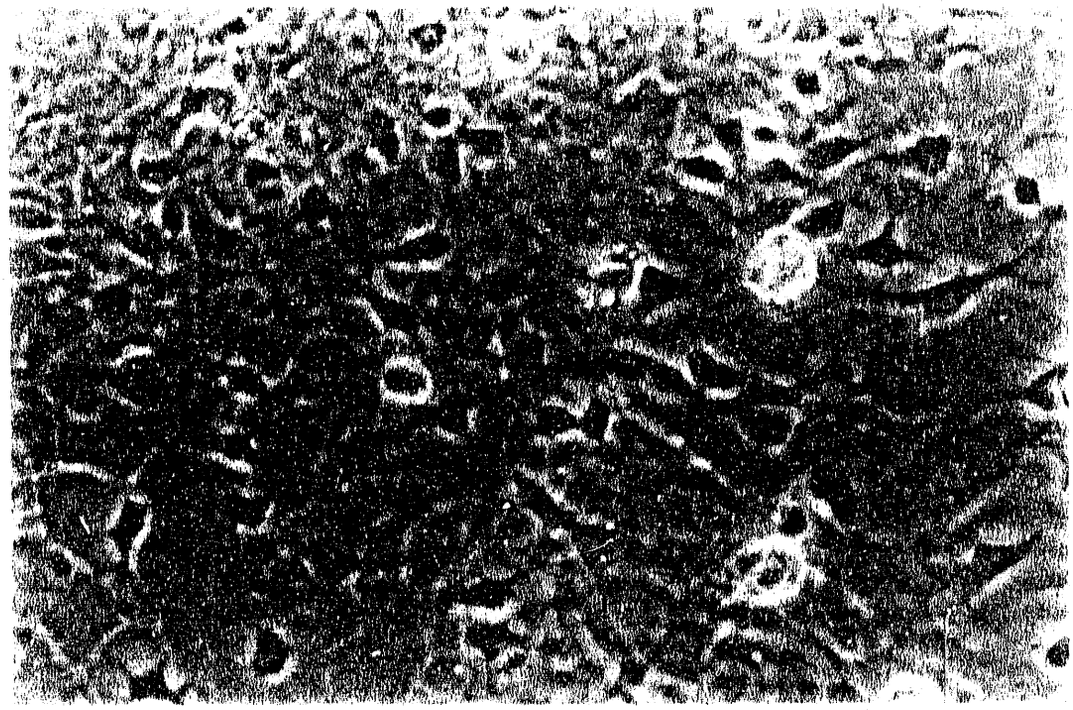

Figure 5.9

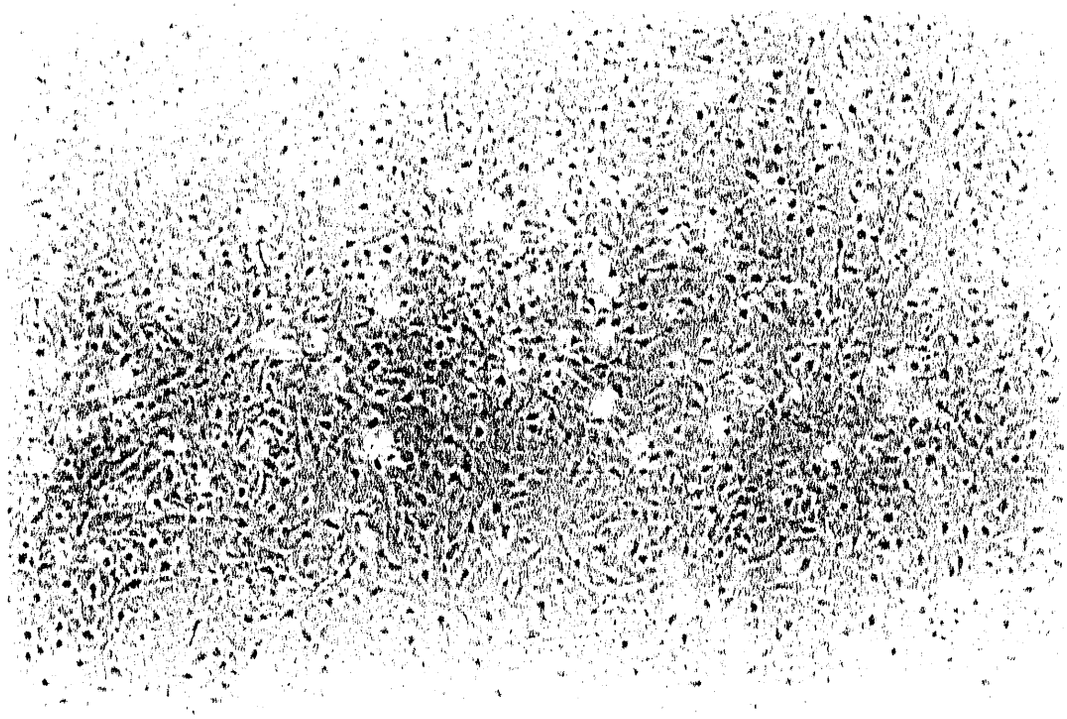

XBB 908-6566A

Figure 5.10

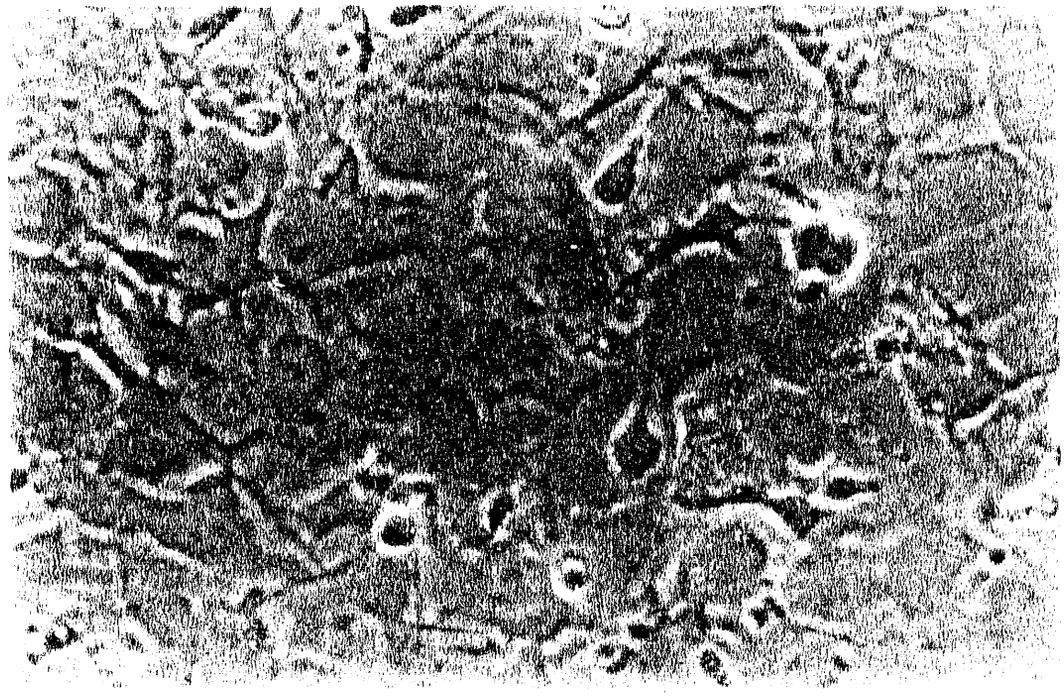

Figure 5.11

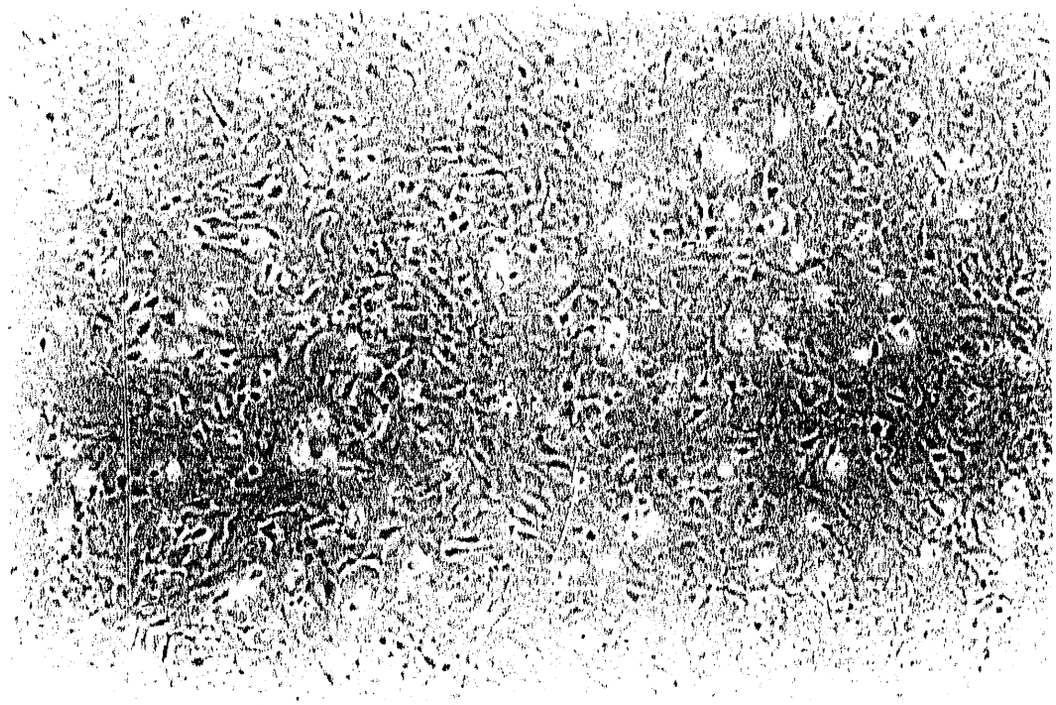

XBB 908-6567A

Figure 5.12

Figure 5.13

Representative high-power ($\times 100$) phase contrast photomicrograph of an unirradiated primary mixed glial cell culture at DIC 12. The astrocyte monolayer is fully confluent. (Cf Figure 5.14.)

Figure 5.14

A representative low-power ($\times 25$) phase contrast photomicrograph from the unirradiated primary mixed glial cell culture shown in Figure 5.13. Oligodendrocytes are abundant throughout the field.

Figure 5.15

Representative high-power ($\times 100$) phase contrast photomicrograph of a primary mixed glial cell culture at DIC 12, 6 d following 2 Gy 225 kVp x-irradiation. The astrocyte monolayer is fully confluent. (Cf Figure 5.16.)

Figure 5.16

A representative low-power ($\times 25$) phase contrast photomicrograph from the 2-Gy irradiated primary mixed glial cell culture shown in Figure 5.15.

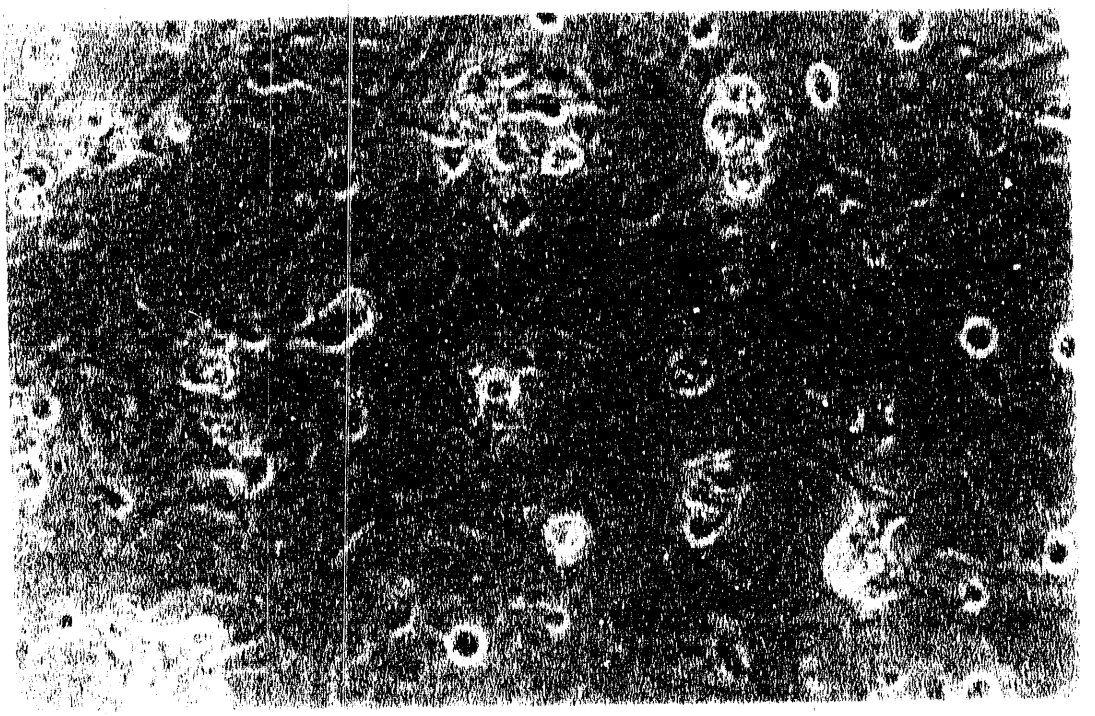

Figure 5.13

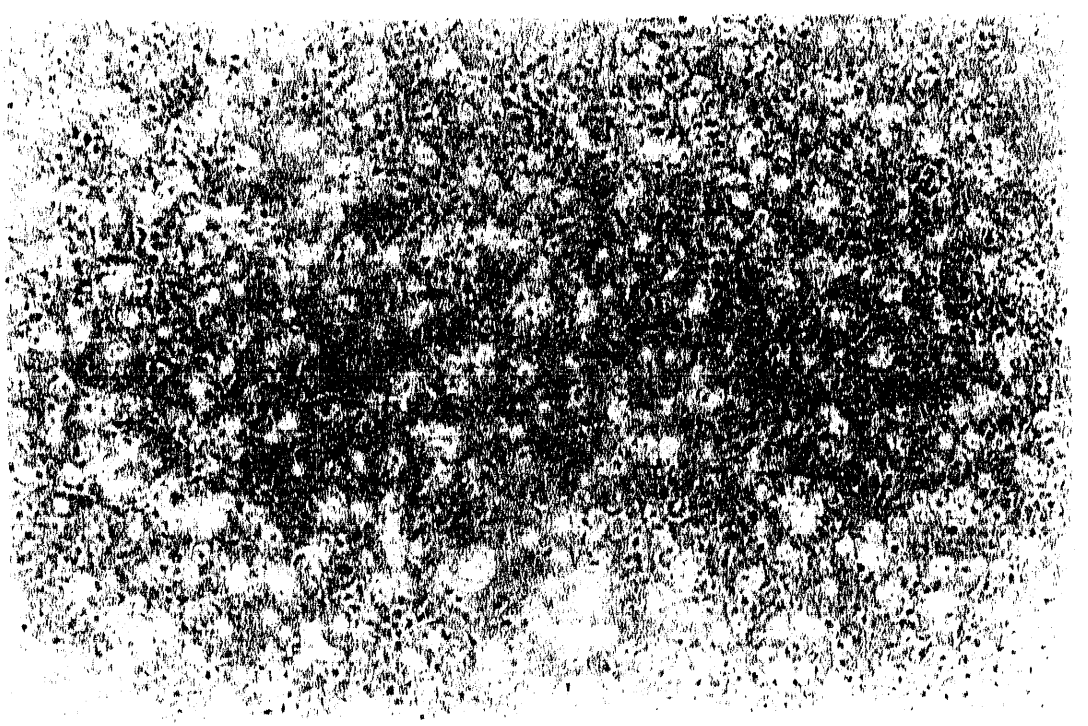

XBB 908-6585A

Figure 5.14

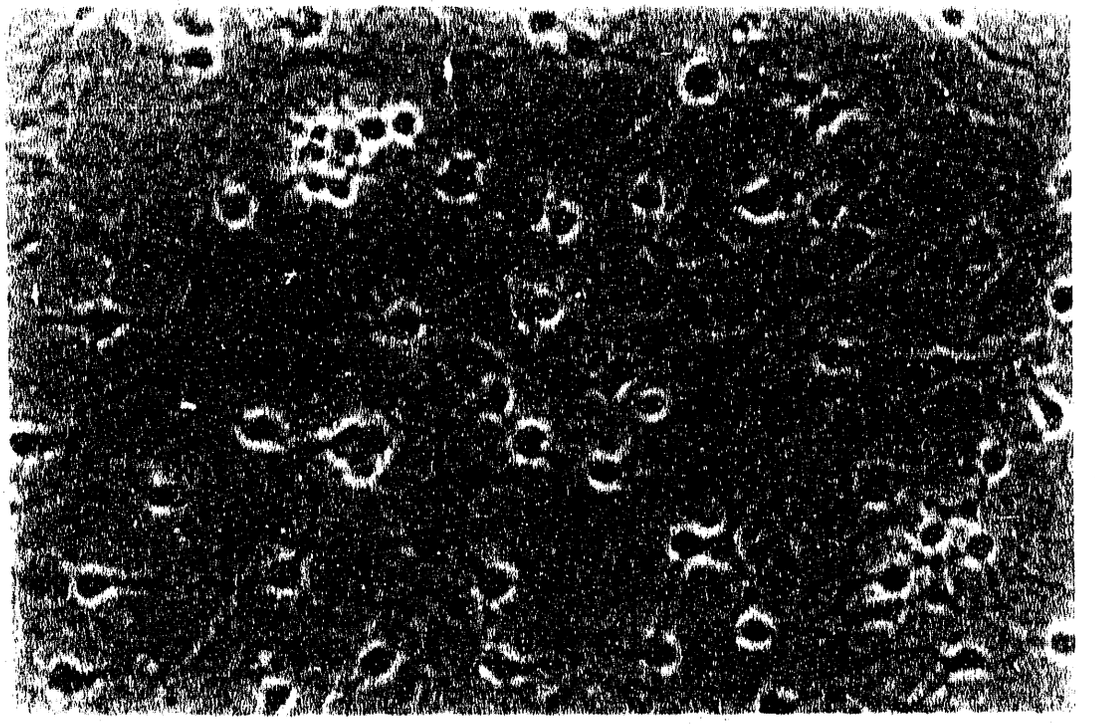

Figure 5.15

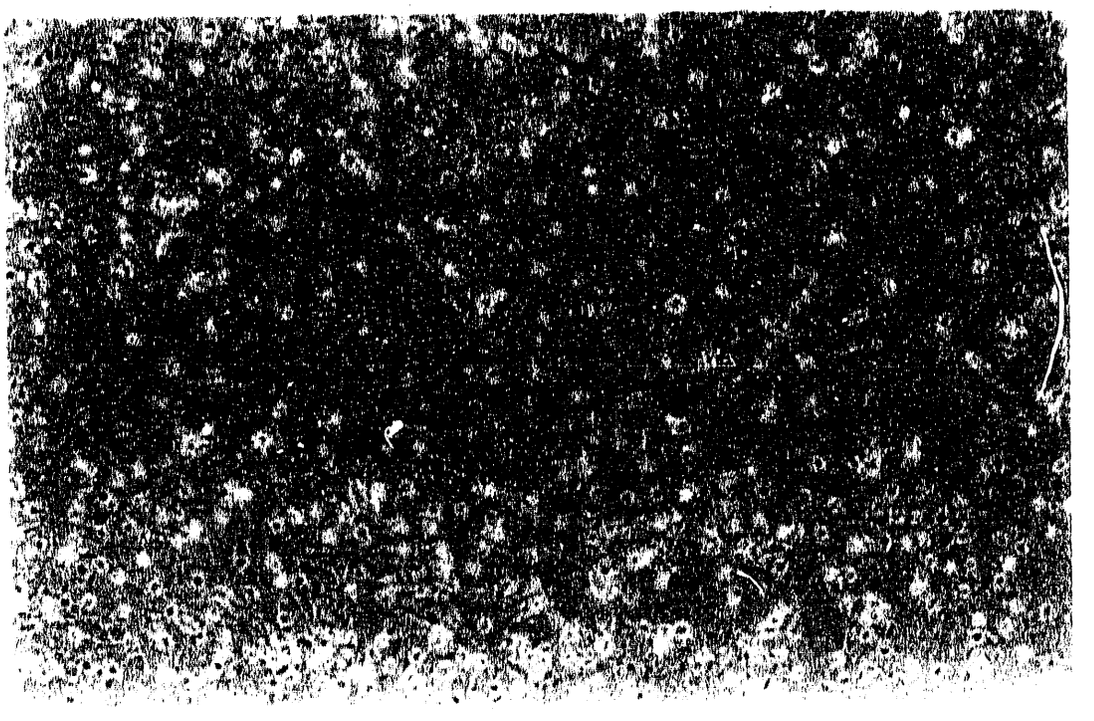

XBB 908-6587A

Figure 5.16

Figure 5.17

Representative high-power (×100) phase contrast photomicrograph of a primary mixed glial cell culture at DIC 12, 6 d following 5 Gy 225 kVp x-irradiation. The extent of recovery in the oligodendrocyte population is illustrated by comparison with Figures 5.5 and 5.11. (Cf Figure 5.18.)

Figure 5.18

A representative low-power (×25) phase contrast photomicrograph from the 5-Gy irradiated primary mixed glial cell culture shown in Figure 5.17. The astrocyte monolayer is nearly confluent.

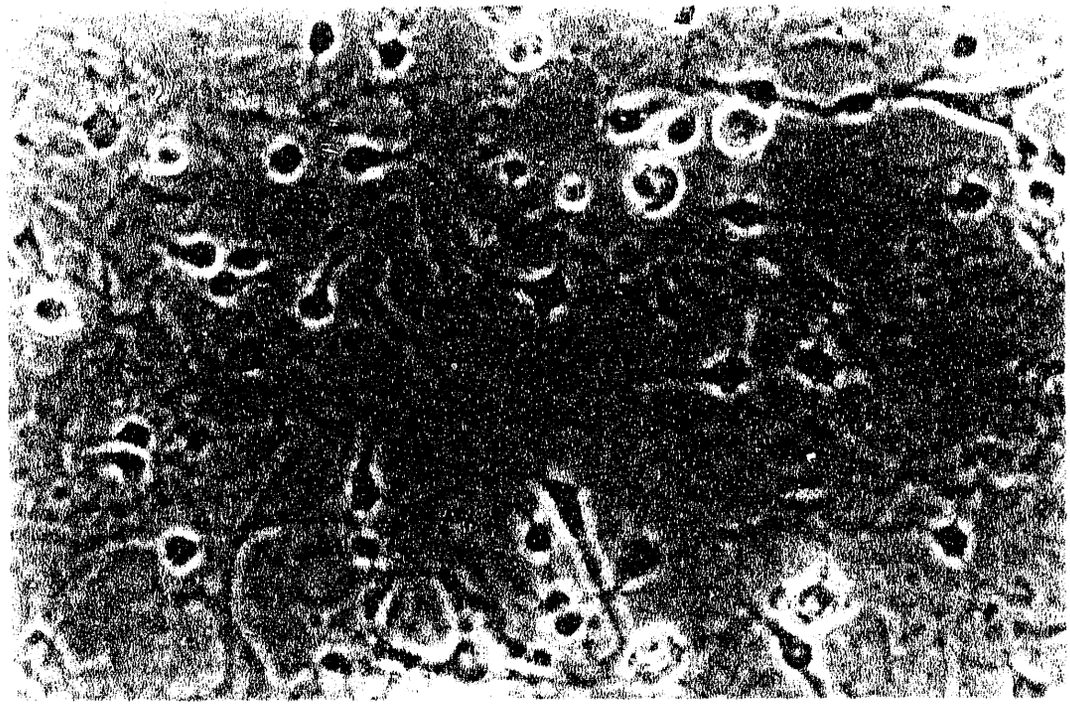

Figure 5.17

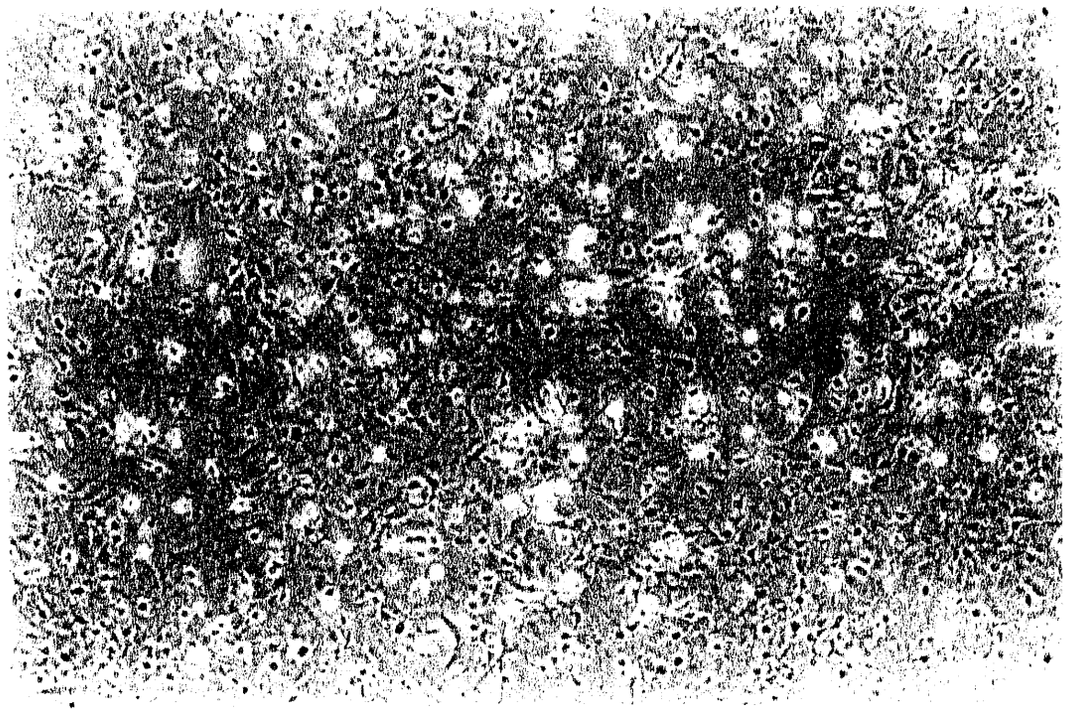

Figure 5.18

XBB 908-6588A

glial cell response can also be appreciated with low-power microscopy; here, the oligodendrocytes appear as small dark process-bearing cells scattered irregularly throughout the field of view and are seen positioned atop the astrocyte carpet.

The astrocyte monolayer was also responsive to irradiation. Acellular regions in the relatively amorphous gray astrocyte carpet (see Section 4.2.1) were observed to increase with radiation dose (Figures 5.4 and 5.6). Astrocyte confluence was attained at DIC 9 in unirradiated cultures and DIC 12 in cultures irradiated with 2 Gy (Figures 5.8 and 5.16); the astrocyte monolayer in cultures irradiated with 5 Gy also recovered quickly, but some acellular regions still remained at DIC 12 (Figure 5.18).

The responses of the oligodendrocyte and astrocyte populations to doses of 10 Gy or 30 Gy were much more profound and longer-lasting than those observed after 5 Gy irradiation. These higher doses were considered to be in excess of that required to induce obvious morphologic changes. Conversely, a dose of 1 Gy did not induce morphologic changes consistently. On the basis of these observations, it was determined that subsequent quantitative irradiation experiments would be limited to evaluation of the response to doses of 2 Gy and/or 5 Gy. Sampling of culture data was designated for DIC 14 and/or DIC 21 because, in unirradiated glial cultures, oligodendrocyte counts were found to reach a plateau at about DIC 14 (see Section 4.2.4) and myelin basic protein (MBP) values were found to increase up to and beyond DIC 21 (see Section 4.5).

5.3 OLIGODENDROCYTE RESPONSE IN γ-IRRADIATED GLIAL CELL CULTURES

5.3.1 General Morphologic Effects

The general morphologic response of mixed glial cultures to ^{60}Co γ-irradi-

ation was quite comparable to the response pattern observed after glial irradiation with corresponding doses of 225 kVp x-rays. The findings with phase contrast microscopy were essentially as described in Section 5.2, and will not be reiterated here. The remaining portions of this section describe the quantitative response of the oligodendrocyte population to ^{60}Co γ-irradiation as a function of dose and dose-rate, and the response to split-dose irradiation. All experiments described henceforth involved culture irradiation at DIC 8.

5.3.2 Dose and Dose-Rate Response

A series of experiments was designed to evaluate the dose and dose-rate response of oligodendrocytes at DIC 14 and DIC 21 (i.e., 6 d and 14 d, respectively, after irradiation). The oligodendrocyte population was counted at DIC 14 following culture irradiation at dose rates of 0.12 Gy/min and 0.49 $\pm$0.02 Gy/min (Figures 5.19–5.21). Statistical evaluation using analysis of variance confirmed in all cases the null hypothesis that no significant difference in response of the oligodendrocyte population existed between cultures irradiated at the different dose rates evaluated; this dose-rate response was found after total doses of either 2 Gy or 5 Gy were used. When the oligodendrocyte response was analyzed as a function of total dose, significant differences existed for all but one permutation tested; significance was approached, but not demonstrated at the 95% level, in one of the two trials comparing cultures irradiated with 2 Gy at a rate of 0.49 Gy/min to unirradiated control cultures.

Given the general absence of a dose-rate response at DIC 14, the total dose-response at this time was evaluated by grouping together for each experiment all specimens irradiated to a specific total dose. In two separate trials, mean oligodendrocyte counts were 55% of unirradiated-control values following irradiation with 2 Gy, and 36% of control values after 5 Gy (Figures 5.19 and

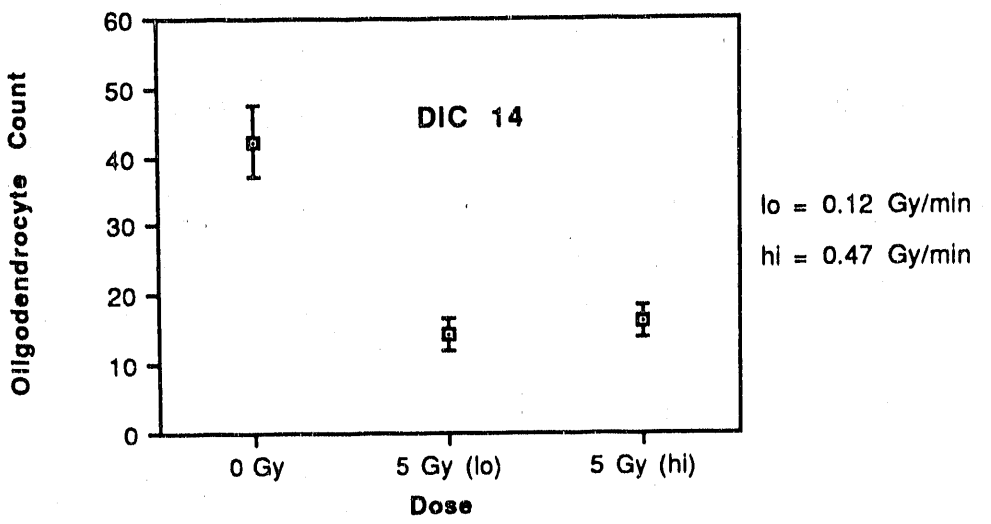

Comparison:	Mean Diff.:	Fisher PLSD:
Gy0 vs. Gy5Hi	26.21	4.52*
Gy0 vs. Gy5Lo	27.78	5.06*
Gy5Hi vs. Gy5Lo	1.57	5.06

* Significant at 95%

Figure 5.19. Oligodendrocyte counts (mean ± S.D.) in primary mixed glial cell cultures at DIC 14, following 5 Gy γ-irradiation at DIC 8. The oligodendrocyte response was examined at dose rates of 0.12 Gy/min and 0.47 Gy/min. No significant dose-rate effect was found between irradiated groups, but both 5-Gy groups had significantly lower counts than unirradiated controls.

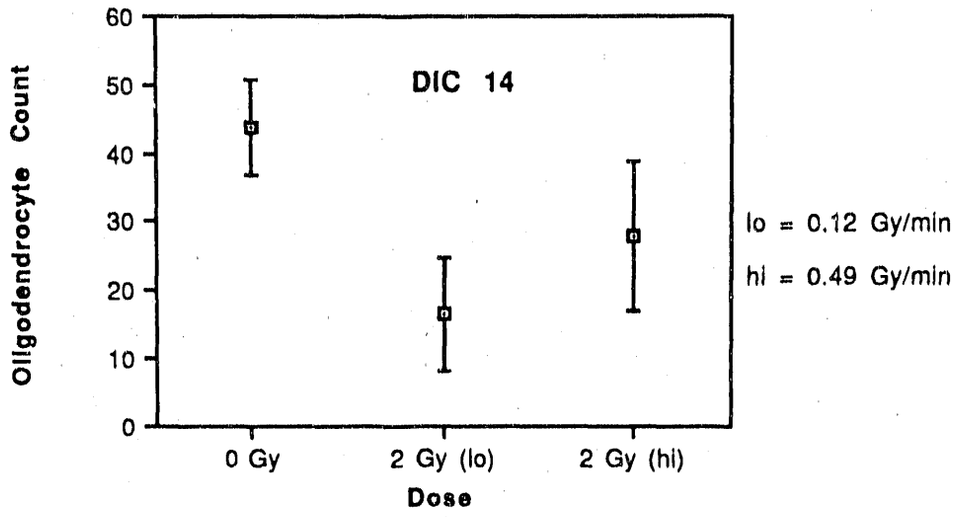

Comparison:	Mean Diff.:	Fisher PLSD:
Gy0 vs. Gy2Hi	15.66	17.22
Gy0 vs. Gy2Lo	27.22	18.86*
Gy2Hi vs. Gy2Lo	11.56	13.34

* Significant at 95%

Figure 5.20. Oligodendrocyte counts (mean ± S.D.) in primary mixed glial cell cultures at DIC 14, following 2 Gy γ-irradiation at DIC 8. The oligodendrocyte response was examined at dose rates of 0.12 Gy/min and 0.49 Gy/min. No significant dose-rate effect was found between irradiated groups, but both 2-Gy groups had significantly lower counts than unirradiated controls.

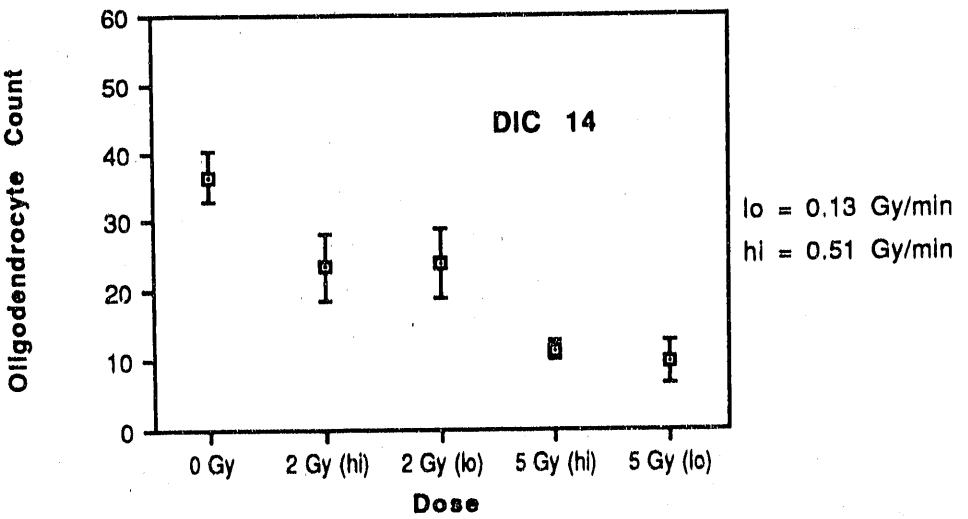

Comparison:	Mean Diff.:	Fisher PLSD:
Gy0 vs. Gy2Hi	13.06	4.05*
Gy0 vs. Gy2Lo	12.52	4.35*
Gy0 vs. Gy5Hi	25.25	4.18*
Gy0 vs. Gy5Lo	26.86	4.18*
Gy2Hi vs. Gy2Lo	-.55	4.22
Gy2Hi vs. Gy5Hi	12.18	4.05*
Gy2Hi vs. Gy5Lo	13.79	4.05*
Gy2Lo vs. Gy5Hi	12.73	4.35*
Gy2Lo vs. Gy5Lo	14.34	4.35*
Gy5Hi vs. Gy5Lo	1.61	4.18

* Significant at 95%

Figure 5.21. Oligodendrocyte counts (mean ± S.D.) in primary mixed glial cell cultures at DIC 14, following 2 Gy and 5 Gy γ-irradiation at DIC 8. The oligodendrocyte response was examined at dose rates of 0.13 Gy/min and 0.51 Gy/min. The response to total dose was significant, but no significant dose-rate effect was found at either 2 Gy or 5 Gy total dose.

5.20). These findings were subsequently confirmed when cultures irradiated with doses of 2 Gy and 5 Gy were evaluated concurrently, and oligodendrocyte counts were 65% and 29%, respectively, of control values (Figure 5.21).

The response of the oligodendrocyte population at DIC 21 was measured at dose rates ranging from 0.12 Gy/min to 1.97 Gy/min in cultures receiving 2 Gy total dose, and at dose rates from 0.03 Gy/min to 1.97 Gy/min in cultures receiving 5 Gy total dose. The permutations of dose and dose-rate studied are illustrated in Figures 5.22–5.24. The null hypothesis for dose-rate response was confirmed in the majority of trials comparing dose rates between 0.12 Gy/min and 1.97 Gy/min. However, one of two trials suggested that a dose rate of 0.12 Gy/min was less effective in reducing oligodendrocyte population than were higher dose rates (Figures 5.22 and 5.23). Moreover, a significant difference in response of the oligodendrocyte population was observed following irradiation with 5 Gy total dose, when cultures irradiated at a rate of 0.03 Gy/min were compared with cultures irradiated at 1.57 Gy/min; in this comparison, the lower dose rate was less effective in reducing the oligodendrocyte counts (Figure 5.24).

When the oligodendrocyte response at DIC 21 was evaluated as a function of total dose, mean oligodendrocyte counts were generally inversely related to dose; however, statistically significant differences could not be demonstrated consistently (Figures 5.22–5.24).

When the dose-response at DIC 21 was examined by grouping together all specimens irradiated to a given dose within each trial (for dose rates not found to effect different responses), it was apparent that there had been considerable recovery of the oligodendrocyte population in irradiated cultures as compared with that seen at DIC 14. In consecutive studies, mean oligodendrocyte counts in cultures irradiated to 2 Gy were 110% and 83%, respectively, of counts in unirradiated control cultures (Figures 5.22 and 5.23). When cultures irradiated

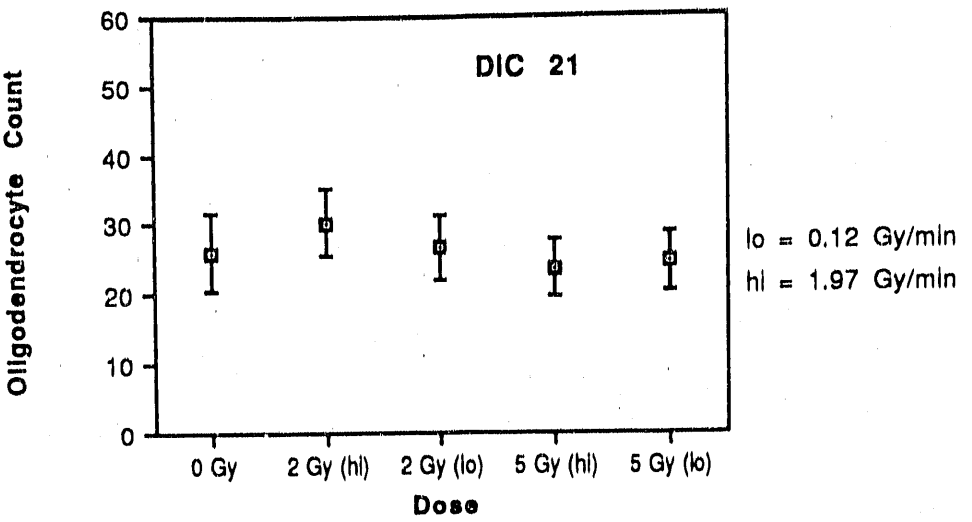

Comparison:	Mean Diff.:	Fisher PLSD:
Gy0 vs. Gy2Hi	-4.26	5.03
Gy0 vs. Gy2Lo	-.75	5.03
Gy0 vs. Gy5Hi	2.74	4.81
Gy0 vs. Gy5Lo	1.41	4.81
Gy2Hi vs. Gy2Lo	3.51	4.66
Gy2Hi vs. Gy5Hi	7	4.42*
Gy2Hi vs. Gy5Lo	5.67	4.42*
Gy2Lo vs. Gy5Hi	3.48	4.42
Gy2Lo vs. Gy5Lo	2.15	4.42
Gy5Hi vs. Gy5Lo	-1.33	4.17

* Significant at 95%

Figure 5.22. Oligodendrocyte counts (mean ± S.D.) in primary mixed glial cell cultures at DIC 21, following 2 Gy and 5 Gy γ-irradiation at DIC 8. The oligodendrocyte response was examined at dose rates of 0.12 Gy/min and 1.97 Gy/min. No significant dose-rate effect was found at either 2 Gy or 5 Gy total dose. Overall, considerable recovery of irradiated oligodendrocyte populations to near-control values was apparent.

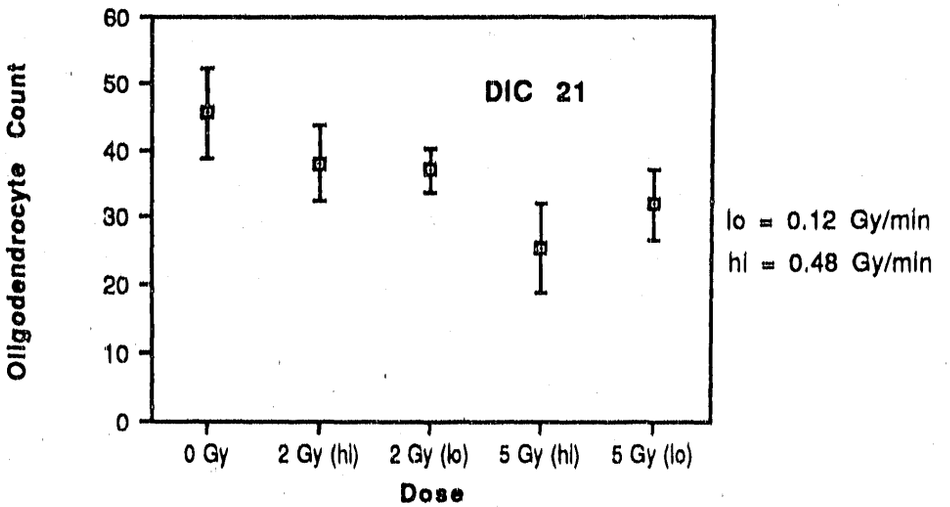

Comparison:	Mean Diff.:	Fisher PLSD:
Gy0 vs. Gy2Hi	7.44	5.37*
Gy0 vs. Gy2Lo	8.43	5.58*
Gy0 vs. Gy5Hi	20.03	5.37*
Gy0 vs. Gy5Lo	13.5	5.37*
Gy2Hi vs. Gy2Lo	.98	5.98
Gy2Hi vs. Gy5Hi	12.59	5.77*
Gy2Hi vs. Gy5Lo	6.06	5.77*
Gy2Lo vs. Gy5Hi	11.6	5.98*
Gy2Lo vs. Gy5Lo	5.08	5.98
Gy5Hi vs. Gy5Lo	-6.53	5.77*

* Significant at 95%

Figure 5.23. Oligodendrocyte counts (mean ± S.D.) in primary mixed glial cell cultures at DIC 21, following 2 Gy and 5 Gy γ-irradiation at DIC 8. The oligodendrocyte response was examined at dose rates of 0.12 Gy/min and 0.48 Gy/min. A possible dose-rate effect was noted at 5 Gy total dose; here, a dose rate of 0.12 Gy/min was less effective in reducing the oligodendrocyte population than was a dose rate of 0.48 Gy/min. However, this was not confirmed in a separate experiment (cf Figure 5.22).

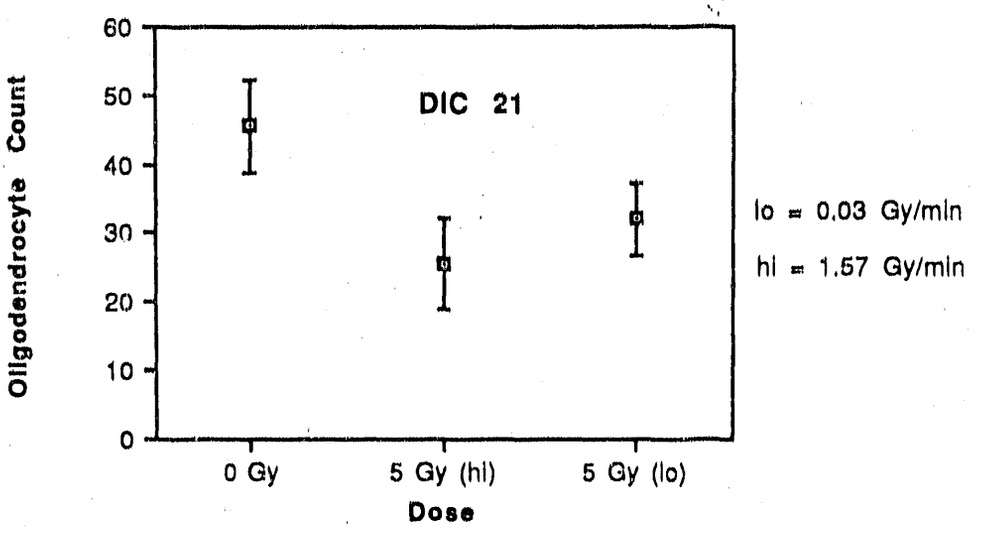

Comparison:	Mean Diff.:	Fisher PLSD:
Gy0 vs. Gy5Hi	12.79	2.52*
Gy0 vs. Gy5Lo	9.38	2.52*
Gy5Hi vs. Gy5Lo	-3.41	2.52*

* Significant at 95%

Figure 5.24. Oligodendrocyte counts (mean ± S.D.) in primary mixed glial cell cultures at DIC 21, following 5 Gy γ-irradiation at DIC 8. The oligodendrocyte response was examined at dose rates of 0.03 Gy/min and 1.57 Gy/min. A dose rate of 0.03 Gy/min was less effective in reducing the oligodendrocyte population than was a dose rate of 1.57 Gy/min.

to 5 Gy were considered in two separate studies, mean oligodendrocyte counts were 63% and 92% of control values, respectively (Figures 5.22 and 5.23).

5.3.3 Split-Dose Radiation Response

In order to evaluate the potential for repair of sublethal damage in γ-irradiated oligodendrocytes, the effects of split-dose irradiation were studied in a series of specimens given a total dose of 5 Gy in two 2.5-Gy fractions. Interfraction time was varied in hourly increments from 0 h (i.e., 5 Gy in one fraction) to 6 h. Separate experiments were conducted for analysis at DIC 14 and DIC 21 (Figures 5.25 and 5.26). The general response of the irradiated groups at DIC 14 was similar to that described in Section 5.3.2 (i.e., marked lowering of oligodendrocyte counts). Statistical evaluation using analysis of variance demonstrated that all irradiated groups had significantly lower counts than unirradiated controls; mean counts in irradiated groups ranged from 34% to 58% of control values (Figure 5.25). Cultures irradiated to 5 Gy in one fraction had significantly lower oligodendrocyte counts than cultures irradiated to 5 Gy at all split-dose time intervals tested. No significant difference in counts was found between any groups irradiated with two 2.5-Gy fractions, regardless of the permutation of time intervals compared.

At DIC 21, the general response was of marked oligodendrocyte recovery toward control values (see Section 5.3.2). Cultures irradiated with interfraction times of 3 h to 6 h exhibited a greater degree of recovery than cultures irradiated with shorter interfraction times (Figure 5.26). No difference was found when culture groups irradiated at intervals of 4 h to 6 h were compared with each other or with unirradiated controls. Culture groups irradiated at intervals of 0 h (i.e., 5 Gy in one fraction) to 2 h were similar to each other, but had significantly lower counts than unirradiated controls or cultures irradiated at intervals of 4 h to 6 h.

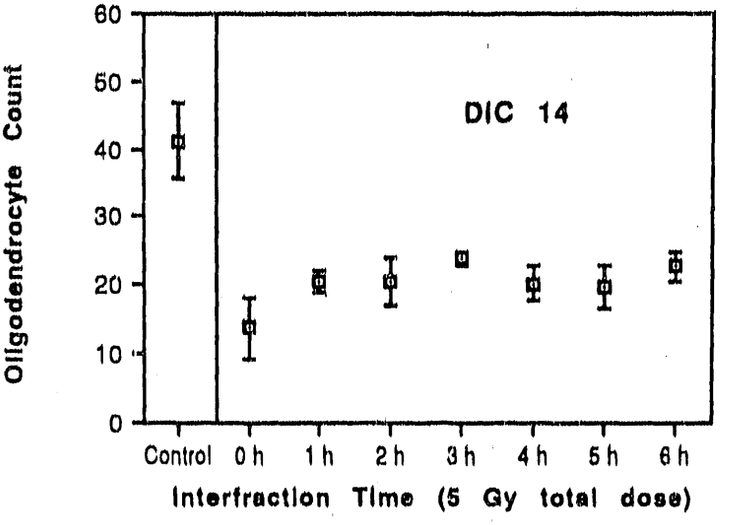

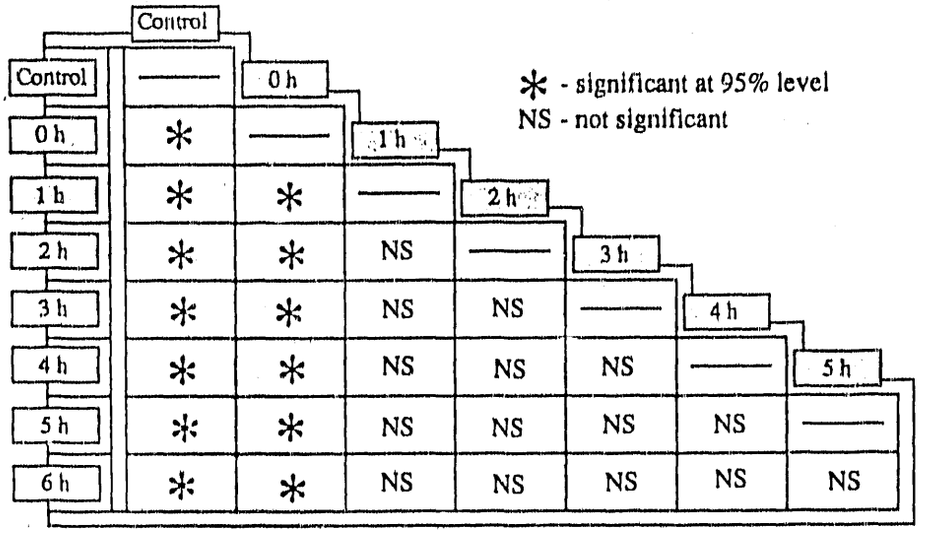

Figure 5.25. Oligodendrocyte counts (mean ± S.D.) in primary mixed glial cell cultures at DIC 14, following 5 Gy split-dose γ-irradiation at DIC 8. Cultures irradiated to 5 Gy in one fraction had significantly lower oligodendrocyte counts than cultures irradiated at any split-dose interval tested. No difference was found between any groups irradiated with two 2.5-Gy fractions.

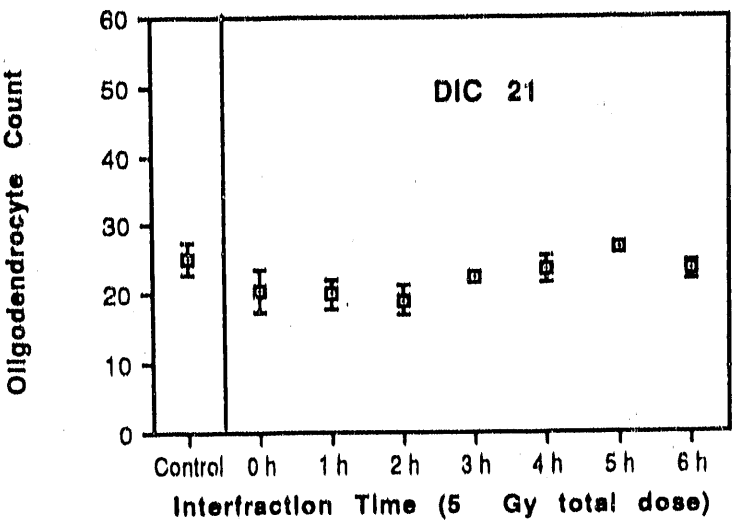

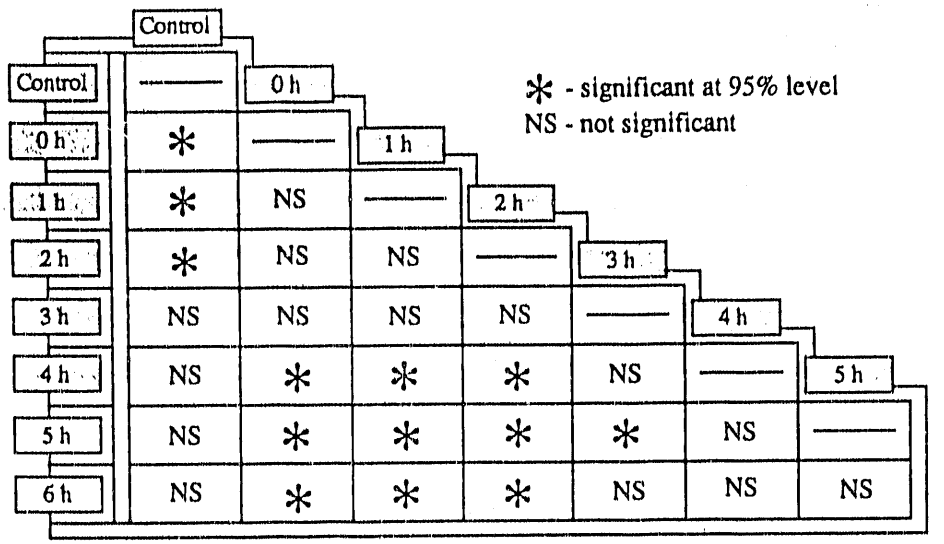

Figure 5.26. Oligodendrocyte counts (mean ± S.D.) in primary mixed glial cell cultures at DIC 21, following 5 Gy split-dose γ-irradiation at DIC 8. Cultures irradiated at intervals of 0 h to 2 h were similar to each other, but had significantly lower counts than unirradiated controls or cultures irradiated at intervals of 4 h to 6 h.

5.4 MYELIN BASIC PROTEIN SYNTHESIS IN γ-IRRADIATED GLIAL CELL CULTURES

5.4.1 Dose and Dose-Rate Response

A series of experiments was designed to evaluate the biochemical response of glial cell cultures to γ-irradiation as a function of dose and dose-rate. Cultures were analyzed at DIC 14 and DIC 21. Myelin basic protein (MBP) content was measured at DIC 14 following culture irradiation at dose rates of 0.12 Gy/min and 0.49 $\pm$0.02 Gy/min (Figures 5.27–5.29). Statistical evaluation using analysis of variance confirmed in all but one case the null hypothesis that no significant difference in MBP production existed between cultures irradiated at different dose rates; in one trial an unusually low MBP result in the 0.12 Gy/min group following a dose of 5 Gy was significantly lower than the MBP measurement in the higher dose-rate group.

When the MBP response was assessed as a function of total dose, significant differences were found for all but one permutation tested; MBP measurements clearly decreased with increasing dose (Figures 5.27–5.29). In the one exception, significance was approached, but not demonstrated at the 95% level, in one of the four combinations evaluated to compare cultures irradiated with 2 Gy to unirradiated control cultures.

The pattern of dose and dose-rate response of MBP was defined even more clearly at DIC 21 than at DIC 14. MBP was assayed following irradiation at dose rates ranging from 0.12 Gy/min to 1.97 Gy/min in cultures receiving 2 Gy total dose, and at dose rates from 0.03 Gy/min to 1.97 Gy/min in cultures receiving 5 Gy total dose. The permutations of dose and dose-rate studied are illustrated in Figures 5.30–5.32. No significant difference in MBP production as a function of dose rate was detected in any combination of dose rates studied. Production

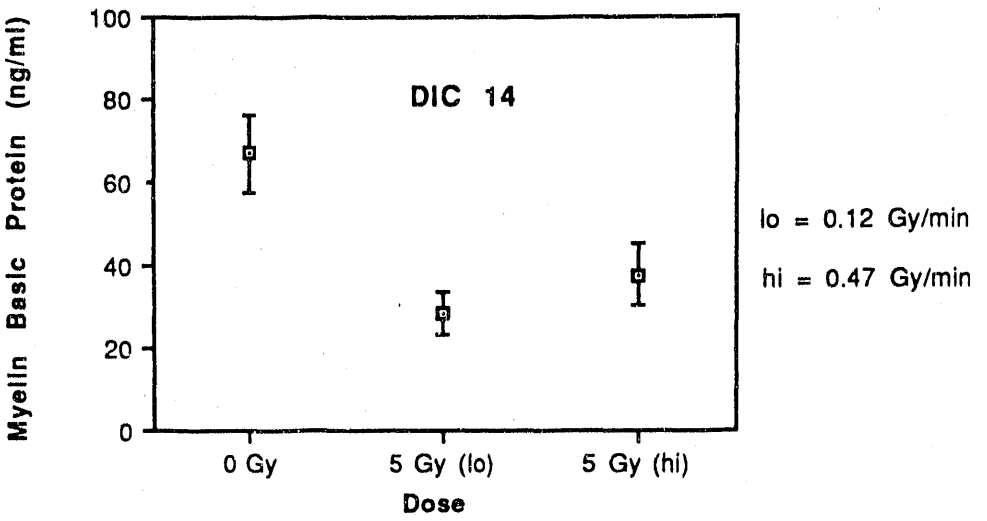

Comparison:	Mean Diff.:	Fisher PLSD:
Gy0 vs. Gy5Hi	29.19	11.21*
Gy0 vs. Gy5Lo	33.7	12.53*
Gy5Hi vs. Gy5Lo	4.51	12.53

* Significant at 95%

Figure 5.27. Myelin basic protein (MBP) levels (mean ± S.D.) in primary mixed glial cell cultures at DIC 14, following 5 Gy γ-irradiation at DIC 8. The MBP response was examined at dose rates of 0.12 Gy/min and 0.47 Gy/min. No significant dose-rate effect was found between irradiated groups, but both 5-Gy groups had significantly lower MBP levels than unirradiated controls.

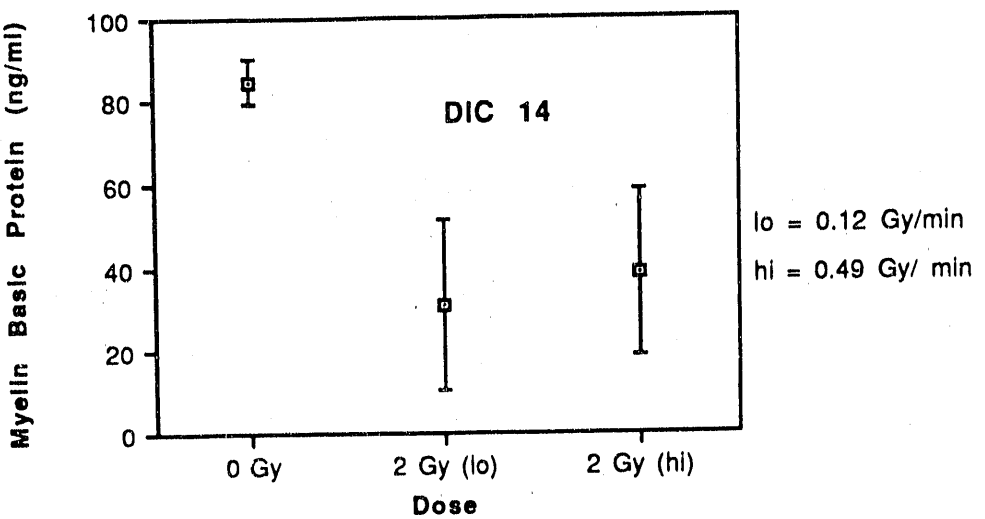

Comparison:	Mean Diff.:	Fisher PLSD:
Gy0 vs. Gy2Hi	46.29	33.68*
Gy0 vs. Gy2Lo	53.83	36.89*
Gy2Hi vs. Gy2Lo	7.53	26.09

* Significant at 95%

Figure 5.28. Myelin basic protein (MBP) levels (mean ± S.D.) in primary mixed glial cell cultures at DIC 14, following 2 Gy γ-irradiation at DIC 8. The MBP response was examined at dose rates of 0.12 Gy/min and 0.49 Gy/min. No significant dose-rate effect was found between irradiated groups, but both 2-Gy groups had significantly lower MBP levels than unirradiated controls.

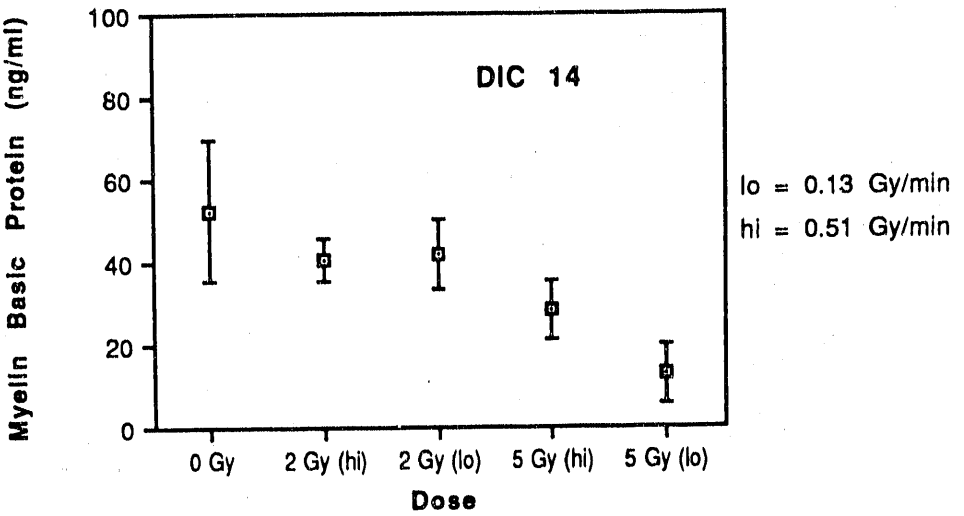

Comparison:	Mean Diff.:	Fisher PLSD:
Gy0 vs. Gy2Hi	11.8	10.43*
Gy0 vs. Gy2Lo	10.55	11.22
Gy0 vs. Gy5Hi	24.09	10.78*
Gy0 vs. Gy5Lo	39.66	10.78*
Gy2Hi vs. Gy2Lo	-1.24	10.89
Gy2Hi vs. Gy5Hi	12.29	10.43*
Gy2Hi vs. Gy5Lo	27.86	10.43*
Gy2Lo vs. Gy5Hi	13.53	11.22*
Gy2Lo vs. Gy5Lo	29.1	11.22*
Gy5Hi vs. Gy5Lo	15.57	10.78*

* Significant at 95%

Figure 5.29. Myelin basic protein (MBP) levels (mean ± S.D.) in primary mixed glial cell cultures at DIC 14, following 2 Gy and 5 Gy γ-irradiation at DIC 8. The MBP response was examined at dose rates of 0.13 Gy/min and 0.51 Gy/min. MBP levels decreased with increasing dose. In one group (5 Gy total dose at 0.13 Gy/min), an unusually low MBP result was obtained and this value was significantly lower than the MBP level in the higher dose-rate group.

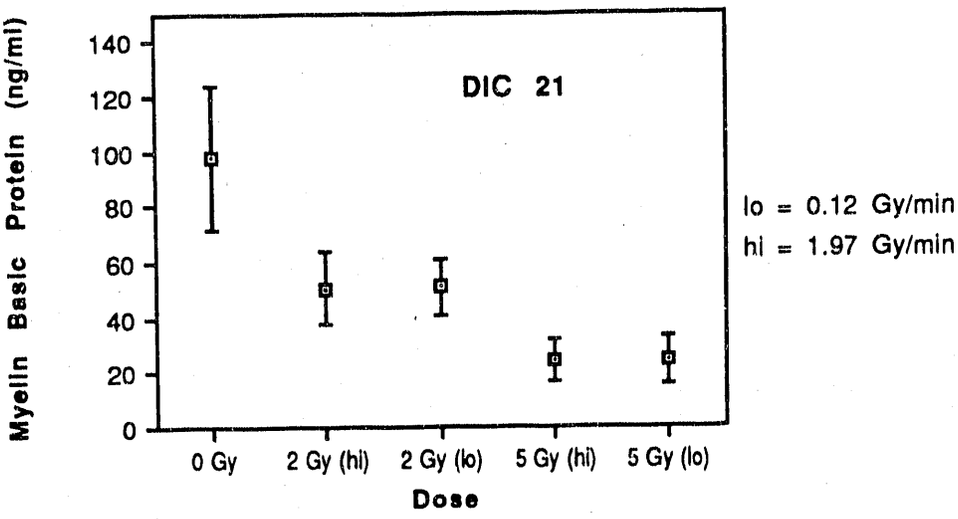

Comparison:	Mean Diff.:	Fisher PLSD:
Gy0 vs. Gy2Hi	47.25	14.61*
Gy0 vs. Gy2Lo	47	14.61*
Gy0 vs. Gy5Hi	73.8	13.97*
Gy0 vs. Gy5Lo	73.95	13.97*
Gy2Hi vs. Gy2Lo	-.25	13.53
Gy2Hi vs. Gy5Hi	26.55	12.84*
Gy2Hi vs. Gy5Lo	26.7	12.84*
Gy2Lo vs. Gy5Hi	26.8	12.84*
Gy2Lo vs. Gy5Lo	26.95	12.84*
Gy5Hi vs. Gy5Lo	.15	12.1

* Significant at 95%

Figure 5.30. Myelin basic protein (MBP) levels (mean ± S.D.) in primary mixed glial cell cultures at DIC 21, following 2 Gy and 5 Gy γ-irradiation at DIC 8. The MBP response was examined at dose rates of 0.12 Gy/min and 1.97 Gy/min. MBP levels clearly decreased with increasing dose. No dose-rate effect was found.

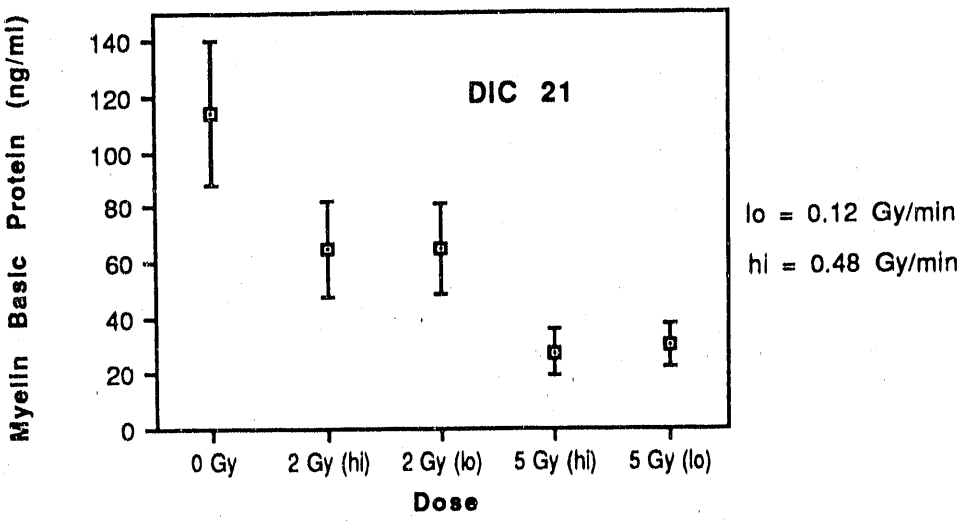

Comparison:	Mean Diff.:	Fisher PLSD:
Gy0 vs. Gy2Hi	49	16.54*
Gy0 vs. Gy2Lo	49.14	17.22*
Gy0 vs. Gy5Hi	86.75	16.54*
Gy0 vs. Gy5Lo	83.81	16.54*
Gy2Hi vs. Gy2Lo	.14	18.43
Gy2Hi vs. Gy5Hi	37.75	17.8*
Gy2Hi vs. Gy5Lo	34.81	17.8*
Gy2Lo vs. Gy5Hi	37.61	18.43*
Gy2Lo vs. Gy5Lo	34.67	18.43*
Gy5Hi vs. Gy5Lo	-2.94	17.8

* Significant at 95%

Figure 5.31. Myelin basic protein (MBP) levels (mean ± S.D.) in primary mixed glial cell cultures at DIC 21, following 2 Gy or 5 Gy γ-irradiation at DIC 8. The MBP response was examined at dose rates of 0.12 Gy/min and 0.48 Gy/min. MBP levels decreased with increasing dose. No dose-rate effect was found.

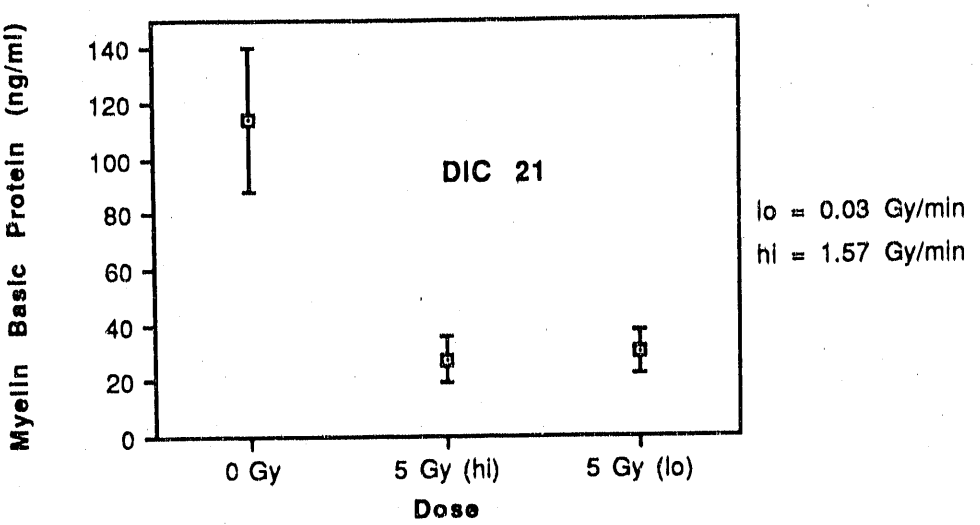

Comparison:	Mean Diff.:	Fisher PLSD:
Gy0 vs. Gy5Hi	104.7	15.62*
Gy0 vs. Gy5Lo	91	15.62*
Gy5Hi vs. Gy5Lo	-13.7	15.62

* Significant at 95%

Figure 5.32. Myelin basic protein (MBP) levels (mean ± S.D.) in primary mixed glial cell cultures at DIC 21, following 5 Gy γ-irradiation at DIC 8. The MBP response was examined at dose rates of 0.03 Gy/min and 1.57 Gy/min. No dose-rate effect was found.

of MBP at DIC 21 was demonstrated unequivocally to decrease with increasing total dose (Figures 5.30–5.32). Statistically significant differences were found in each trial for every permutation tested.

5.4.2 Split-Dose Radiation Response

The potential effects of repair of sublethal damage on MBP synthesis in γ-irradiated glial cells were evaluated by split-dose irradiation experiments in a series of cultures irradiated to a total dose of 5 Gy in two 2.5-Gy fractions (Figures 5.33 and 5.34). The time interval between doses was varied from 0 h to 6 h. At DIC 14, MBP production was significantly lower in all irradiated groups than in unirradiated controls (Figure 5.33). Intergroup comparison was significant in only three of 21 permutations investigated, all of which resulted from an unusually low MBP measurement in the group irradiated with an interfraction time of 6 h.

In a separate experiment, MBP production at DIC 21 was significantly lower in all irradiated groups than in unirradiated controls (Figure 5.34). The null hypothesis that variation in interfraction time would not be associated with alteration in MBP synthesis was confirmed in all 21 intergroup permutations investigated.

5.5 TOTAL CELLULAR PROTEIN SYNTHESIS IN γ-IRRADIATED GLIAL CELL CULTURES

5.5.1 Dose and Dose-Rate Response

Total cellular protein synthesis was determined in glial cultures at DIC 14 following irradiation at dose rates of 0.12 Gy/min and 0.49 $\pm$0.02 Gy/min, and at DIC 21 following irradiation at dose rates of 0.03 Gy/min to 1.97 Gy/min

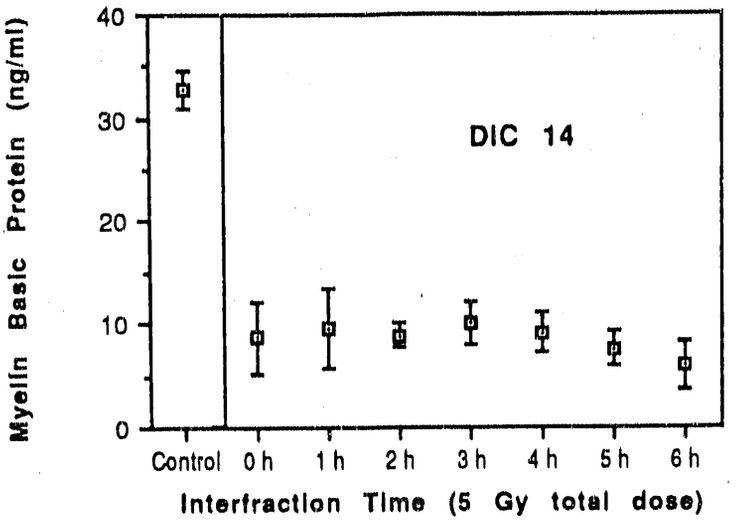

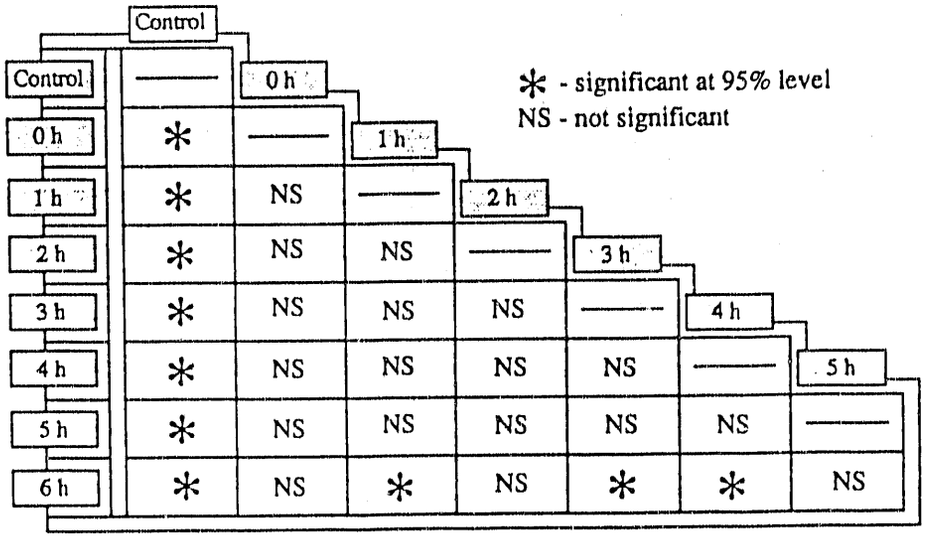

Figure 5.33. Myelin basic protein (MBP) levels (mean ± S.D.) in primary mixed glial cell cultures at DIC 14, following 5 Gy split-dose γ-irradiation at DIC 8. Intergroup comparison was significant in only three of 21 permutations tested, all of which resulted from an unusually low MBP value in the 6-h group.

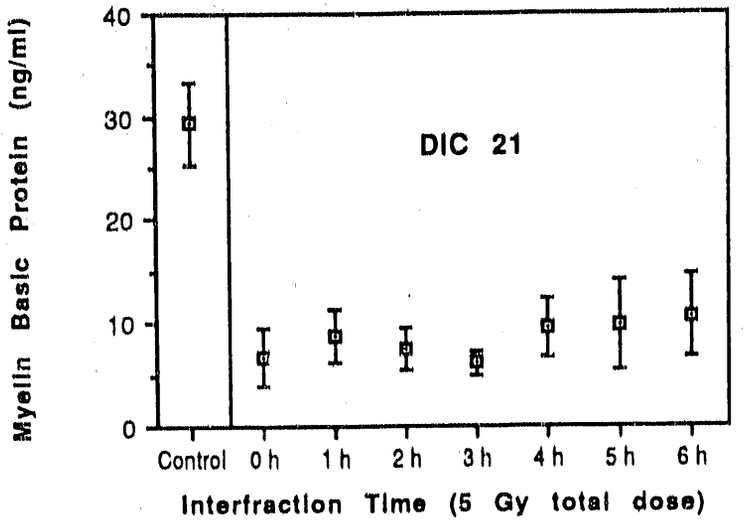

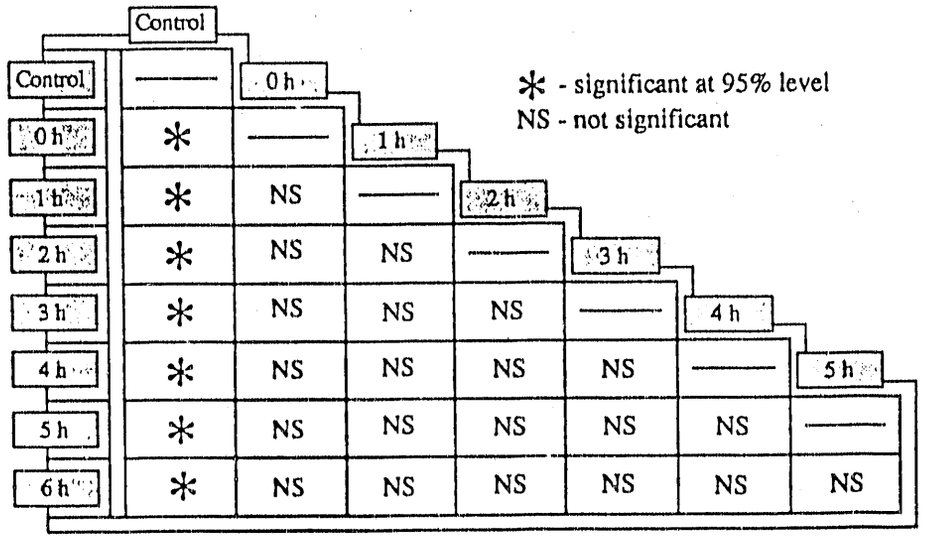

Figure 5.34. Myelin basic protein (MBP) levels (mean ± S.D.) in primary mixed glial cell cultures at DIC 21, following 5 Gy split-dose γ-irradiation at DIC 8. No significant difference could be detected in any of the 21 permutations tested.

(Figures 5.35–5.40). No significant dose-rate effect was noted at either DIC 14 or DIC 21 for any combination of dose and dose rate studied.

At DIC 14, mean total cellular protein measurements were lower than control values in all cases, but were significantly lower in only one of three experiments performed, due to large variance of data (Figures 5.35–5.37). A similar pattern was observed at DIC 21 (Figures 5.38–5.40). Mean total protein measurements decreased with increasing total dose. However, significant differences were found consistently only when cultures irradiated with total doses of 5 Gy were compared with unirradiated controls. Total protein levels in cultures irradiated with doses of 2 Gy had essentially recovered to control levels by this time.

5.5.2 Split-Dose Radiation Response

Split-dose irradiation had little impact on total cellular protein synthesis. A series of experiments was performed as described in Sections 5.3.3 and 5.4.2 (Figures 5.41 and 5.42). At DIC 14, intergroup comparison was significant in 4 of 21 permutations investigated. Only one permutation remained significant at DIC 21.

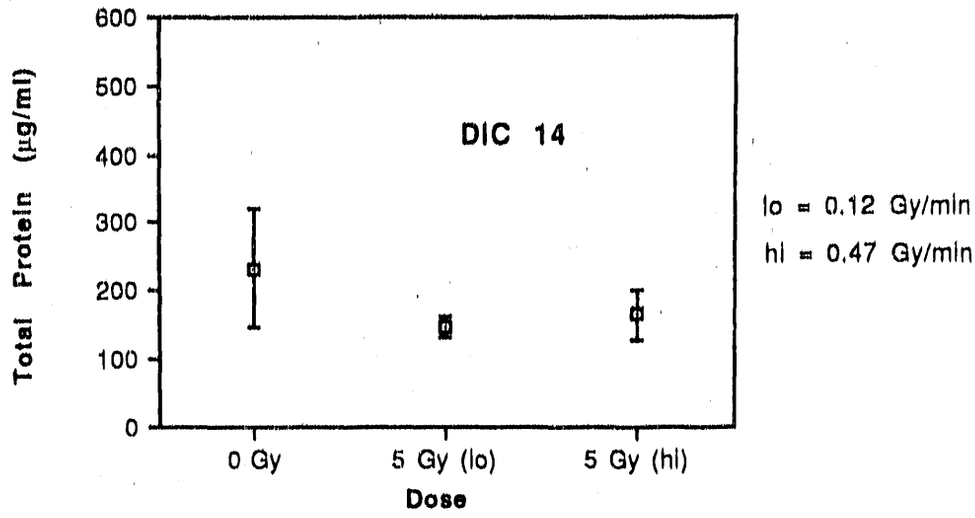

Comparison:	Mean Diff.:	Fisher PLSD:
Gy0 vs. Gy5Hi	68.33	76.31
Gy0 vs. Gy5Lo	86.67	93.46
Gy5Hi vs. Gy5Lo	18.33	93.46

Figure 5.35. Total cellular protein levels (mean ± S.D.) in primary mixed glial cell cultures at DIC 14, following 5 Gy γ-irradiation at DIC 8. The total protein response was examined at dose rates of 0.12 Gy/min and 0.47 Gy/min. No significant difference was found between any groups.

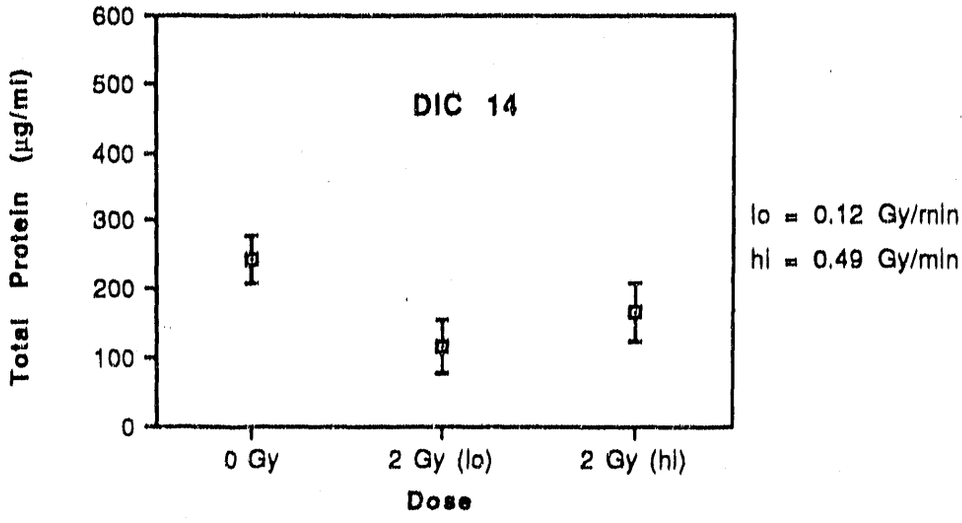

Comparison:	Mean Diff.:	Fisher PLSD:
Gy0 vs. Gy2Hi	78.75	72.59*
Gy0 vs. Gy2Lo	130	79.51*
Gy2Hi vs. Gy2Lo	51.25	56.22

* Significant at 95%

Figure 5.36. Total cellular protein levels (mean ± S.D.) in primary mixed glial cell cultures at DIC 14, following 2 Gy γ-irradiation at DIC 8. The total protein response was examined at dose rates of 0.12 Gy/min and 0.49 Gy/min. No significant dose-rate effect was found.

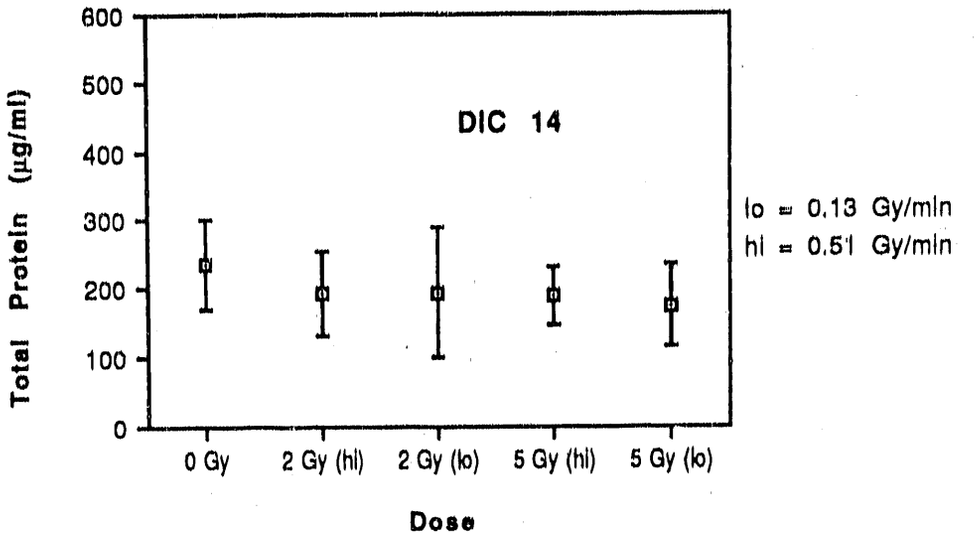

Comparison:	Mean Diff.:	Fisher PLSD:
Gy0 vs. Gy2Hi	43.39	69.3
Gy0 vs. Gy2Lo	42.14	74.5
Gy0 vs. Gy5Hi	48.57	71.57
Gy0 vs. Gy5Lo	61.43	71.57
Gy2Hi vs. Gy2Lo	-1.25	72.32
Gy2Hi vs. Gy5Hi	5.18	69.3
Gy2Hi vs. Gy5Lo	18.04	69.3
Gy2Lo vs. Gy5Hi	6.43	74.5
Gy2Lo vs. Gy5Lo	19.29	74.5
Gy5Hi vs. Gy5Lo	12.86	71.57

Figure 5.37. Total cellular protein levels (mean ± S.D.) in primary mixed glial cell cultures at DIC 14, following 2 Gy and 5 Gy γ-irradiation at DIC 8. The total protein response was examined at dose rates of 0.13 Gy/min and 0.51 Gy/min. No significant difference was found between any groups.

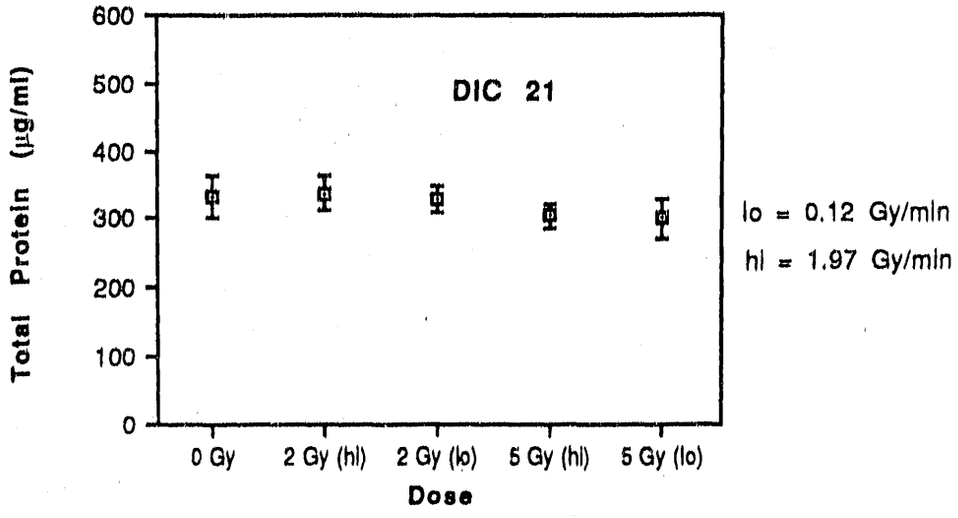

Comparison:	Mean Diff.:	Fisher PLSD:
Gy0 vs. Gy2Hi	-5.12	28.36
Gy0 vs. Gy2Lo	3	28.36
Gy0 vs. Gy5Hi	29	27.25*
Gy0 vs. Gy5Lo	32	27.25*
Gy2Hi vs. Gy2Lo	8.12	24.87
Gy2Hi vs. Gy5Hi	34.12	23.6*
Gy2Hi vs. Gy5Lo	37.12	23.6*
Gy2Lo vs. Gy5Hi	26	23.6*
Gy2Lo vs. Gy5Lo	29	23.6*
Gy5Hi vs. Gy5Lo	3	22.25

* Significant at 95%

Figure 5.38. Total cellular protein levels (mean ± S.D.) in primary mixed glial cell cultures at DIC 21, following 2 Gy and 5 Gy γ-irradiation at DIC 8. The total protein response was examined at dose rates of 0.12 Gy/min and 1.97 Gy/min. No dose-rate effect was present. Protein levels in the 2-Gy groups have returned to normal values; levels in the 5-Gy groups have returned to near-normal values.

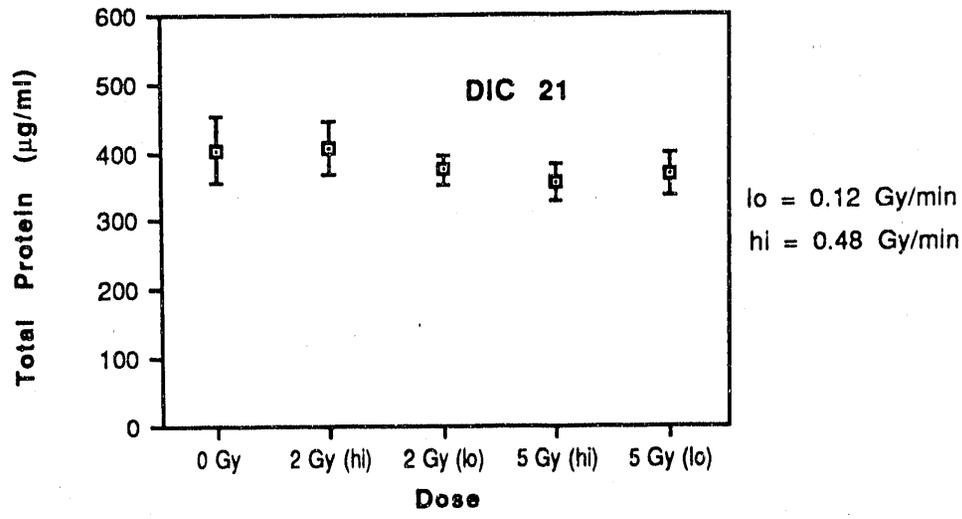

Comparison:	Mean Diff.:	Fisher PLSD:
Gy0 vs. Gy2Hi	-1.36	34.08
Gy0 vs. Gy2Lo	29.35	35.46
Gy0 vs. Gy5Hi	46.14	34.08*
Gy0 vs. Gy5Lo	34.89	34.08*
Gy2Hi vs. Gy2Lo	30.71	37.96
Gy2Hi vs. Gy5Hi	47.5	36.67*
Gy2Hi vs. Gy5Lo	36.25	36.67
Gy2Lo vs. Gy5Hi	16.79	37.96
Gy2Lo vs. Gy5Lo	5.54	37.96
Gy5Hi vs. Gy5Lo	-11.25	36.67

* Significant at 95%

Figure 5.39. Total cellular protein levels (mean ± S.D.) in primary mixed glial cell cultures at DIC 21, following 2 Gy and 5 Gy γ-irradiation at DIC 8. The total protein response was examined at dose rates of 0.12 Gy/min and 0.48 Gy/min. No dose-rate effect was present. Only minor differences in protein content were found as a function of total dose.

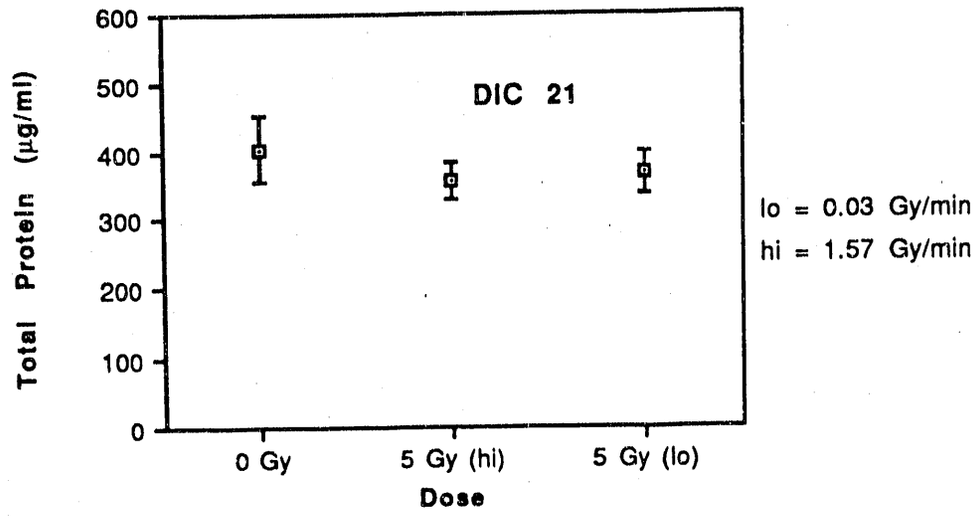

Comparison:	Mean Diff.:	Fisher PLSD:
Gy0 vs. Gy5Hi	107	30.33*
Gy0 vs. Gy5Lo	101	30.33*
Gy5Hi vs. Gy5Lo	-6	30.33

* Significant at 95%

Figure 5.40. Total cellular protein levels (mean ± S.D.) in primary mixed glial cell cultures at DIC 21, following 5 Gy γ-irradiation at DIC 8. The total protein response was examined at dose rates of 0.03 Gy/min and 1.57 Gy/min. Differences in protein content were minor.

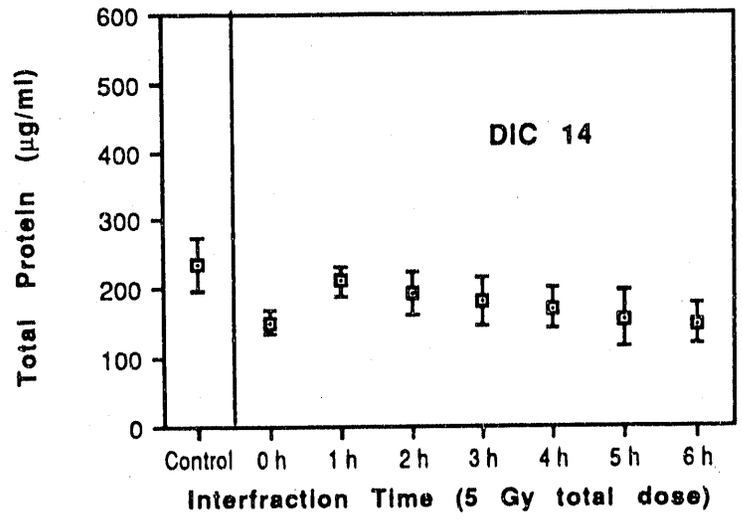

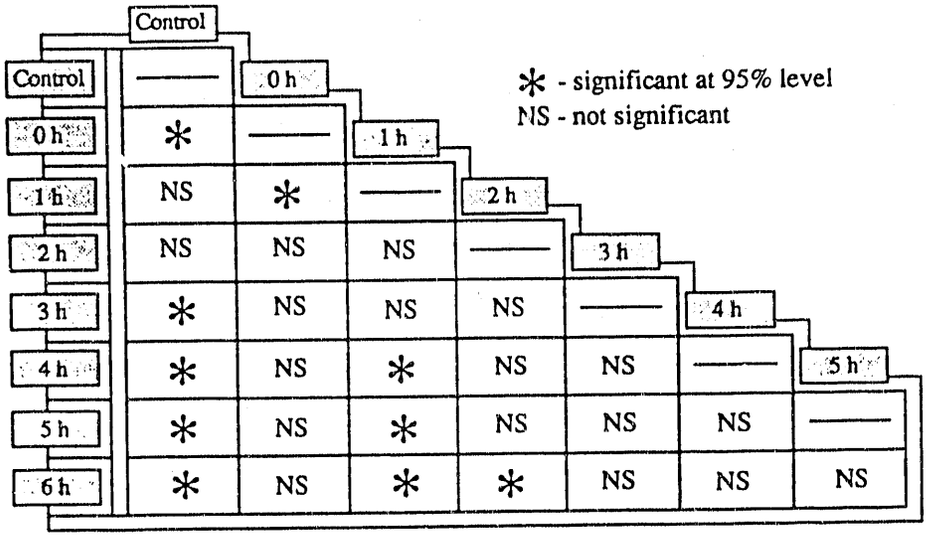

Figure 5.41. Total cellular protein levels (mean ± S.D.) in primary mixed glial cell cultures at DIC 14, following 5 Gy split-dose γ-irradiation at DIC 8. Intergroup comparison was significant in four of 21 permutations tested, but differences in total protein content were small.

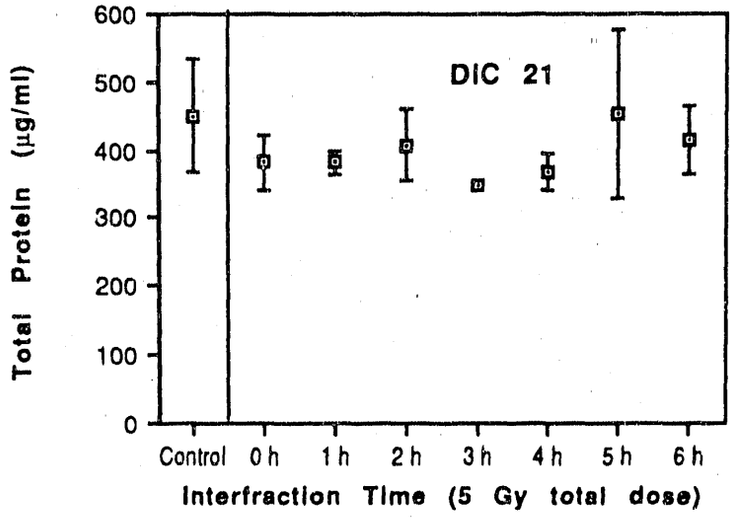

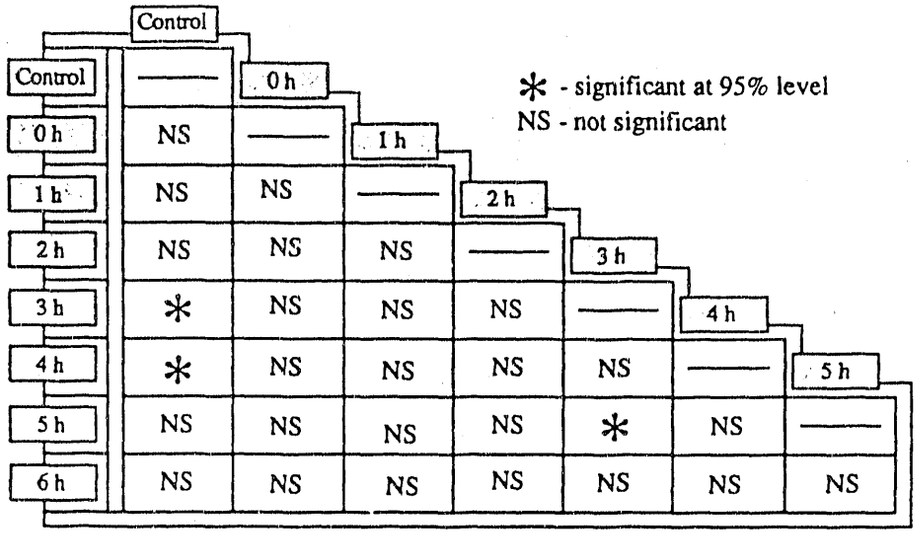

Figure 5.42. Total cellular protein levels (mean ± S.D.) in primary mixed glial cell cultures at DIC 21, following 5 Gy split-dose γ-irradiation at DIC 8. Intergroup comparison was significant in only one of 21 permutations tested.

5.6 MYELIN SYNTHESIS INDEX IN γ-IRRADIATED GLIAL CELL CULTURES

The complex temporal patterns of dose-response observed in the oligodendrocyte population (Section 5.3) and in the synthesis of MBP (Section 5.4) led to the hypothesis that MBP synthesis per oligodendrocyte might be a useful index of oligodendrocyte function (see Chapter 6). In three separate experiments, the MBP per oligodendrocyte ratio was determined for each irradiated and control culture at DIC 21 (Figures 5.43–5.45). The myelin synthesis index at a given dose was remarkably consistent from one experiment to the next, and appeared to be independent of initial plating conditions.

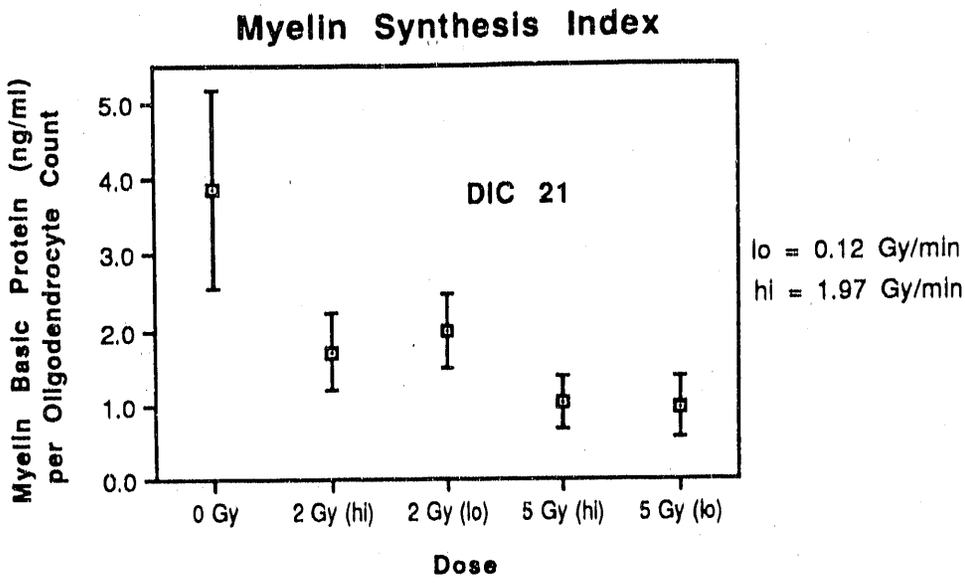

Kruskal-Wallis X 1 : Dose Y 1 : MBP/Oligo

DF	4
# Groups	5
# Cases	42
H	29.46 p = .0001

Group:	# Cases:	Σ Rank:	Mean Rank:
Gy0	6	234	39
Gy2Hi	8	209	26.12
Gy2Lo	8	230	28.75
Gy5Hi	10	120	12
Gy5Lo	10	110	11

Figure 5.43. Myelin synthesis index (mean ± S.D.) in primary mixed glial cell cultures at DIC 21, following 2 Gy and 5 Gy γ-irradiation at DIC 8. Dose rates of 0.12 Gy/min and 1.97 Gy/min were examined. The index is defined as the ratio of myelin basic protein level (ng/ml) to mean oligodendrocyte grid count. This parameter appears to be a useful gauge of functional maturity of the average oligodendrocyte in culture. The index was quite sensitive to dose, but no dose-rate effect was detected (cf Figures 5.44 and 5.45.)

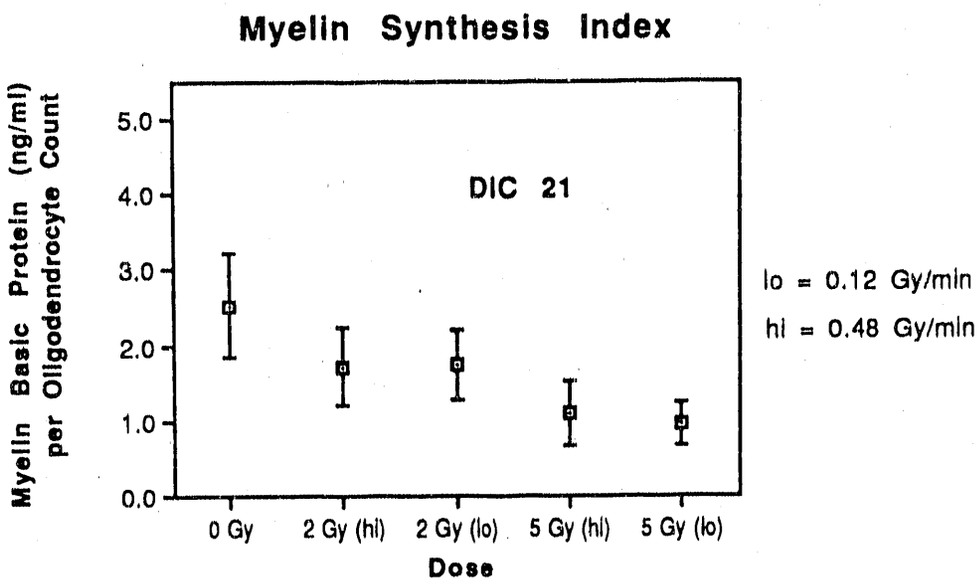

Kruskal-Wallis X 1 : Dose Y 1 : MBP/Oligo

DF	4
# Groups	5
# Cases	42
H	30.3 p = .0001

Group:	# Cases:	Σ Rank:	Mean Rank:
Gy0	11	391	35.55
Gy2Hi	8	189	23.62
Gy2Lo	7	169	24.14
Gy5Hi	8	91	11.38
Gy5Lo	8	63	7.88

Figure 5.44. Myelin synthesis index (mean ± S.D.) in primary mixed glial cell cultures at DIC 21, following 2 Gy and 5 Gy γ-irradiation at DIC 8. No difference was found between 0.12 Gy/min and 0.48 Gy/min.

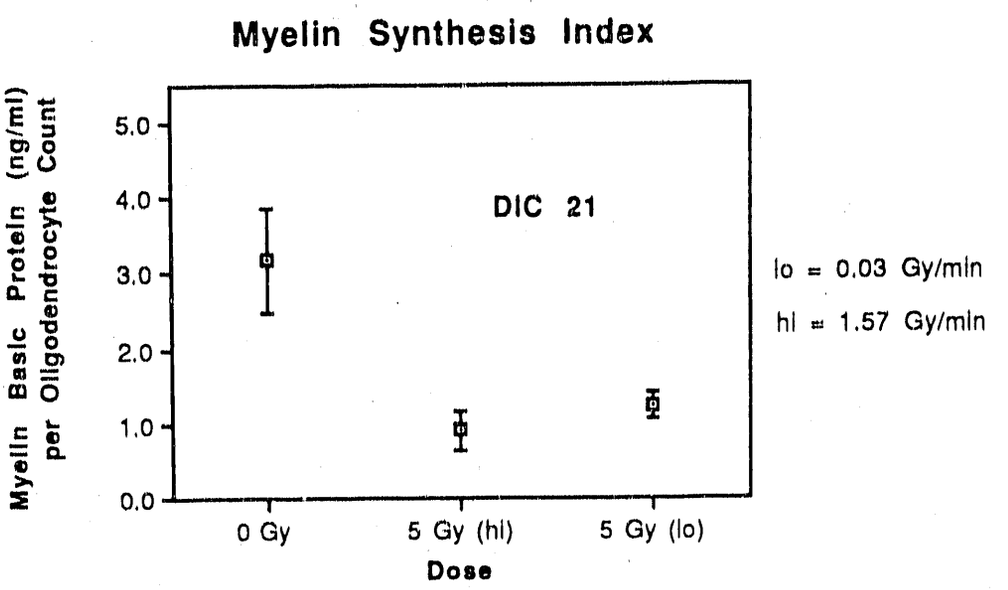

Kruskal-Wallis X 1 : Dose Y 1 : MBP/Oligo

DF	2
# Groups	3
# Cases	30
H	22.89 p = .0001

Group:	# Cases:	Σ Rank:	Mean Rank:
Gy0	10	255	25.5
Gy5Hi	10	68	6.8
Gy5Lo	10	142	14.2

Figure 5.45. Myelin synthesis index (mean ± S.D.) in primary mixed glial cell cultures at DIC 21, following 2 Gy or 5 Gy γ-irradiation at DIC 8. No difference was found between 0.03 Gy/min and 1.57 Gy/min.

CHAPTER 6
DISCUSSION

6.1 INTRODUCTION

Brain tissue is composed primarily of three types of highly differentiated neural cells - neurons, astrocytes and oligodendrocytes - that are clearly distinguished by their characteristic morphology and function. These cells all have long elaborate cytoplasmic processes which intertwine intimately with one another to form a highly integrated network of cell populations comprising the brain tissue. The complexity of these cellular relationships is increased further by an extensive and intricate vascular system. This profound heterogeneity and integration of hierarchical structure and function make it very difficult to investigate biochemical and metabolic mechanisms in defined cell types in intact tissue. The problem of cellular heterogeneity is exacerbated that much more when the brain has been subject to pathologic alterations [70].

The reaction of the brain to radiation injury involves a complex series of cellular events that interact to produce changes in neurophysiologic function [13,29,35,36,39,118,119,120]. Since delayed injury was first recognized to be a potential outcome of brain irradiation at high doses, opinions have been divided as to whether the pathogenesis of delayed injury reflects primarily glial (oligodendrocyte-mediated) or vascular origin [13,39,78,120]. The dose-dependency of white matter necrosis and vascular damage has further confused the issue of pathogenesis [120]. A fundamental approach to resolving the intrinsic responses to irradiation of the glial and endothelial cell populations is to isolate the populations from one another prior to irradiation. An *in vitro* cell culture system is essential to accomplish this goal, so that the cellular basis of the reaction to

radiation injury can be investigated.

Historically, cell culture techniques have been developed for evaluation of quantitative clonogenic cell-survival following irradiation in selected transformed "immortal" cell lines typically derived from mammalian, and occasionally human, malignant tissue [28,91]. For example, the radiation-response of glioma-derived cell clones has been studied extensively [25,34]. However, the metabolic properties of transformed cerebral cells growing *in vitro* can not be extrapolated readily to normal cerebral cells. Transformed cells generally lack the distinguishing metabolic characteristics of normal differentiated cells and they typically manifest a markedly different response to irradiation [34]. Accordingly, the development of methods for the isolation and maintenance of normal brain cells in culture and for the characterization of their response to irradiation *in vitro* was considered essential to this dissertation research.

The experimental goals of the thesis are summarized in a series of fundamental questions regarding delayed radiation injury of the brain.

1. What are the roles of the oligodendrocyte population and the myelination process in delayed radiation injury, in the absence of a vascular component of injury?

2. What are the metabolic correlates, extent and temporal patterns of functional recovery?

3. What is the capacity of the oligodendrocyte for repair of sublethal radiation injury?

4. Can the *in vitro* findings of the oligodendrocyte reaction to radiation injury be used to elucidate and predict the *in vivo* radiation response?

A series of experimental studies was designed and carried out to address

the fundamental questions posed above. The findings of these investigations are discussed in Section 6.2. The proliferative and functional responses of the oligodendrocyte and astrocyte populations are described in control and irradiated glial cultures. The variables studied include dose, dose rate and alterations in timing of split-dose irradiation. The implications for repair of sublethal oligodendrocyte damage are discussed. In Section 6.3, an *in vitro* compartmental model of glial cell reaction to radiation injury is proposed to explain the experimental results and to predict the outcome of selected investigations in progress. The proliferation and maturation characteristics of the oligodendrocyte and astrocyte populations are considered, and the relationships of these populations to each other and to a putative stem cell compartment are described. The proposed *in vitro* model is discussed in relation to previously described *in vivo* models of the determinants of reaction to radiation injury in the brain. Finally, future research directions are proposed.

6.2 EXPERIMENTAL FINDINGS

6.2.1 Unirradiated Glial Cell Cultures

Oligodendrocyte Line

In unirradiated glial cell cultures, the most striking finding was the time lag between the period of increase in the number of oligodendrocytes growing *in vitro* and the concomitant pattern of myelin synthesis. The oligodendrocyte population, as identified by morphologic criteria (see Section 3.3.1), increased approximately 70% between day-in-culture (DIC) 7 and DIC 14 and reached a steady-state level shortly thereafter (see Section 4.2.4 and Figure 4.7). This increase in oligodendrocyte number appears to result from differentiation and/or proliferation of previously committed, but morphologically and immunocyto-

chemically indistinct and unrecognized, precursor cells rather than from proliferation of oligodendrocytes with characteristic morphologic and immunocytochemical properties. This conclusion is supported by the tritiated-thymidine incorporation studies detailed in Section 4.4.1. No thymidine uptake was detected at DIC 7 in those cells determined by anti-galactocerebroside (GC) staining to correspond to the characteristic phase-dark cells counted as oligodendrocytes during these investigations. The absence of demonstrable oligodendrocyte proliferation at this stage confirmed previously reported studies in mixed glial and isolated oligodendrocyte cultures [72,113].

A different temporal pattern was apparent, however, when the *functional* capacity of the oligodendrocyte population was examined. During the initial stage of cell population increase, the amount of myelin synthesis per cell remained limited. This growth phase yielded to a period of rapid oligodendrocyte differentiation, accompanied by extensive and concurrent synthesis of myelin membrane. Myelin basic protein (MBP) levels, which strongly correlate with myelin synthesis, increased 35-fold from DIC 7 through DIC 28 (see Figure 4.34) [23]. This nearly exponential rate of increase in MBP *in vitro* corresponded well to the very high rate of myelin synthesis that occurs at comparable cellular age *in vivo* [82].

The regulatory factors controlling population growth, maturation and differentiation in oligodendrocytes and their precursors are not well understood. However, various studies suggest the importance of extra-oligodendroglial factors in the overall process of myelin formation. For example, neurons [130], rodent brain extract [87], and soluble extracts from astrocyte-enriched cultures [9] all stimulate oligodendrocyte development *in vitro*. Insulin, transferrin and fibroblast growth factor synergistically induce more than 90% of isolated oligodendrocytes cultured in a serum-free, chemically defined medium to undergo cell division [99]. Surgical brain trauma in adult mice causes mature oligodendro-

cytes to incorporate tritiated thymidine [60]. Conversely, a factor found in fetal calf serum has an inhibitory effect on oligodendrocyte proliferation [92]. Normal oligodendrocyte-specific end-products (e.g., selected myelin components and enzymes) may also play a role, by exerting local inhibitory control if threshold concentrations are exceeded in the culture milieu. Reversible inhibition of oligodendrocyte progenitor differentiation by a monoclonal antibody against surface galactolipids has been demonstrated *in vitro* [6].

Astrocyte Line

The astrocyte population *in vitro*, as observed microscopically and as examined indirectly by changes in total cellular protein levels, rapidly increased its numbers during the period from DIC 7 to DIC 14 (see Figure 4.35). Tritiated-thymidine incorporation studies using fluorescence-activated cell sorting demonstrated active deoxyribonucleic acid (DNA) synthesis in the astrocyte population at DIC 7 (see Section 4.4.1). Astrocyte proliferation continued until inhibited by apparently extrinsic cellular factors (e.g., contact inhibition).

Although further astrocyte proliferation in culture appeared to be halted by contact inhibition once cellular confluence was attained, total cellular protein synthesis continued unabated at least to DIC 28. The sustained protein synthesis presumably reflected continuing metabolic function of the maturing astrocyte population rather than unrestrained proliferation. Accordingly, the total cellular protein level is viewed more appropriately as an index of composite functional activity of the astrocyte population rather than a direct measure of cell number.

Whether additional factors play a role in controlling astrocyte population growth and differentiation in the experimental mixed glial culture system is not well established. When purified monolayer cultures of astrocytes were grown in a chemically defined medium, hydrocortisone, putrescine, prostaglandin $F_{2\alpha}$,

insulin and fibroblast growth factor were all found to stimulate astrocyte proliferation and subsequent differentiation [77].

Active proliferation of astrocytes *in vivo* is tightly regulated during the normal development of the brain, and proliferation of the astrocyte population typically ceases in the adult [131]. However, in selected pathologic conditions, including traumatic and degenerative brain injury, the astrocytes are capable of resuming proliferative activity [17,51,106].

6.2.2 Irradiated Glial Cell Cultures: Dose Response

Oligodendrocyte Line

The behavior of the oligodendrocyte population following single doses of γ-irradiation suggested that the highly differentiated cells are moderately radiosensitive; the response was dose-dependent, and the initiation and duration of recovery was dose-dependent, as well. At DIC 14, when the counts of morphologically distinct oligodendrocytes in control cultures reached maximal levels, oligodendrocyte counts in irradiated cultures lagged far behind (see Section 5.3.2). Counts were only 55% to 65% of control values after 2 Gy irradiation, and 29% to 36% of control values after 5 Gy irradiation. However, the oligodendrocyte populations in irradiated cultures increased in number considerably over the following week, reaching near-normal levels at DIC 21 in the 2-Gy irradiated group and about 75% of normal levels in the 5-Gy irradiated group (Figure 6.1).

The temporal pattern of MBP production in irradiated cultures demonstrated that the recovery of the functional capacity of the oligodendrocyte population following irradiation was also dose-dependent, and that the temporal pattern of recovery was not well correlated with changes in the oligodendrocyte counts (Figure 6.2). At DIC 14, MBP levels attained about 60% of control values in cultures irradiated with 2 Gy, and 40% of control values in cultures irradiated

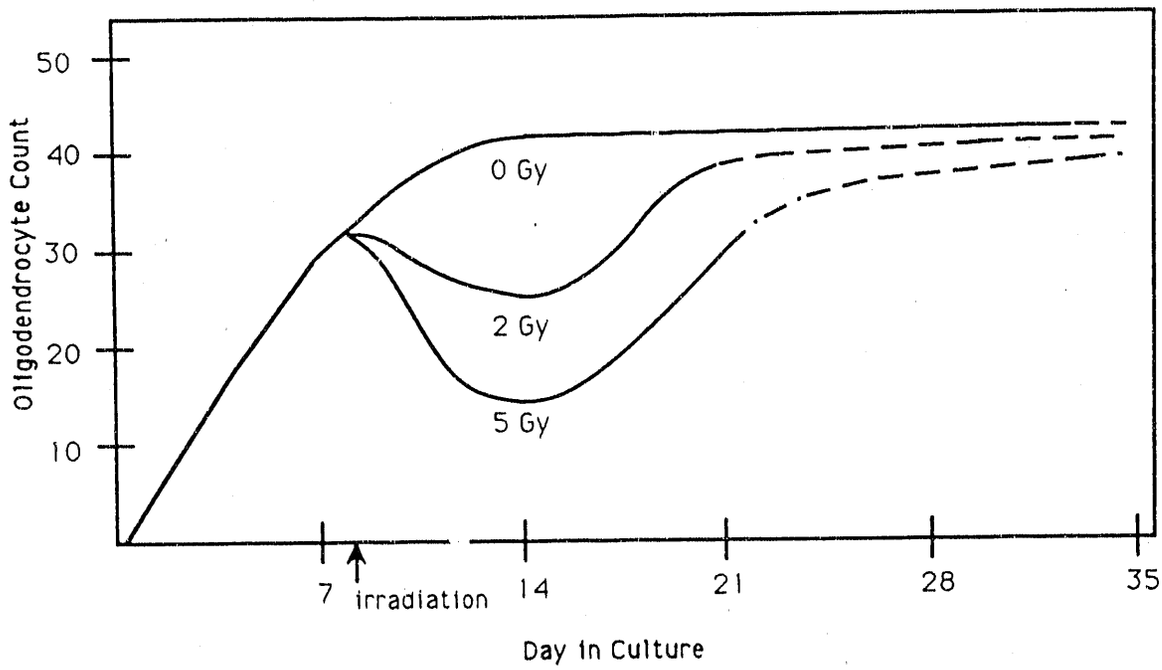

Figure 6.1. Schematic representation of the response of the oligodendrocyte population as a function of DIC and radiation dose. The temporal pattern of response is shown for unirrradiated control cultures and cultures irradiated with 2 Gy or 5 Gy γ-irradiation at DIC 8. Solid lines represent experimental data. Dashed lines represent projected patterns of response. Cultures irradiated with higher doses sustain more dramatic and longer-lasting decrements in oligodendrocyte counts than cultures irradiated with lower doses. However, even 5 Gy-irradiated cultures show significant recovery of oligodendrocyte counts by DIC 21 (see Section 6.2.2).

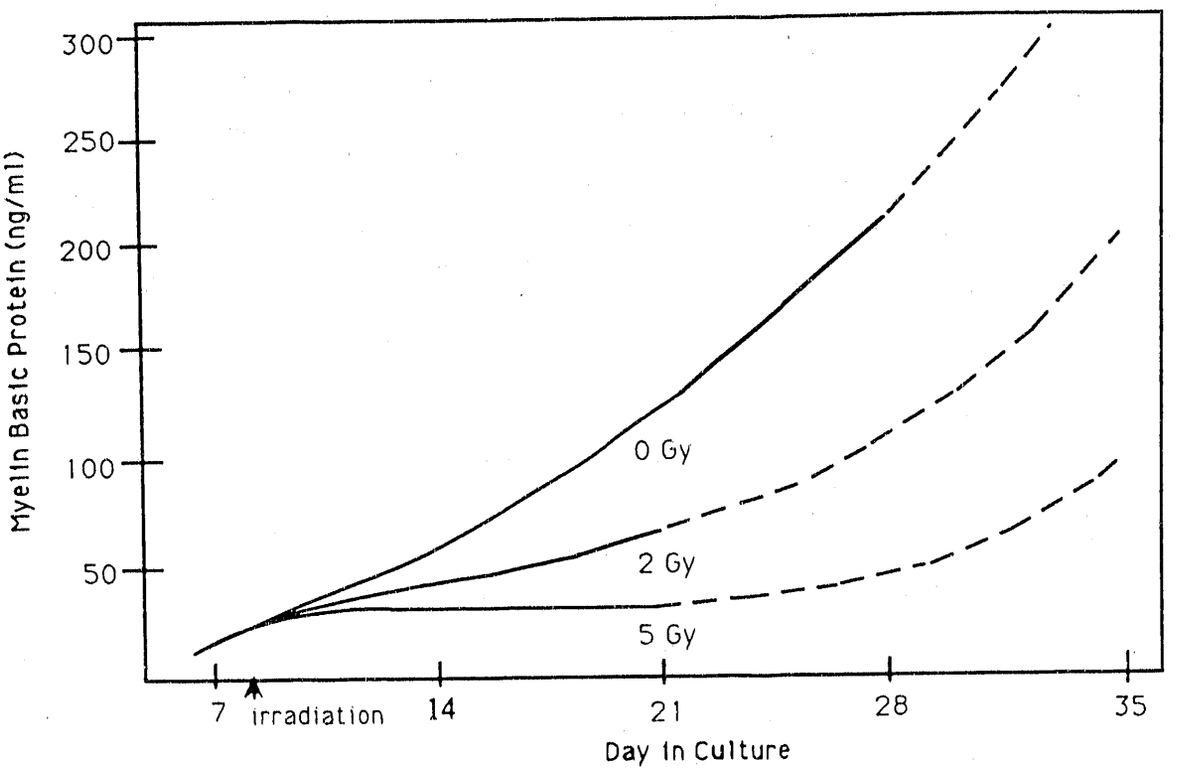

Figure 6.2. Schematic representation of the temporal pattern of MBP synthesis as a function of DIC and radiation dose. The response is shown for unirrradiated control cultures and for cultures exposed to 2 Gy or 5 Gy γ-irradiation at DIC 8. Solid lines represent experimental data. Dashed lines represent projected patterns of response. Cultures irradiated with higher doses sustain more dramatic and longer-lasting impairment in MBP production. At DIC 21, 5-Gy irradiated cultures show no recovery in MBP synthesis and 2-Gy irradiated cultures show modest recovery, even while the counts of oligodendrocytes have increased considerably from their nadirs (see Figure 6.1). It is projected that MBP renewal will gradually recover as the new replacement oligodendrocytes differentiate and mature.

with 5 Gy. These MBP values (as a function of control values) were roughly proportional to the oligodendrocyte counts at DIC 14 in similarly irradiated cultures. Based on these findings, it could be concluded that irradiation reduced the number of oligodendrocytes reaching maturity, but that the surviving oligodendrocytes continued to differentiate and function normally, or that oligodendrocytes ultimately fated to die continue to carry on biochemical function. In this situation, MBP levels would be considered simply as an index of the number of oligodendrocytes in culture. However, at DIC 21 a different relationship between MBP levels and oligodendrocyte counts began to emerge. At this time, the absolute MBP level in cultures irradiated with 2 Gy was about 45% greater than that observed at DIC 14, but the MBP level as a fraction of age-matched control MBP values dropped from about 60% to 50% during this same interval. When cultures irradiated with 5 Gy were considered, absolute MBP levels changed little between DIC 14 and DIC 21, but MBP levels relative to control cultures decreased from about 40% to 25%. It was concluded, therefore, that the oligodendrocyte population in irradiated cultures was qualitatively different than the oligodendrocyte population in control cultures, the former manifesting a significantly lower functional capacity following exposure. This difference was dose-dependent and was quantifiable in the myelin synthesis index (see Section 5.6).

The saturation of the MBP response between DIC 14 and DIC 21 following 5-Gy irradiation is proposed to be the composite result of several different factors.

1. The population of normally functioning oligodendrocytes is markedly decreased by irradiation injury.

2. Undamaged oligodendrocytes continue to differentiate and synthesize rapidly increasing quantities of myelin.

3. Damaged oligodendrocytes ultimately fated to die continue to synthesize myelin in the interim.

4. The oligodendrocyte population begins to recover as the progenitor cells proliferate and mature in response to the loss of inhibitory feedback control (and/or other regulatory factors); however, the replacement cells initially have very low synthetic capabilities commensurate with cell age.

Analysis of radiation response by plotting oligodendrocyte survival as a function of radiation dose, in a manner analogous to that classically used to describe the response to irradiation of immortal mammalian cells grown in tissue culture, introduced a number of methodologic problems and technical difficulties. With immortal cell lines, the natural logarithm of the surviving fraction of clonogenic cells, when plotted as a function of dose, demonstrates an initial shoulder in the low-dose range followed by a linear exponential portion [2,3,28]. The generally accepted interpretation of this mathematical relationship assumes that cells with surviving clonogenic capacity will proliferate to form discrete colonies that can be counted, and that cells rendered nonclonogenic will not form colonies (and therefore not be counted). This pattern of response, however, does not occur with mature oligodendrocytes. These cells do not form discrete colonies even under optimal growth conditions, preferring instead to interact with one another via their extended network of processes, and their numbers reach a steady-state plateau fairly early in culture (see Section 6.2.1). Additionally, since oligodendrocytes typically have limited mitotic activity, some radiation-damaged cells will appear morphologically normal throughout the duration of the experiment and will be counted as if they were unaffected. A more detailed discussion of the limitations of clonogenic assays in evaluating radiation response of normal tissues is found in reference [74].

Another confounding variable is the uncertainty regarding the extent to which committed oligodendrocyte-precursor cells and/or pluripotential stem cells in the culture recognize the damage to the oligodendrocyte population and the degree to which these cells are capable of responding to the radiation insult. The concentrations of those humoral factors hypothesized to play an inhibitory role in controlling the oligodendrocyte-population growth phase in unirradiated cultures (see Section 6.2.1) might be expected, in cultures damaged by irradiation, to drop below the threshold levels required to suppress the progenitor-cell population. Whether additional factors (e.g., soluble moieties of astrocyte origin [9,87]) may play a role in stimulating or suppressing *in vitro* growth and development of the oligodendrocyte population following irradiation injury is not established [10,71].

The reproductively viable stem cells and oligodendrocyte precursors present in the culture will themselves lose clonogenic potential in significant numbers due to irradiation, in a dose-dependent fashion. Thus, the degree to which the oligodendrocyte progenitors are capable of replenishing the mature oligodendrocyte population will be compromised. With increasing radiation dose, fewer viable progenitors will remain and the surviving ones will require more time to restore the population to pre-irradiation numbers. If the dose is high enough, the progenitor population will be sterilized completely and no recovery will be possible.

Oligodendrocyte-Progenitor Cells

The subependymal cell layer is presumed to represent an anatomically defined stem cell compartment with self-renewal properties [49,65,85,118]. Glial cell kinetics have been studied extensively in rodents. Korr, Schultze and colleagues [49,103] concluded that glial cells continue to proliferate throughout life. Proliferating glial cells have a cell cycle time of about 20 h, but the growth frac-

tion declines from about 0.1 in the 2-wk-old rat to 0.004 in the adult mouse. Approximately half of newly formed cells leave the growth fraction, but some nonproliferating cells re-enter the growth fraction and begin to proliferate [49]. These findings support the contention that differentiated glial cells retain the capability to revert to a proliferative state, and that an increased proportion may do so when cells are lost after a cytotoxic insult (see Section 6.2.1).

Paterson et al [85] studied the migration and maturation of cells originating in the rat subependymal cell layer by using autoradiographic evaluation following intraventricular injection of tritiated thymidine. Subependymal cells migrated to the cerebral cortex at the level of the corpus callosum, where they were termed "free subependymal" cells; these cells then differentiated into progressively mature oligodendricytes, as identified by morphologic criteria. The proliferation of glial cells *in situ* is similar in different regions of the brain, and most likely is independent of proliferative activity in the subependymal plate [49].

Radiation injury to the subependymal cell compartment has been demonstrated in the rodent brain brain, and the kinetics of injury and repair have been characterized [20,40,41,42,49,65]. However, the relationship between acute radiation changes in the subependymal plate and late damage in other regions of the brain is not well established. The morphologically indistinct progenitor cells, previously hypothesized to explain some of the experimental findings of this dissertation, correspond well to the "free subependymal" cells described *in situ* by Paterson et al [85]. These cells may be considered to constitute a *functional* stem cell compartment in dissociated cell culture, analogous to the *anatomic* stem cell compartment of the subependymal plate *in vivo*.

The nature and origin of the oligodendrocyte-specific progenitor population are not well understood. The existence of pluripotential glial progenitor

cells was established by *in vitro* studies demonstrating that cells with stem-cell properties could be isolated from perinatal rat optic nerve [92]. These cells (termed O-2A progenitor cells) differentiated into oligodendrocytes or type-2 astrocytes depending on the culture medium. (The processes of type-2 astrocytes contact the nodes of Ranvier; glutamate receptors on the surface of these cells suggest glial-neuronal signalling at the node [123].) O-2A cells have clonogenic colony-forming properties when cultured under certain conditions; recently, van der Maazen et al [122,123] have used these clonogenic properties to develop an *in vitro* colony-counting assay for stem-cell survival following irradiation.

Further support for the pluripotential origins of the oligodendrocyte population comes from immunocytochemical evaluation of purified oligodendrocyte cultures derived from neonatal rat cerebrum and grown in a serum-free, chemically defined medium found to encourage oligodendrocyte proliferation [99]. A marked increase in the number of cells positive for MBP, GC and A2B5 (an antigen typically found in O-2A progenitor cells [26,92]) was found. The addition of serum to the defined medium at the time of oligodendrocyte isolation, however, resulted in the appearance of phase-dark cells expressing reactivity to glial fibrillary acidic protein (GFAP). Taken together, these findings suggest that isolated oligodendrocyte cultures in these cultures are developmentally immature and that a subpopulation can be induced to differentiate into GFAP-positive cells by manipulation of the culture environment [99].

Additional indirect evidence for the presence of pluripotential precursor cells derives from correlative electron microscopic and immunohistochemical studies of human fetal spinal cord; "transitional" cells were found with cytologic, ultrastructural and immunohistochemical features intermediate between those of astroglial and oligodendroglial cells [21].

Astrocyte Line

Total cellular protein levels *in vitro* recovered toward normal values rather quickly after irradiation, reflecting the very high capacity of the astrocyte population for recovery from radiation injury. Through active proliferation and differentiation, the astrocyte population was rapidly replaced. Following doses in the 2 Gy to 5 Gy range at DIC 8, total protein levels at DIC 14 were about 60% to 70% of unirradiated age-matched controls. By DIC 21, however, even 5-Gy irradiated cultures had total protein levels at 90% to 100% of control values.

6.2.3 Irradiated Glial Cell Cultures: Repair of Sublethal Damage

The theoretical considerations underlying the concept of sublethal radiation damage and repair in mammalian cells were discussed in Section 2.4.3. In this investigation, the extent and temporal pattern of repair in populations of irradiated glial cells were evaluated by characterizing the oligodendrocyte response to split-dose irradiation and to variation in dose rate.

Split-Dose Irradiation

The response of the oligodendrocyte population to split-dose γ-irradiation suggested that these cells were capable of a significant degree of repair of sublethal damage (see Sections 5.3.3 and 5.4.2). The general response of the irradiated cultures at DIC 14 (i.e., 6 d following irradiation with 5 Gy) was that of marked and statistically significant lowering of oligodendrocyte counts as compared with control cultures. Cultures irradiated with 5 Gy in one fraction had significantly lower oligodendrocyte counts than did cultures in all other irradiated groups; however, no significant differences in response were found between any groups irradiated with two 2.5-Gy fractions (see Figure 5.25). These findings were paralleled by the response to irradiation of MBP synthesis at DIC 14 – marked lowering of

MBP levels in all irradiated cultures, but no significant differences referable to the split-dose time interval (see Figure 5.33). A different pattern of response became apparent when irradiated cultures were evaluated at DIC 21 (i.e., 13 d following irradiation). Cultures irradiated with split-dose intervals of 0 h (i.e., 5 Gy in a single dose) to 2 h had similar oligodendrocyte counts to one another, but these counts were significantly lower than found in cultures irradiated with dose intervals of 4 h to 6 h or in unirradiated controls (see Figure 5.26). Cultures irradiated with a split-dose interval of 3 h had intermediate oligodendrocyte counts at DIC 14. However, the MBP levels remained severely depressed at DIC 21 for all irradiated cultures, with no significant split-dose response observed (see Figure 5.34).

The general temporal patterns of the morphologic and biochemical responses to irradiation demonstrated in the split-dose experiments described above were consistent with those seen in the single-dose experiments discussed in Section 6.2.2 (Figures 6.1 and 6.2). Specifically, oligodendrocyte counts were decreased markedly at DIC 14 following 5-Gy irradiation, but recovered considerably by DIC 21; MBP counts, on the other hand, remained severely depressed at least through DIC 21. However, the relative improvement in recovery of oligodendrocyte counts observed in cultures irradiated with longer split-dose intervals was highly suggestive of repair of sublethal damage. Differential MBP recovery could not be demonstrated in these experiments, but split-dose studies planned with lower doses and or longer followup periods (to DIC 28 and beyond) may well show a corresponding, albeit delayed, MBP response (see Section 6.2.1).

The experimental data suggest that nearly all of the sublethal damage in the oligodendrocyte population (and its precursors) caused by the initial conditioning dose is repaired within 3 h to 4 h. This estimate corresponds reasonably well to that of a repair-rate model that assumes repair to be a mono-exponential

function of time following irradiation [7,56]. The unrepaired fraction (U_f) of the repairable damage as a function of time (t) following irradiation can be described by:

$$U_f = e^{-\mu t}, \tag{6.1}$$

where μ is a rate constant that may vary for different tissues. Expressed in half-time of repair, $T_{1/2}$ values are in the range of 0.4 h to 1.6 h [115]. For example, if $T_{1/2}$ = 1 h, an interval of 3 h to 4 h corresponds to 88% to 94% of maximal repair. Van der Kogel [121] estimated a $T_{1/2}$ value of about 90 min for lumbosacral paralysis following 300 kVp x-irradiation of rat spinal cord; this value corresponds to 75% to 84% of maximal repair in a 3 h to 4 h period. Similar $T_{1/2}$ values were found for cervical spinal cord irradiation [4].

The astrocyte population did not demonstrate any significant differential response *in vitro* at DIC 14 or DIC 21 to variation in split-dose intervals. This finding was consistent with the previously described experimental data, which had suggested that the high proliferative capacity of the astrocyte population would overwhelm any effect that might arise from differences in sublethal repair.

Dose-Rate Response

The cellular response to low dose-rate irradiation reflects the ability of a tissue to recover from sublethal damage. In contrast to split-dose or fractionated irradiation, however, the repair processes take place during the radiation exposure. As a consequence, the degree to which sublethal damage is repaired during low dose-rate irradiation depends both on the capacity and on the kinetics of cellular repair, since competition exists during exposure between the rate of production and the rate of repair of sublethal damage [100].

The response of the oligodendrocyte population to variation in dose rate

was evaluated *in vitro* at DIC 14 and DIC 21. Dose rates examined included 0.03, 0.12, 0.48, 1.57 and 1.97 Gy/min. One of two trials suggested that a dose rate of 0.12 Gy/min was less effective in reducing oligodendrocyte population than were higher dose rates (Figures 5.22 and 5.23). Moreover, a dose rate of 0.03 Gy/min was less effective in producing radiation damage than a dose rate of 1.57 Gy/min in 5-Gy irradiated cultures examined at DIC 21 (Figure 5.24).

It is of interest that the dose rates found (0.03 Gy/min) or suggested (0.12 Gy/min) to have decreased effectiveness were comparable to dose rates found *in vivo* to have similar effects in the spinal cord and other late-responding tissues and organs (see Section 2.4.3) [31]. In Figure 6.3, the spinal cord irradiation data of Scalliet et al [100] and van der Kogel [121] are plotted as a function of dose rate [31]; the arrows indicate the dose rates examined experimentally in this dissertation. Oligodendrocyte response in the region of 0.03 Gy/min to 0.12 Gy/min must be examined in more detail (e.g., at still lower dose rates and at doses other than 5 Gy) to confirm the presence of a dose-rate effect *in vitro*.

No differential response was found for MBP synthesis or for total cellular protein synthesis for any permutation of dose rates examined at DIC 14 or DIC 21. These experimental results are consistent with the related experimental data reported previously (see Sections 5.4 and 5.5), and their fundamental interpretation is correspondingly similar and will not be reiterated here (see Section 6.2.2).

6.3 MODELS OF DELAYED RADIATION INJURY OF THE BRAIN

6.3.1 Theoretical Approaches

There are many different theoretical models of delayed radiation injury in the brain and they can be grouped into three major classes [57]: (1) repair-

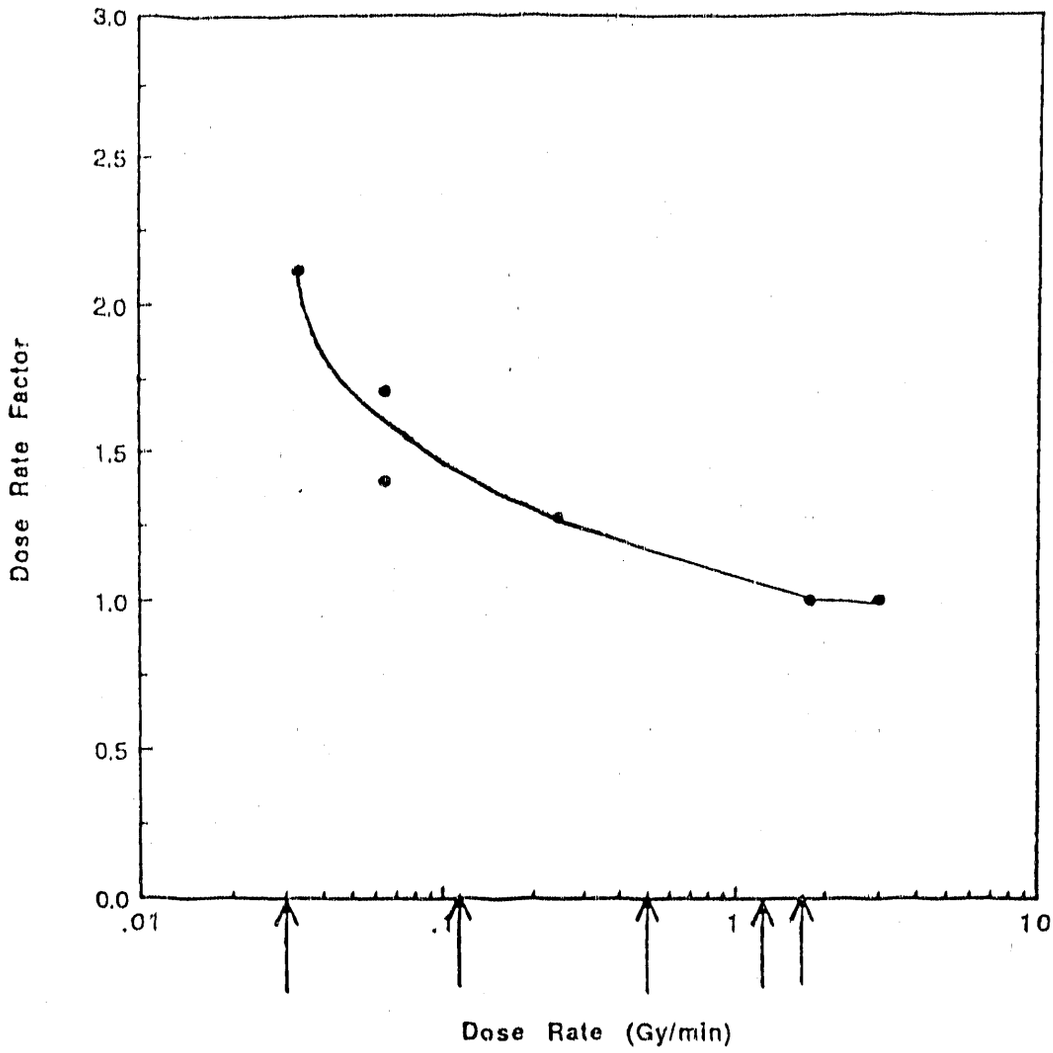

Figure 6.3. The spinal cord irradiation data of Scalliet et al [100] and van der Kogel [121] are plotted as a function of dose rate. The dose-rate factor, defined as the ratio of isoeffect dose for a given dose rate to the isoeffect dose for a reference dose rate, is shown. The arrows indicate the dose rates examined experimentally here. A dose rate of 0.03 Gy/min was less effective in suppressing oligodendrocyte counts at DIC 21 than were higher dose rates in 5-Gy irradiated cultures; a dose rate of 0.12 Gy/min was equivocally less effective than were higher dose rates. It is seen that these dose rates correspond to dose rates found *in vivo* to be on the rising portion of the dose-rate factor curve.

misrepair models, which evaluate response at the subcellular (DNA) level [24, 46,117]; (2) target cell models, which examine responses at the cellular level in crucial cell populations [39,120]; and (3) dose-volume models, which describe neurophysiologic response at the tissue and organ level in terms of the volume of brain irradiated and the dose received [30,102].

Repair-misrepair models focus on the temporal response of lesions formed at the subcellular level. Radiation-induced lesions are created by the interaction of DNA with electrons and their delta rays produced by the primary ionizing event. The initial energy transfer events, which comprise the track structure of the radiation beam, require about 10^{-16} sec; subsequent physicochemical processes, including formation of radicals and propagation of indirect DNA injury occur in about 10^{-3} sec [19,117]. Enzymatic repair mechanisms are considered to be competitive with other molecular processes that fix the lesions irreversibly. However, DNA repair rates are not well established, and are estimated to range from the order of seconds ("fast" repair) to hours or days ("slow" repair) [18,19,98]. Fast and slow repair kinetics may both be operational and are considered complementary. More detailed discussions of repair-misrepair models are found in references [24] and [117].

The application of dose-volume parameters to explain and predict determinants of delayed radiation injury represents the opposite end of the theoretical-model spectrum from the subcellular (DNA) model described above. Here, the response at the organ level is considered as a function of dose, fractionation and volume of brain irradiated. This approach has great utility in clinical radiotherapy, but it does not specifically address fundamental mechanisms of delayed radiation injury. A more detailed discussion of dose-volume-injury considerations can be found in reference [54].

Various target cell models have been proposed to bridge between the subcellular and tissue- and organ-level responses [39,78,118,120]. The oligodendrocytes and the cerebral endothelial cells are generally considered to be the target cells involved in mediating delayed radiation injury, although there is considerable debate regarding the relative contributions of these two cell types. The experimental background supporting these models is discussed in Section 2.4. A primary goal of this dissertation has been to investigate the behavior of the oligodendrocyte population in response to radiation injury, free of the potential influence or contribution of the vascular system. A proposed theoretical model of oligodendrocyte behavior is presented to integrate the experimental observations discussed above.

6.3.2 A Compartmental Model of Oligodendroglial Cell Response to Irradiation

A compartmental model of glial cell response to irradiation *in vitro* is proposed to explain the experimental findings described. In this section, an overview of the model is presented. Supporting arguments are drawn concurrently from the experimental data in this investigation (see Section 6.2) and from findings reported by others in the neuroscience and radiobiology literature. The model consists of pathways of proliferation and differentiation/maturation for oligodendrocyte lineages, arising from a precursor population of pluripotential stem cells (Figure 6.4). Parallel pathways of proliferation and differentiation for the astrocyte lineage *in vitro* and the interdependency of oligodendrocyte and astrocyte populations are important functional components of the model. Regulatory feedback loops and potential sites of irradiation action are postulated.

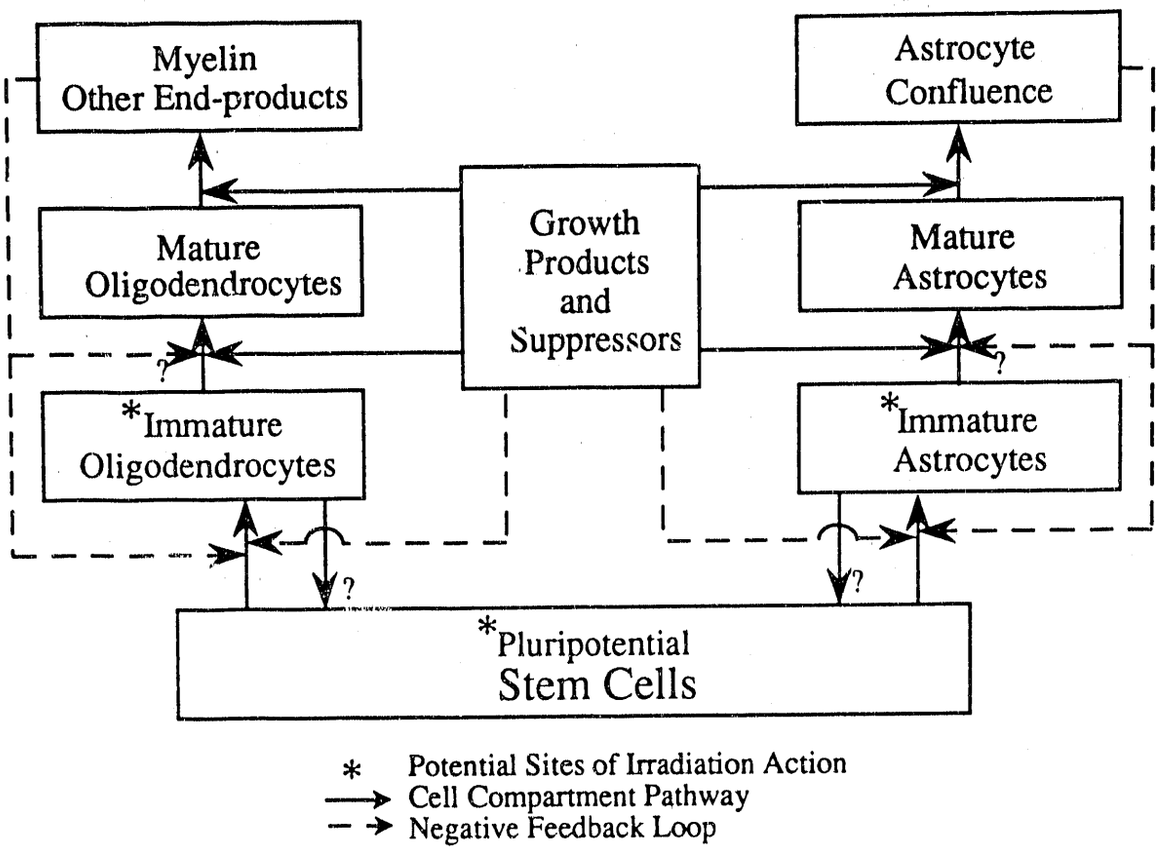

Figure 6.4. Compartmental model of glial cell response to irradiation *in vitro*. The model consists of parallel pathways of proliferation, differentiation and maturation for cells of oligodendrocyte and astrocyte lineages, each lineage arising from a precursor population of pluripotential stem cells (see Section 6.3.2). Regulatory negative feedback loops are shown as dashed arrows. Pathways of cellular maturation and differentiation and sites of action for stimulatory/growth agents are shown as solid arrows. Potential sites of irradiation action are denoted by asterisks. It is not known whether immature "committed" cells are capable of de-differentiating under certain conditions.

Unirradiated Glial Cell Cultures

The application of the model to the unirradiated cell culture system is described first. Immature undifferentiated committed cells destined for either oligodendrocyte or astrocyte lineage are present in the initial culture of neonatal brain cells. These original committed progenitor populations give rise to or coexist with newly committed undifferentiated cells arising from pluripotential stem cells also present in the initial neonatal cell culture. The immature oligodendrocytes and astrocytes undergo proliferation to expand their respective populations, and this is followed by differentiation to achieve ultimately appropriately sized populations of mature differentiated cells.

Astrocyte proliferation continues unabated *in vitro* until the surface of the culture flask is fully covered; regulation by contact inhibition then turns off the proliferative process. Thereafter, the astrocytes continue to synthesize protein as they undergo further differentiation, but they no longer increase in cell number.

The initial increase in number of phase-dark oligodendrocytes in unirradiated control cultures can be explained by two alternative hypotheses or a combination of the two: (1) proliferation of oligodendrocyte-specific progenitors and/or recruitment of pluripotential stem cells [103]; or (2) maturation of morphologically unrecognized, but previously committed, cells into more-differentiated oligodendrocytes with typical phase-microscopic characteristics [129]. In response to intrinsic (genetically programmed intracellular signals) and/or extrinsic (culture milieu) factors, the period of oligodendrocyte population increase terminates at about DIC 14. Since the oligodendrocyte population never achieves confluence, the relevant regulatory control mechanism must be other than contact inhibition. Various components of myelin and/or other oligodendrocyte end-products, if present in sufficient concentration in the culture milieu, are postulated in the proposed model to be inhibitory to oligodendrocyte proliferation. As the oligo-

dendrocyte population reaches its maximum number at about DIC 14, individual cells undergo progressive differentiation and manifest greatly enhanced capacity to synthesize myelin. If the metabolic integrity of the culture is compromised for any reason, a consequent loss of inhibitory feedback control may ensue if the amplitude of the inhibitory signal is lowered below its threshold for effectiveness. This process would stimulate replacement activity in the stem cell compartment, and may induce transfer of reversibly committed immature glial cells or unrecognized precursors back into the stem cell pool. Here, transfer would only occur from committed to uncommitted progenitor state, and would not involve mature functional end-cells.

Irradiated Glial Cell Cultures

When the glial cell cultures at DIC 6 to DIC 8 are irradiated with single doses in the range of 2 Gy to 5 Gy, perturbation of oligodendroglial cell proliferation kinetics involves both intracellular repair and recovery. Some committed stem cells and immature oligodendrocytes undergo reproductive cell death during the days immediately following irradiation, resulting in decreased numbers of morphologically identifiable oligodendrocytes. The surviving oligodendrocytes continue to differentiate and synthesize myelin. Committed oligodendrocyte precursors and stem cells undergo active compensatory proliferation, increasing the number of mature oligodendrocytes *in vitro* with return to control values over a period of 2 to 3 wk. The newly formed oligodendrocytes lag behind the surviving (or unirradiated) oligodendrocytes in their functional capacity, but these new cells mature and differentiate over the next several weeks, ultimately achieving comparable metabolic capabilities. While the experimental data at present do not demonstrate recovery of MBP synthesis to near-normal control values, 2-Gy irradiated cultures have begun to show recovery of MBP levels by DIC

21. This pattern of functional recovery will require experimental confirmation by extending culture analysis out to beyond DIC 28 (Figure 6.2).

The astrocytes at DIC 6 to DIC 8 are actively engaged in cell proliferation, and are quite sensitive to radiation injury. Initially, the astrocyte population decreases promptly following exposure. However, the surviving astrocytes and surviving committed stem cells have very high proliferative capacities, and rapidly compensate for the cells lost to irradiation. Cellular confluence on the culture flask surface is restored within 1 to 2 wk, and astrocyte function quickly returns to normal levels.

A Model for Delayed Radiation Injury

The experimental results and cell compartmental model discussed above describe patterns of radiation-induced injury and recovery in the oligodendrocyte population *in vitro* analogous in a number of ways to the situation that obtains *in vivo*:

1. The number of oligodendrocytes *in vitro* decreases following irradiation. The magnitude of this response is sensitive to variations in total dose, dose-rate and split-dose intervals, in a manner similar to that observed *in vivo*.

2. The temporal patterns of *cellular* recovery in the oligodendrocyte population *in vitro* (i.e., gradual recovery to a seemingly *predetermined* level) are consistent with homeostatic regulatory controls typically manifested *in vivo*.

3. The patterns of *functional* loss and recovery in culture (as measured by myelin synthesis) appear analogous to patterns of demyelination and remyelination found *in vivo*. The magnitude of functional loss and the timing

and the ultimate extent of functional recovery are dose-dependent. This phenomenon corresponds to eventual tissue breakdown and loss of functional end-cells *in vivo* when the radiation-damaged pool of progenitor cells can no longer compensate effectively due to damage in the stem-cell and proliferative compartments of a renewing cell population [120].

The proposed model is, at present, incomplete and may not accurately include recruitment of *in vivo* mechanisms of target cell response, depletion and recovery, and their relationship to delayed radiation injury. However, the model helps in the design of further experimental studies to elucidate the cellular bases of delayed injury by examining the individual cell-specific metabolic determinants of the cell populations involved.

6.4 PERSPECTIVES AND FUTURE DIRECTIONS

The response of mammalian brain tissue to ionizing radiation involves a complex cascade of sequential and interdependent cellular events, the first stages of which are completed in time frames ranging from small fractions of a second to several days (see Section 6.3.1). These cellular responses *in vivo* to the presence of damaged DNA may not become apparent for many months after irradiation, because the mammalian brain is comprised of a hierarchy of terminally differentiated cells that do not proliferate (neurons) or cells that have very long turnover periods (glial and cerebral endothelial cells) [39,103,120,128]. Furthermore, these cellular changes may not become manifest at the tissue level for several months or years [29,35,36,105]. The functional integrity of the brain requires that damaged or senescent differentiated cells of both parenchymal and vascular cell populations are replenished efficiently. Under optimal conditions, both rapidly and slowly proliferating cell renewal systems are maintained in a

steady-state equilibrium of cell production and differentiation and cell death, and regulated by complex feedback control mechanisms. Under the stress of radiation injury, this equilibrium is threatened and may be overwhelmed by concomitant expression of overt cellular damage and consequent brain dysfunction.

Given the extreme complexity of the neurophysiologic responses to radiation injury, it is inevitable that a variety of experimental strategies have evolved to examine and to characterize these responses. These various approaches have been described in Section 2.4 and earlier in this chapter. In general, the methods can be categorized as emphasizing either quantitative *population-specific* endpoints or more qualitative *functional* endpoints. For example, quantitative *in vitro* assays have been developed to examine DNA strand breaks (but without specific *functional* endpoints) or to evaluate clonogenic survival in glioma-derived cells (which have limited functional similarity to normal brain cells). Other quantitative assays evaluate highly selected populations of glial cell precursors, including mitotically active cells of the subependymal plate (quantitative high-resolution autoradiography for evaluation of cell cycle kinetics) and O-2A progenitor clones (colony-counting assay). On the other hand, functional *in vivo* assays, which examine endpoints at the tissue level (histopathologic changes and limb paralysis), typically obscure the unique roles of specific cell types in the pathogenesis of radiation injury and recovery, and they integrate the response of the parenchymal and vascular components.

The experimental model developed here is viewed as complementary to the approaches described above, and not as a replacement for them. Although using an experimental system of dissociated cell cultures for evaluation of brain function requires the conversion of a complex three-dimensional tissue structure into a quasi-two-dimensional array of cells, this *in vitro* model has many similarities and correlates to the situation *in vivo*. The approach is designed to integrate

the *population-specific* and the *functional* approaches for evaluation of delayed radiation injury of the brain. For example, oligodendrocytes *in vitro* are identified and quantified by morphologic and/or immunocytochemical criteria comparable to those applicable in tissue section. Functional responses *in vitro* (e.g., myelin synthesis) are also analogous to the situation at the *tissue* level *in vivo*. Thus, the quantitative response of the oligodendrocyte population and its functional response can now be assessed concurrently and without the confounding influences of the complex hierarchy of intertwined and functionally interdependent cell populations and particularly that of the vascular system. Furthermore, the experimental culture system contains progenitor cells capable of differentiating and proliferating in response to changes in the regional cellular environment.

A wide range of cellular parameters can now be examined using the techniques and analytical methods developed in these investigations. Thus far, experimental results have been presented demonstrating that the reaction to radiation injury is cell-specific, that it involves metabolic events in the highly differentiated oligodendrocytes, and that the system can be used to study sublethal radiation injury and repair, and to evaluate the temporal and morphologic patterns of response to injury of the oligodendrocyte lineage. It is planned to expand these investigations to evaluate the effects of low dose-rate and split-dose irradiation in greater detail. A number of other research directions are currently in progress or under consideration.

1. The response to irradiation of the oligodendrocyte population *in vitro* has been experimentally determined to DIC 21. It is now necessary to extend the investigation to DIC 28 and beyond to verify projections made regarding the time course and extent of cellular recovery. A broader range of doses will be evaluated.

2. Evaluation of antigen-specific subpopulations (e.g., GC, MBP, GFAP, A2-B5) should provide further insights into patterns of recovery following demyelination injury. Immunocytochemical labeling can be used to improve cell-specificity in grid-counting procedures and fluorescence-activated cell sorting, or in combination with autoradiographic examination of tritiated precursor incorporation.

3. Preliminary studies have demonstrated that the oligodendrocyte population is capable of repairing a significant degree of sublethal damage. This property must now be examined with a wider range of doses and dose rates. Examination of the oligodendroglial response to very low dose rates has potential implications for assessment of risk factors in exposed human populations (e.g., carcinogenesis in the workplace or in extraterrestrial environments). An understanding of the degree of oligodendrocyte repair following exposure to densely ionizing radiations (e.g., heavy ions or neutrons) should have implications for both experimental clinical radiotherapy and manned space travel.

4. The role of the vascular system in mediating delayed radiation injury in the brain is not fully understood, but it is believed to play some dominant role in the pathogenesis of delayed injury. Development of an *in vitro* technique for endothelial cell growth would permit concurrent examination of this important "target cell" population. This should have ultimate application to influence treatment stategies, notably in the radiotherapy of brain cancer.

5. The functional information derived from the experimental approach developed here is considered complementary to that of recently developed assays for clonogenic glial stem cell survival. The integration of these two approaches should help elucidate the regulatory control mechanisms

of oligodendrocyte proliferation and differentiation required to respond in a coordinated manner to cytotoxic insult. *In vitro* investigation of the metabolic basis of radiation sensitizers and protectors is possible; evaluation may be improved by an integrated approach.

There has been a predictable sequence in our progress in understanding the cellular determinants of radiation injury in the brain. Early studies focused on descriptive aspects of behavioral response. Next the pathology of brain injury was described, and attempts were made to correlate these findings with the behavioral response. More than 130 years ago, Rudolf Virchow stated, "Life is cell activity; its uniqueness is the uniqueness of the cell." Despite major advances in cellular neuroradiobiology, many questions remain unanswered in our quest to understand the cellular bases of neurologic disease. With improved capabilities for isolation and examination of the functional and metabolic responses of the different cell types, we can hope to further our investigation of basic cellular mechanisms in various pathologic conditions, including radiation injury of the brain.

CHAPTER 7
SUMMARY AND CONCLUSIONS

The response of mammalian brain tissue to ionizing radiation involves a complex cascade of sequential and interdependent events. Oligodendrocytes and cerebral endothelial cells are generally considered to be the target cells involved in mediating delayed radiation injury in the brain, although the relative contribution of these two cell types is not fully understood. Various target cell models have been proposed to explain the large spectrum of observed neurophysiologic perturbations, to integrate the subcellular and tissue-level models of radiation response, and to provide a framework for investigating the cellular bases of delayed radiation injury and repair in heterogenous and hierarchical brain cell populations.

An experimental *in vitro* cell culture system using neuroglial cells from dissociated neonatal rat brain was developed to examine oligodendroglial response to ionizing radiation. The oligodendrocyte population was assessed morphologically with grid counting, immunocytochemically with indirect antigen-specific immunofluorescent staining and fluorescence-activated cell sorting, and biochemically with measurement of myelin basic protein (MBP). The astrocyte population and its composite functional activity were assessed by determination of total cellular protein levels.

Following ^{60}Co γ-irradiation at day-in-culture (DIC) 8, oligodendrocyte counts at DIC 14 were 55% to 65% of control values after 2 Gy irradiation, and 29% to 36% of control values after 5 Gy irradiation. Oligodendrocyte counts in irradiated cultures increased considerably over the following week, reaching near-normal levels at DIC 21 in the 2-Gy irradiated group and about 75% of normal levels in the 5-Gy irradiated group. At DIC 14, MBP levels (as a fraction of

control values) were roughly proportional to oligodendrocyte counts; MBP measurements were about 60% of control values in cultures irradiated with 2 Gy, and 40% of control values in cultures irradiated with 5 Gy. At DIC 21, the absolute MBP level in cultures irradiated with 2 Gy was about 45% greater than that observed at DIC 14, but the MBP level, as a fraction of age-matched control values, dropped from about 60% to 50% during this same interval. When cultures irradiated with 5 Gy were considered, absolute MBP levels changed little between DIC 14 and DIC 21, but MBP levels relative to control cultures decreased from about 40% to 25%. It was concluded that the oligodendrocyte population in irradiated cultures was qualitatively different than the oligodendrocyte population in control cultures, the former manifesting a significantly lower functional capacity per cell following radiation exposure.

The response of the oligodendrocyte population to split-dose γ-irradiation suggested that these cells were capable of a significant degree of repair of sublethal damage. The general response of the irradiated cultures at DIC 14 was that of marked and statistically significant lowering of oligodendrocyte counts as compared with control cultures. Cultures irradiated with 5 Gy in a single fraction had significantly lower counts than those found in any group given split-dose irradiation. However, no significant differences in response were associated with the timing of the second dose. These findings were paralleled by the response to irradiation of MBP synthesis at DIC 14 – marked lowering of MBP levels in all irradiated cultures, but no significant differences referable to the split-dose time interval. A different pattern of response was apparent when irradiated cultures were evaluated at DIC 21. Cultures irradiated with split-dose intervals of 0 h (i.e., 5 Gy in a single dose) to 2 h had similar oligodendrocyte counts to one another, but these counts were significantly lower than found in cultures irradiated with dose intervals of 4 h to 6 h or in unirradiated controls. However, MBP

levels remained severely depressed at DIC 21 for all cultures irradiated with 5 Gy, and no significant split-dose response was observed. The experimental data suggest that nearly all sublethal damage in the oligodendrocyte population (and its precursors) induced by the initial conditioning dose is repaired within 3 h to 4 h. The response of the oligodendrocyte population to variation in dose rate was evaluated *in vitro* at DIC 14 and DIC 21. Dose rates examined included 0.03, 0.12, 0.48, 1.57 and 1.97 Gy/min. A dose rate of 0.03 Gy/min was less effective in suppressing oligodendrocyte counts at DIC 21 than were higher dose rates in 5-Gy irradiated cultures; a dose rate of 0.12 Gy/min was equivocally less effective than were higher dose rates.

Total cellular protein levels *in vitro* recovered to near-normal values rather quickly after irradiation, reflecting the very high capacity of the depleted astrocyte population for recovery from radiation injury. Through active proliferation and differentiation, the astrocyte population was rapidly replaced. Following doses in the 2 Gy to 5 Gy range at DIC 8, total protein levels at DIC 14 were about 60% to 70% of unirradiated age-matched controls. By DIC 21, however, even 5-Gy irradiated cultures had total protein levels at 90% to 100% of control values. No dose-rate or split-dose irradiation effects were noted.

The experimental system described has properties intermediate between clonogenic colony-counting systems and histopathologic approaches, and it should prove to be a useful method for elucidating cellular repair mechanisms and for correlating morphologic observations with tissue responses. Oligodendrocytes and/or their progenitors respond *in vitro* to changes in the regional cellular environment in a manner consistent with *in vivo* regulatory control mechanisms. Similarly, the observed temporal patterns of myelin loss and renewal *in vitro* appear analogous to patterns of demyelination and functional recovery *in vivo*. This experimental system may also prove useful for examining potential regu-

latory factors controlling population growth, maturation and differentiation in neuroglial cells and their precursors, and for examining the neurobiologic basis of radiation sensitization and protection.

Based on experimental results presented here, a new compartmental cell model of the *in vitro* reaction of glial cells to radiation injury is proposed to describe the correlations between the numerical and functional responses in the oligodendrocyte population. The model consists of parallel pathways of proliferation and differentiation/maturation for oligodendrocyte and astrocyte lineages, and their relationship to a precursor population of pluripotential stem cells. Regulatory feedback loops and potential sites of irradiation action are proposed.

In conclusion, an experimental tissue-culture-based model for brain irradiation was developed to examine the morphologic and functional reaction of the oligodendroglial population to radiation injury, while circumventing the potentially confounding presence of neuronal and vascular endothelial cell populations *in vivo*. The resulting experimental system is responsive to variations in dose, dose rate, and split-dose irradiation, and it should prove of value in elucidating fundamental mechanisms of delayed radiation injury of the brain.

Bibliography

[1] Agrawal HC and Hartman BK. Proteolipid protein and other lipids of myelin. In Bradshaw RA and Schneider DM (eds): *Proteins of the Nervous System, 2nd ed.*, pp. 145–169, Raven Press, New York, 1980.

[2] Alpen EL. *Radiation Biophysics.* Prentice Hall, Englewood Cliffs, 1990.

[3] Alper T. *Cellular Radiobiology.* Cambridge University Press, Cambridge, 1979.

[4] Ang KK, van der Kogel AJ, van Dam J, and van der Schueren E. The kinetics of repair of sublethal damage in the rat cervical spinal cord during fractionated irradiations. *Radiother Oncol* 1:247–253, 1984.

[5] Armitage P and Berry G. *Statistical Methods in Medical Research.* Blackwell Scientific Publications, Oxford, 1987.

[6] Bansal R and Pfeiffer SE. Reversible inhibition of oligodendrocyte progenitor differentiation by a monoclonal antibody against surface galactolipids. *Proc Natl Acad Sci USA* 86:6181–6185, 1989.

[7] Barendsen GW. Influence of fractionation on normal tissue tolerance. In Gutin PH, Leibel SA, and Sheline GE (eds): *Radiation Injury to the Nervous System*, pp. 57–67, Raven Press, New York, 1991.

[8] Benjamins JA. Protein metabolism of oligodendroglial cells in vivo. In Norton WT (ed): *Oligodendroglia. Advances in Neurochemistry. Vol. 5*, pp. 87–124, Plenum Press, New York, 1984.

[9] Bhat S and Pfeiffer SE. Stimulation of oligodendrocytes by extracts from astrocyte-enriched cultures. *J Neurosci Res* 15:19–27, 1986.

[10] Bologa L, Cole R, Chiappelli F, Saneto RP, and de Vellis J. Serum contains inducers and repressors of oligodendrocyte differentiation. *J Neurosci Res* 20:182–188, 1988.

[11] Brent RL. Response of the $9\frac{1}{2}$ day-old-rat embryo to variations in exposure rate of 150 R X-irradiation. *Radiat Res* 45:127–136, 1971.

[12] Bunge RP. Glial cells and the central myelin sheath. *Physiol Rev* 48:197–251, 1968.

[13] Calvo W, Hopewell JW, Reinhold HS, and Yeung TK. Time and dose-related changes in the white matter of the rat brain after single doses of x-rays. *Br J Radiol* 61:1043–1052, 1988.

[14] Campagnoni AT, Campagnoni CW, Dutton GR, and Cohen J. A regional study of developing rat brain: The accumulation and distribution of proteolipid protein. *J Neurobiol* 7:313–324, 1976.

[15] Campagnoni AT and Hunkeler MJ. Synthesis of the myelin proteolipid protein in developing mouse brain. *J Neurobiol* 11:355–364, 1980.

[16] Carpenter MB. *Core Text of Neuroanatomy.* Williams & Wilkins, Baltimore, 1976.

[17] Cavanagh JB. The proliferation of astrocytes around a needle wound in the rat brain. *J Anat* 106:471–487, 1970.

[18] Cerda H and Rosander K. DNA damage in irradiated endothelial cells of the rat cerebral cortex. Protective action of cysteamine in vivo. *Radiat Res* 95:317–326, 1983.

[19] Chapman JD and Gillespis CJ. Radiation-induced events and their timescale in mammalian cells. *Adv Radiat Biol* 9:143–199, 1981.

[20] Chauser B, Morris C, Field SB, and Lewis PD. The effects of fast neutrons and X rays on the subependymal layer of the rat brain. *Radiology* 122:821–823, 1977.

[21] Choi BH, Kim RC, and Lapham LW. Do radial glia give rise to both astroglial and oligodendroglial cells? *Dev Brain Res* 8:119–130, 1983.

[22] Cochran FB, Yu RK, and Ledeen RW. Myelin gangliosides in vertebrates. *J Neurochem* 39:773–779, 1982.

[23] Cohen SR and Guarnieri M. Immunochemical measurement of myelin basic protein in developing rat brain: An index of myelin synthesis. *Dev Biol* 49:294–299, 1976.

[24] Curtis SB. Lethal and potentially lethal lesions induced by radiation - a unified repair model. *Radiat Res* 106:252–270, 1986.

[25] Dwarkanath BS and Jain VK. Energy-linked modifications of the radiation response in a human cerebral glioma cell line. *Int J Radiat Oncol Biol Phys* 17:1033–1040, 1989.

[26] Eisenbarth GS, Walsh FS, and Nirenberg M. Monoclonal antibody to a plasma membrane antigen of neurons. *Proc Natl Acad Sci USA* 76:4913–4917, 1979.

[27] Elkind MM and Sutton H. X-ray damage and recovery in mammalian cells in culture. *Nature* 184:1293–1295, 1959.

[28] Elkind MM and Whitmore GF (eds): *The Radiobiology of Cultured Mammalian Cells.* Gordon and Breach, New York, 1967.

[29] Fajardo LF (ed): *Pathology of Radiation Injury.* Masson Publishing, New York, 1982.

[30] Flickinger JC. An integrated logistic formula for prediction of complication from radiosurgery. *Int J Radiat Oncol Biol Phys* 17:879–885 1989.

[31] Fu KK. Influence of dose rate on normal tissue tolerance. In Gutin PH, Leibel SA, and Sheline GE (eds): *Radiation Injury to the Nervous System*, pp. 69–87, Raven Press, New York, 1991.

[32] Gebicke-Härter PJ, Althaus HH, Rittner I, and Neuhoff V. Bulk separation and long-term culture of oligodendrocytes from adult pig brain. I. Morphological studies. *J Neurochem* 42:357–368, 1984.

[33] Gebicke-Härter PJ, Althaus HH, and Neuhoff V. Bulk separation and long-term culture of oligodendrocytes from adult pig brain. II. Some biochemical data. *J Neurochem* 42:369–376, 1984.

[34] Gerweck LE, Kornblith PL, Burlett P, Wang J, and Sweigert S. Radiation sensitivity of cultured human glioblastoma cells. *Radiology* 125:231–234, 1977.

[35] Gilbert HA and Kagan AR (eds): *Radiation Damage to the Nervous System. A Delayed Therapeutic Hazard.* Raven Press, New York, 1980.

[36] Gutin PH, Leibel SA, and Sheline GE (eds): *Radiation Injury to the Nervous System.* Raven Press, New York, 1991.

[37] Hall EJ. *Radiobiology for the Radiologist, 3rd ed.*. Chapter 12. Time, dose, and fractionation in radiotherapy, pp. 239–259, JB Lippincott Co., Philadelphia, 1988.

[38] Herndon RM, Price DL, and Weiner LP. Regeneration of oligodendroglia during recovery from demyelinating disease. *Science* 195:693–694, 1977.

[39] Hopewell JW. Late radiation damage to the central nervous system: A radiobiological interpretation. *Neuropathol Appl Neurobiol* 5:329–343, 1979.

[40] Hopewell JW. The subependymal plate and the genesis of gliomas. *J Pathol* 117:101–103, 1975.

[41] Hopewell JW and Cavanagh JB. Effects of X irradiation on the mitotic activity of the subependymal plate of rats. *Br J Radiol* 45:461–465, 1972.

[42] Hubbard BM and Hopewell JW. Quantitative changes in the cellularity of the rat sub-ependymal plate after X-irradiation. *Cell Tissue Kinet* 13:403–413, 1980.

[43] Jack JJB, Noble D, and Tsien RW. *Electric Current Flow in Excitable Cells.* Clarendon Press, Oxford, 1975.

[44] Janssen P, Klatzo I, Miquel J, Brustad T, Behar A, Haymaker W, Lyman J, Henry J, and Tobias CA. Pathologic changes in the brain from exposure to alpha particles from a 60-inch cyclotron. In Haley TJ and Snider RS (eds): *Response of the Nervous System to Ionizing Radiation (First International Symposium*, pp. 383–409, Academic Press, New York, 1962.

[45] Johns HE and Cunningham JR. *The Physics of Radiology.* Charles C Thomas, Springfield, IL, 1983.

[46] Kellerer AM and Rossi HH. A generalized formulation of dual radiation action. *Radiat Res* 75:471–488, 1978.

[47] Korr H, Koeser K, Oldenkott S, Schmidt H, and Schultze B. X-ray dose-effect relationship on unscheduled DNA synthesis in mouse brain cells studied in vivo. *Radiat Environ Biophys* 28:13–26, 1989.

[48] Korr H and Schultze B. In vivo synthesis of unscheduled DNA in various cell types of the mouse brain. *Exp Brain Res* 74:573–578, 1989.

[49] Korr H, Schultze B, and Maurer W. Autoradiographic investigations of glial proliferation in the brain of adult mice. I. The DNA synthesis phase of neuroglia and endothelial cells. *J Comp Neurol* 150:169–176, 1973.

[50] Larsson B. Blood vessel changes following local irradiation of the brain with high-energy protons. *Acta Soc Med Uppsala* 65:61–71, 1960.

[51] Latov N, Nilayer G, Zimmerman EA, Johnson WG, Silverman JA, Detenionini R, and Cote L. Fibrillary astrocytes proliferate in response to brain injury. *Dev Biol* 72:381–384, 1979.

[52] Leith JT, Dewyngaert JK, and Glicksman AS. Radiation myelopathy in the rat: An interpretation of dose effect relationships. *Int J Radiat Oncol Biol Phys* 7:1673–1677, 1981.

[53] Leksell L, Larsson B, Andersson B, Rexed B, Sourander P, and Mair W. Lesions in the depth of the brain produced by a beam of high energy protons. *Acta Radiol* 54:251–264, 1960.

[54] Levy RP, Lo EH, and Fabrikant JI. Biologic rationale for stereotactic radiosurgery. In Phillips MH (ed): *Physical Aspects of Stereotactic Rdaiosurgery*, Plenum Publishing, New York (in press).

[55] Lisak RP, Pleasure DE, Silberberg DH, Manning MC, and Saida T. Long term culture of bovine oligodendroglia isolated with a Percoll gradient. *Brain Res* 223:107–122, 1981.

[56] Liversage WE. A general formula for equating protracted and acute regimes of radiation. *Radiology* 42:432–440, 1969.

[57] Lo EH. *Neurophysiologic Reaction to Radiation Injury in the Brain.* PhD Thesis, University of California, Berkeley, Berkeley, 1990.

[58] Lo EH, Frankel KA, Steinberg GK, DeLaPaz RL, and Fabrikant JI. Single fraction high-dose brain irradiation: MRI, cerebral blood flow, electrophysiological and histological studies. *Int J Radiat Oncol Biol Phys* (in press).

[59] Ludwin SK. Pathology of demyelination and remyelination. In Waxman SG and Ritchie JM (eds): *Demyelinating Disease: Basic and Clinical Electrophysiology*, pp. 123–168, Raven Press, New York, 1981.

[60] Ludwin SK. The reaction of oligodendrocytes and astrocytes to trauma and implantation. *Lab Invest* 52:20–30, 1985.

[61] Ludwin SK and Johnson ES. An autoradiographic study of cellular proliferation in remyelination of the central nervous system. *Am J Pathol* 95:683–690, 1979.

[62] Ludwin SK and Johnson ES. Evidence for a "dying-back" gliopathy in demyelinating disease. *Ann Neurol* 9:301–305, 1981.

[63] Lundqvist H, Rosander K, Lomanov M, Lukjashim V, Shimchuk G, Zolotov V, and Minakova E. Permeability of the blood-brain barrier in the rat after local proton irradiation. *Acta Radiol Oncol* 21:267–271, 1982.

[64] Mamoon A-M. *Effects of Ionizing Radiation on Myelin Formation in Rat Brain Cultures.* PhD Thesis, University of California, Berkeley, Berkeley, 1969. UCRL-19481.

[65] Manley NB. *Cell and Tissue Kinetics of the Subependymal Layer in Mouse Brain Following Heavy Charged Particle Irradiation.* PhD Thesis, University of California, Berkeley, Berkeley, 1988.

[66] Manuelidis L and Manuelidis EE. An autoradiographic study of the proliferation and differentiation of glial cells *in vitro*. *Acta Neuropathol (Berl)* 18:193–213, 1971.

[67] Manuelidis L and Manuelidis EE. Proliferation and response of oligodendrocytes. *Lab Invest* 52:1–2, 1985.

[68] Martin PG. Response of the developing ra' brain to varying doses and dose-rates of gamma-radiation. *Growth* 41:41–49, 1977.

[69] McCarthy KD and de Vellis J. Preparation of separate astroglial and oligodendroglial cell cultures from rat cerebral tissue. *J Cell Biol* 85:890–902, 1980.

[70] McKhann GM. A cellular approach to neurological disease. *Johns Hopkins Med J* 143:48–57, 1978.

[71] McMorris FA and Dubois-Dalcq M. Insulin-like growth factor I promotes cell proliferation and oligodendroglial commitment in rat glial progenitor cells developing in vitro. *J Neurosci Res* 21:199–209, 1988.

[72] Meir D and Schachner. Immunoselection of oligodendrocytes by magnetic beads. II. In vitro maintenance of immunoselected oligodendrocytes. *J Neurosci Res* 7:135–145, 1982.

[73] Mendonca MS, Rodriguez A, and Alpen EL. Quiescence in 9L cells and correlation with radiosensitivity and PLD repair. *Radiat Res* 117:433–447, 1989.

[74] Michalowski A. Effects of radiation on normal tissues: Hypothetical mechanisms and limitations of *in situ* assays of clonogenicity. *Radiat Environ Biophys* 19:157–172, 1981.

[75] Mirsky R, Winter J, Abney ER, Pruss RM, Gavrilovic J, and Raff MC. Myelin-specific proteins and glycolipids in rat Schwann cells and oligodendrocytes in culture. *J Cell Biol* 84:483–494, 1980.

[76] Mori S and Leblond CP. Electron microscopic identification of three classes of oligodendrocytes and a preliminary study of their proliferative activity in the corpus callosum of young rats. *J Comp Neurol* 139:1–30, 1970.

[77] Morrison RS and de Vellis J. Growth of purified astrocytes in a chemically defined medium. *Proc Natl Acad Sci USA* 78:7205–7209, 1981.

[78] Myers R, Rogers MA, and Hornsey SA. A reappraisal of the roles of glial and vascular elements in the development of white matter necrosis in irradiated rat spinal cord. *Br J Cancer* 53:221–223, 1986.

[79] Nilsson A, Wennerstrand J, Leksell D, and Backlund EO. Stereotactic gamma irradiation of the basilar artery in cat. Preliminary experiences. *Acta Radiol Oncol* 17:150–160, 1978.

[80] Noback CR and Demarest RJ (eds): *The Human Nervous System. Basic Principles of Neurobiology, 3rd ed.* McGraw-Hill, New York, 1981.

[81] Norton WT. Biochemistry of myelin. In Waxman SG and Ritchie JM (eds): *Demyelinating Disease: Basic and Clinical Electrophysiology*, pp. 93–121, Raven Press, New York, 1981.

[82] Norton WT. Formation, structure and biochemistry of myelin. In Siegel GJ, Albers RW, Agranoff BW, and Katzman R (eds): *Basic Neurochemistry*, pp. 63–92, Little, Brown, Boston, 1981.

[83] Norton WT. Recent advances in the neurobiology of oligodendroglia. In Fedoroff S and Hertz L (eds): *Cellular Neurobiology. Vol. 4*, pp. 3–55, Academic Press, New York, 1983.

[84] Ostertag CB. Experimental central nervous system injury from implanted isotopes. In Gutin PH, Leibel SA, and Sheline GE (eds): *Radiation Injury to the Nervous System*, pp. 183–190, Raven Press, New York, 1991.

[85] Paterson JA, Privat A, Ling EA, and LeBlond CP. Investigation of glial cells in semithin sections. III. Transformation of subependymal cells into glial cells, as shown by radioautography after ^{3}H-thymidine injection into the lateral ventricle of the brain of young rats. *J Comp Neurol* 149:83–102, 1973.

[86] Peters A. *The Fine Structure of the Nervous System: The Neurons and Supporting Cells*, Chapter VII. The Neuroglial Cells, pp. 231–263. W B Saunders, Philadelphia, 1976.

[87] Pettmann B, Delannoy JP, Cumageot J, Devilliers G, and Sensenbrenner M. Rat brain glial cells in culture: Effects of brain extract on the development of oligodendrocyte-like cells. *Dev Biol* 75:278–287, 1980.

[88] Pfeiffer SE. Oligodendrocyte development in culture systems. In Norton WT (ed): *Oligodendroglia. Advances in Neurochemistry. Vol. 5*, pp. 233–298, Plenum Press, New York, 1984.

[89] Plotnikova ED, Levitmann MK, Shaspovnikova VV, Koshevoj JV, and Eidus LK. Protection of microvasculature in rat brain against late radiation injury by gammaphos. *Int J Radiat Oncol Biol Phys* 15:1197–1201, 1988.

[90] Poduslo SE, Miller K, and McKhann GM. Metabolic properties of maintained oligodendroglia purified from brain. *J Biol Chem* 253:1592–1597, 1978.

[91] Puck TT and Marcus PI. A rapid method for viable cell titration and clone production with HeLa cells in tissue culture: The use of x-irradiated cells to supply conditioning factors. *Proc Natl Acad Sci USA* 41:432–437, 1955.

[92] Raff MC, Miller RH, and Noble M. A glial progenitor cell that develops *in vitro* into an astrocyte or an oligodendrocyte depending on culture medium. *Nature* 303:390–399, 1983.

[93] Raff MC, Mirsky R, Fields KL, Lisak RP, Dorfman SH, Silberberg DH, Gregson NA, Leibowitz S, and Kennedy MC. Galactocerebroside is a specific cell-surface antigenic marker for oligodendrocytes in culture. *Nature* 274:813–816, 1978.

[94] Raine CS. Neurocellular anatomy. In Siegel Gj, Albers RW, Katzman R, and Agranoff BW (eds): *Basic Neurochemistry, 3rd ed.*, pp. 21–47, Little, Brown, Boston, 1981.

[95] Reinhold HS, Calvo W, Hopewell JW, and Van Der Berg AP. Development of blood-vessel related radiation damage in the fimbria of the CNS. *Int J Radiat Oncol Biol Phys* 18:37–42, 1990.

[96] Reiss DS, Lees MB, and Sapirstein VS. Is Na^+K^+-ATPase a myelin-associated enzyme? *J Neurochem* 36:1418–1426, 1981.

[97] Remler MP, Marcussen WH, and Tiller-Borsich J. The late effects of radiation on the blood brain barrier. *Int J Radiat Oncol Biol Phys* 12:1965–1969, 1986.

[98] Rosander K, Frankel KA, Cerda H, Phillips MH, Lo EH, Fabrikant I, Fabrikant JI, and Levy RP. DNA damage in mammalian cells after heavy-ion irradiation. In Steiner L (ed): *Radiosurgery: Baseline and Trends*, pp 121–127, Raven Press, New York, 1992.

[99] Saneto RP and de Vellis J. Characterization of cultured rat oligodendrocytes proliferating in a serum-free, chemically defined medium. *Proc Natl Acad Sci USA* 82:3509–3513, 1985.

[100] Scalliet P, Landuyt W, and van der Schueren E. Repair kinetics as a determining factor for late tolerance of central nervous system to low dose rate irradiation. *Radiother Oncol* 14:345–353, 1989.

[101] Schmitt FO (ed): *The Neurosciences, Second Study Program.* Rockefeller University Press, New York, 1970.

[102] Schultheiss TE, Orton CG, and Peck RA. Models in radiotherapy: Volume effects. *Med Phys* 10:410–415, 1983.

[103] Schultze B and Korr H. Cell kinetic studies of different cell types in the developing and adult brain of the rat and mouse: A review. *Cell Tissue Kinet* 14:309–325, 1981.

[104] Seil F. Cerebellum in tissue culture. *Rev Neurosci* 4:105–177, 1979.

[105] Sheline GE, Wara WM, and Smith V. Therapeutic irradiation and brain injury. *Int J Radiat Oncol Biol Phys* 6:1215–1228, 1980.

[106] Skoff RP. The fine structure of pulse labelled (^{3}H-thymidine) cells in degenerating rat optic nerve. *J Comp Neurol* 161:595–612, 1975.

[107] Sprinkle TJ, Zaruea ME, and McKhann GM. Activity of 2′,3′-cyclic-nucleotide 3′-phosphodiesterase in regions of rat brain during development: Quantitative relationship to myelin basic protein. *J Neurochem* 30:309–314, 1978.

[108] Steel GG, Down JD, Peacock JH, and Stephens TC. Dose-rate effects and the repair of radiation damage. *Radiother Oncol* 5:321–331, 1986.

[109] Stein BF. *An Introduction to Neuropysiology.* Chapter3. The electric properties of neurones, pp. 23–41, Blackwell Scientific Publications, Oxford, 1982.

[110] Sternberger NH. Patterns of oligodendrocyte function seen by immunocytochemistry. In Norton WT (ed): *Oligodendroglia. Advances in Neurochemistry. Vol. 5*, pp. 125–173, Plenum Press, New York, 1984.

[111] Sternberger NH, Itoyama Y, Kies MW, and Webster HdeF. Immunocytochemical method to identify basic protein in myelin-forming oligodendrocytes of newborn rat C.N.S. *J Neurocytol* 7:251–263, 1978.

[112] Sternberger NH, Itoyama Y, Kies MW, and Webster HdeF. Myelin basic protein demonstrated immunocytochemically in oligodendroglia prior to myelin sheath formation. *Proc Natl Acad Sci USA* 75:2521–2524, 1978.

[113] Szuchet S, Stefansson K, Wollman RL, Dawson G, and Arnason BGW. Maintenance of isolated oligodendrocytes in long-term culture. *Brain Res* 200:151–164, 1980.

[114] Tanaka A, Ueno H, Yamashita Y, and Caveness WF . Regional cerebral blood flow in delayed brain swelling following x-irradiation of the right occipital lobe in the monkey. *Brain Res* 96:233–246, 1975.

[115] Thames HD and Hendry JH. *Fractionation in Radiotherapy.* Taylor and Francis, Ltd., London, 1987.

[116] Tiller-Borsich JK, Fike JR, Phillips TL, and Davis RL. Pathology of delayed radiation brain damage: An experimental canine model. *Radiat Res* 110:161–172, 1987.

[117] Tobias CA. The repair-misrepair model in radiobiology: Comparison to other models. *Radiat Res* 104:S77–S95, 1985.

[118] van der Kogel AJ. The cellular basis of radiation-induced damage in the central nervous system. In Potten CS and Hendry JH (eds): *Cytotoxic Insult to Tissue*, pp. 329–352, Churchill Livingstone, Edinburgh, 1983.

[119] van der Kogel AJ. Central nervous system radiation injury in small animal models. In Gutin PH, Leibel SA, and Sheline GE (eds): *Radiation Injury to the Nervous System*, pp. 91–111, Raven Press, New York, 1991.

[120] van der Kogel AJ. Radiation-induced damage in the central nervous system: An interpretation of target cell responses. *Br J Cancer* 53[Suppl VII]:207–217, 1986.

[121] van der Kogel AJ. Radiation tolerance of the rat spinal cord: Time-dose relationships. *Radiology* 122:505–509, 1977.

[122] van der Maazen RWM, Verhagen I, Kleiboer BJ, and van der Kogel AJ. Radiosensitivity of glial progenitor cells of the perinatal and adult rat optic nerve studied by an in vitro clonogenic assay. *Radiother Oncol* 20:258–264, 1991.

[123] van der Maazen RWM, Verhagen I, and van der Kogel AJ. An *in vitro* clonogenic assay to assess radiation damage in rat CNS glial progenitor cells. *Int J Radiat Biol* 58:835–844, 1990.

[124] Vandyke DC, Janssen P, and Tobias CA. Fluorescein as a sensitive, semi-quantitative indicator of injury following alpha particle irradiation of the brain. In Haley TJ and Snider RS (eds): *Response of the Nervous System to Ionizing Radiation (First International Symposium)*, pp. 369–382, Academic Press, New York, 1962.

[125] Winer BJ. *Statistical Principles in Experimental Design.* McGraw-Hill, New York, 1971.

[126] Withers HR. Biologic basis for altered fractionation schemes. *Cancer* 55:2086-2095, 1985.

[127] Withers HR. The biologic basis of radiation therapy. In Perez CA and Brady LW (eds): *Principles and Practice of Radiation Oncology*, pp. 67–98, J B Lippincott Co., Philadelphia, 1987.

[128] Withers HR, Peters LJ, and Kogelnik HD. The pathobiology of late effects of irradiation. In Myers RJ and Withers HR (eds): *Radiation Biology in Cancer Research*, pp. 439–448. Raven Press, New York, 1980.

[129] Wood P and Bunge RP. The biology of the oligodendrocyte. In Norton WT (ed): *Oligodendroglia. Advances in Neurochemistry. Vol. 5*, pp. 1–46, Plenum Press, New York, 1984.

[130] Wood P, Okada E, and Bunge RP. The use of networks of dissociated rat dorsal root ganglion neurons to induce myelination by oligodendrocytes in culture. *Brain Res* 196:247–252, 1980.

[131] Yong VW, Kim SU, Kim MW, and Shin DH. Growth factors for human glial cells in culture. *Glia* 1:113–123, 1988.

END

DATE
FILMED
5/11/92